FUNCTIONAL ANALYSIS OF KNOTTED-LIKE HOMEOBOX AND OVATE FAMILY PROTEINS INVOLVED IN SECONDARY CELL WALL DEVELOPMENT IN ARABIDOPSIS

by

Shumin Wang

M.Sc., Nanjing Agricultural University, 2011

A THESIS SUBMITTED IN PARTIAL FULFILLMENT OF

THE REQUIREMENTS FOR THE DEGREE OF

DOCTOR OF PHILOSOPHY

in

THE FACULTY OF GRADUATE AND POSTDOCTORAL STUDIES

(BOTANY)

THE UNIVERSITY OF BRITISH COLUMBIA

(Vancouver)

April 2018

Abstract

The formation of plant secondary cell walls requires a complex network of transcriptional regulation, culminating in a coordinated suite of biosynthetic genes depositing walls, in a spatial and temporal fashion. The transcription factor *KNOTTED ARABIDOPSIS THALIANA7* (*KNAT7*) is a Class II KNOTTED1-like homeobox (*KNOX2*) gene, that acts as a negative regulator of secondary cell wall biosynthesis in interfascicular fibers. Previously, members of Ovate Family Proteins (OFP1 and OFP4), were shown to interact with KNAT7 to negatively regulate wall formation. However, the function of other closely related *KNOX2* and *OFP* genes in secondary wall formation remains unclear. Herein, I showed that *knat3knat7* double mutants possess an enhanced *irregular xylem* (*irx*) phenotype relative to single mutants, and decreased interfascicular fiber cell wall thickness. Additionally, unlike the increased lignin content characteristic of *knat7* mutants, *knat3knat7* had no change in lignin content, while the monomeric lignin composition was substantially reduced relative to the wild-type plants. In contrast, *KNAT3* overexpression resulted in thicker interfascicular fiber secondary walls, suggesting a positive regulation of *KNAT3* in wall development.

A thorough examination of *OFP* mutants showed that none of the single mutants revealed any wall defects, including *ofp4*, which was previously shown to interact with KNAT7. However, they do display leaf phenotypes. In contrast, plants overexpressing *OFP* isoforms consistently exhibited cell swelling, disordered microtubules, and dark-grown de-etiolated phenotypes, resembling phenotypes common to brassinosteroid deficient mutants. Using yeast two-hybrid and bimolecular fluorescence complementation assays, I identified two genes that interacted with OFP4, NAP1;1 and NAP1;2, members of the Nucleosome Assembly Protein 1 (NAP1) family. Higher-order, loss-of-function *NAP1* and *OFP* mutants also exhibit altered cotyledon shape and a reduced cotyledon width:length ratio. The kidney-shaped cotyledon phenotype apparent in *OFP4* overexpressing plants was suppressed in the *nap1;1 nap1;2 nap1;3* triple mutant background. Together, my research suggests that in addition to *KNAT7*, *KNAT3* also contributes to cell wall deposition, and that a complex

network of positive and negative regulation governed by KNOX2 proteins regulates secondary wall formation. Moreover, the complex of OFP4 and NAP1 plays a significant role in the cotyledon development.

Lay Summary

Plant secondary cell walls form the foundation of fibers and wood, and understanding their formation has important biological and economic implications. Arabidopsis has proven a useful model for secondary wall biosynthesis, due to it short generation times, amenablity to transformation, substantive gene mutations, and have a plethora of genetic resources. Two proteins, KNAT7 and OFP4, were reported to negatively regulate secondary wall formation in interfascicular fibers. My research attempted to functionally characterize genes closely associated with *KNAT7* and *OFP4*, and elucidate their involvement in secondary wall formation. I clearly showed that *KNAT3* functions together with *KNAT7* to activate xylem vessel secondary wall formation, while acting antagonistically during secondary wall formation in interfascicular fibers. Concurrently, although expressed in the appropriate developmental window, I showed that the *OFP* genes function to maintain plant hormone homeostasis and regulate cotyledon development instead of participating in secondary wall development as originally hypothesized.

Preface

Figures in Chapter 1 were reproduced with permission from the publishers.

Experiments in Chapter 2 employed seeds of transgenic lines obtained graciously from Dr. John Bowman (Monash University, Australia). Dr. Etienne Grienenberger generated the *knat3knat7* double mutants and first documented the weak stem phenotype. Dr. Masatoshi Yamaguchi generated the Pro_{KNAT4}*::GUS* and Pro_{KNAT5}*::GUS* transgenic lines. Shumin Wang, Dr. Carl Douglas, and Dr. Shawn Mansfield designed the experiments. Shumin Wang performed all the experiments and data analysis. Shumin Wang wrote the manuscript with the assistance of Drs. Lacey Samuels, Shawn Mansfield, and Etienne Grienenberger.

Experiments in Chapter 3 employed the seeds of *nap1* mutants and *pUBQ1::mRFP-TUB6* transgenic plants graciously obtained from Dr. Aiwu Dong (Fudan University, China) and Dr. Chris Ambrose (University of Saskatchewan, Canada), respectively. Shumin Wang, Dr. Carl Douglas, Dr. Lacey Samuels, and Dr. Shawn Mansfield designed the experiments. Shumin Wang performed all the experiments and data analysis.

Table of Contents

List of Tables

List of Figures

List of Abbreviations

3-AT	3-Amino-1,2,4-triazole
4CL	*4-Coumarate: Coenzyme A Ligase*
ABA	abscisic acid
BELL	BELL-like
BES1	BRI1-EMS-SUPPRESSOR 1
BET9	*Bromodomain and Extraterminal Domain Protein 9*
bHLHZip	helix-loop-helix leucine zipper
BiFC	Bimolecular Fluorescence Complementation
BIN2	BRASSINOSTEROID-INSENSITIVE 2
BLH6	BELL-LIKE HOMEODOMAIN6
BP	*BREVIPEDICELLUS*
BR	brassinosteroid
C	catechyl
C3H1	*COUMARATE 3-HYDROXYLASE 1*
C4H	*CINNAMATE-4-HYDROXYLASE*
CAD5	*CINNAMYL ALCOHOL REDUCTASE 5*
CCoAOMT1	*CAEEROYL-COA 3-O-METHYLTRANSFERASE 1*
CCR	*Cinnamoyl-CoA Reductase*
CCR1	*CINNAMOYL-COA REDUCTASE 1*
CESA	cellulose synthase
ChIP-seq	chromatin immunoprecipitation sequencing
CMU	CELLULOSE SYNTHASE-MICROTUBULE UNCOUPLING
COMT	*Caffeic acid 3-O-methyltransferase*
CSC	cellulose synthase complex
CSE	*Caffeol Shikimate Esterase*
CSI1	CELLULOSE SYNTHASE INTERACTING1
DEGs	differentially expressed genes

DMCBH	Djavad Mowafaghian Centre for Brain Health
EMS	ethylmethane sulphonate
EMSA	electrophoretic mobility shift assays
epiBL	epibrassinolide
ER	endoplasmic reticulum
F5H	*Ferulate-5-hydroxylase*
FPKM	fragments per kilobase of exon per million fragments mapped
G	guaiacyl
GFP	green fluorescent protein
GO	gene ontology
GUS	*β-GLUCURONIDASE*
H	*p*-hydroxyphenyl
	hydroxycinnamoyl CoA: shikimate/quinate
HCT	hydroxycinnamoyltransferase
HD	homeodomain
HD-ZIP III	Class III homeodomain leucin zipper
His	Histidine
irx	*irregular xylem*
KNAT7	*KNOTTED ARABIDOPSIS THALIANA7*
KNOX	KNOTTED-like homeobox
KNOX2	Class II Knotted-like homeobox
Leu	Leucine
MP	MONOPTEROS
MS	Murashige and Skoog
	metabolic stable isotope labelling immuno-precipitation mass
mSILIP	spectrometry
NAP1	Nucleosome Assembly Protein 1
NAP1;1	*Nucleosome Assembly Protein 1;1*
NAP1;2	*Nucleosome Assembly Protein 1;2*

NHEJ	non-homologous end-joining
NST1	*NAC SECONDARY WALL THICKENING PROMOTING FACTOR1*
OFP	Ovate Family Protein
OX	overexpression
PAL1	*PHENYLALANINE AMMONIA LYASE 1*
PCD	programmed cell death
PHB	*PHABULOSA*
PHV	*PHAVOLUTA*
PME35	*PECTIN METHYLESTERASE35*
PXY	PHLOEM INTERCALATED WITH XYLEM
REV	*REVOLUTA*
RFP	red fluorescent protein
S	syringyl
SND1	*SECONDARY WALL-ASSOCIATED NAC DOMAIN PROTEIN1*
SPR2	*Spiral 2*
STM	*SHOOTMERISTEMLESS*
TALE	Three Amino acid Loop Extension
TRM	TONNEAU1 Recruiting Motif
TRM20	*TON1 Recruiting Motif 20*
Trp	Trptophan
VND6	*VASCULAR-RELATED NAC-DOMAIN6*
VNI2	VND-INTERACTING2
WT	wild-type
X-Gluc	5-bromo-4-chloro-3-indolyl-β-D-glucuronide
XCP1	*XYLEM CYSTEINE PEPTIDASE 1*
XND1	XYLEM NAC DOMAIN1
Y1H	yeast one-hybrid
YFP	yellow fluorescent protein

Acknowledgements

Firstly, I would like to thank Dr. Lacey Samuels and Dr. Shawn Mansfield, my current supervisors. Without their continuous support, encouragement, and advice, I do not think I can finish my thesis. I am truly grateful for having them as my supervisors. Also, I want to express my sincere appreciation to Dr. Carl Douglas, my first supervisor at UBC, for his understanding, encouragement, inspiration, trust, support and care. My gratitude to them is beyond words. I am very fortunate to become their student.

To my committee members, Dr. Xin Li and Dr. Jae-Hyeok Lee, thank you so much for being available, helpful, and supportive all the time. Thank you for being always patient and giving me constructive feedbacks about my projects.

I am also grateful to Dr. Zhiyong Wang, a staff scientist in Carnegie Institution for Science, who hosted me to do my exchanges in his lab. I learned so much there and thank you for taking some time from your busy schedule to teach me some techniques in the lab. Besides, I would like to thank Wang lab's people, Dr. Chanho Park, Dr. Veder Garcia, Dr. Thomas Hartwig and Bi Yang, for all the help, support, care and fun bringing to me.

Working in Douglas lab was very enjoyable. I would like to thank all the people who were working with me at the same time. I would like to give my special thanks to Dr. Etienne Grienenberger for his mentorship. I learned most of my experimental skills from him. Also, I would like to thank Dr. Masatoshi Yamaguchi, for giving me suggestions and help with my KNOX project. I would like to thank all the lab members in Dr. Douglas, Dr. Samuels, and Dr. Mansfiled labs, for being always so kind, helpful and supportive. Lan Tran, Yoichiro (Yoshi) Watanabe, Miranda Meents and Dr. Mathias Schuetz were always helpful with my questions and giving me a lot of support. Dr. Faride Unda, Dr. Eliana Gonzales, Francis de Araujo, Foster Hart, Grant McNair helped me a lot with my chemical analysis. I also would like to thank all people in Botany Department, for being always so nice and willing to help.

Kyra Janot from Dr. Patrick Martone's lab helped me with the biomechanical assays. Dr. Chris Ambrose was trying to help me with my OFP project and Tongjun Sun taught me how to do the transcriptional activity assays using protoplasts. Sean Shang helped me with my RNA-seq analysis.

Funding for my projects was supported by China Scholarship Councils, NSERC (Natural Sciences and Engineering Research Council of Canada) CREATE Grant "Working on Walls", and Dr. Carl Douglas' NSERC Discovery Grant. The Support from of the University of British Columbia Faculty of Science following Dr. Carl Douglas' death is gratefully acknowledged.

Thank you to my parents, Canming Wang and Guihua Tian, my sister Shuyun Wang and my best friend, Aiping Liu, for love, patience, and support.

Dedication

In Memory of

Dr. Carl Douglas

Chapter 1: Introduction

Plant cell walls provide structural support for the "stately trees and other greenery that grace our planet" (Cosgrove, 2005). Primary and secondary cell walls are the two major structures surrounding almost all plant cells. The newly formed wall is first defined by the primary cell wall, which is thin, expandable, and has a relatively constant proportion of the three main cell wall polysaccharide polymers: cellulose, hemicelluloses, and pectin, as well as a minor fraction of protein (Albersheim et al., 2010). In specialized cells, when the primary wall has finished expanding, a secondary cell wall is deposited, which is a thicker layer composed predominantly of cellulose, hemicelluloses and lignin (Albersheim et al., 2010).

Secondary cell walls are the main constituents of plant fibers and wood, which are widely used for construction, paper, furniture, industrial pulp, energy and many other familiar products, so understanding the secondary cell wall development has significant meaning in biology and for the economy. *Arabidopsis thaliana* has proven to be a favorable model for secondary cell wall formation studies as the secondary cell walls are deposited abundantly in the xylem and interfascicular fiber cells in the inflorescence stems (Ehlting *et al.*, 2005; Zhong *et al.*, 2007).

In order to understand what triggers and controls the secondary cell wall deposition, Arabidopsis transcription factors have been intensively studied (Taylor-Teeples *et al.*, 2014). One of the Arabidopsis Class II Knotted-like homeobox (*KNOX2*) genes, *KNOTTED ARABIDOPSIS THALIANA7* (*KNAT7*), was reported to act as a repressor for secondary cell wall formation in interfascicular fibers, with thicker fiber walls observed in *KNAT7* loss-of-function mutants (Li *et al.*, 2012). Members of Ovate Family Proteins (OFPs), OFP1 and OFP4, were shown to interact with KNAT7 and negatively regulate secondary wall formation (Li *et al.*, 2011; Liu and Douglas, 2015). Because of gene duplication and diversification, there are other *KNOX2* and *OFP* genes that are closely related to *KNAT7* and *OFP4*, respectively, and are in the same clade based on the reported phylogenetic

resconstructions (Figure 1.1) (Furumizu *et al.*, 2015; Wang *et al.*, 2016). However, we know little about their roles in secondary cell wall development. For my Ph.D. research, I used a combined molecular and genetic approach to characterize and elucidate the roles of other KNOX2 and OFPs in Arabidopsis secondary cell wall development.

1.1 Secondary cell wall component biosynthesis

Secondary cell walls are strong multilayered structures whose presence provides rigidity and strength to plant organs, and facilitates water transport in specialized cells of the xylem. The major components of secondary cell wall are cellulose, hemicellulose and lignin.

Cellulose consists of a single polymer of β-1, 4-linked glucan chains, and it makes up the main component of secondary cell walls. The hydrogen bonding and van der Waals interactions among the cellulose chains cause it to form a stable crystalline structure called cellulose microfibrils (Kim *et al.*, 2013). Cellulose is synthesized in the plasma membrane by the cellulose synthase complex (CSC), which includes cellulose synthase (CESA) enzymes and accessory proteins (reviewed in McFarlane *et al.*, 2014). In Arabidopsis, CESA4*,* CESA7, and CESA8*,* which correspond to the *irregular xylem* (*irx)* mutants *irx5*, *irx3* and *irx1*, are required for cellulose synthesis in secondary cell wall development (Turner and Somerville, 1997; Taylor *et al.*, 1999; 2000; 2003). The CSC has been found to have a rosette structure at the plasma membrane that forms a cellulose microfibril containing an estimated 18-24 glucan chains (Mueller and Brown, 1980; Oehme *et al.*, 2015; Nixon *et al.*, 2016). Cross-talk between CSCs movement and the cortical microtubules guides cellulose patterning, as CELLULOSE SYNTHASE INTERACTING1 (CSI1)/POM2 interacts with CESAs and guides CSCs moving along cortical microtubules in the early secondary cell wall developmental stage (Schneider *et al.*, 2017). The stability of the cortical microtubule array depends on microtubule-associated proteins such as CELLULOSE SYNTHASE-MICROTUBULE UNCOUPLING (CMU) (Liu *et al.*, 2016). In the loss-of-function *cmu* mutants, CSCs movement along the plasma membrane may lead to microtubule displacement (Liu *et al.*, 2016).

Hemicelluloses are Golgi-synthesized polysaccharides that can bind to cellulose microfibrils by noncovalent bonds in the cell wall. Xyloglucan is the quantitatively most abundant hemicellulose in the primary cell walls of dicotyledons, while xylans and mannans are the dominant hemicelluloses during differentiation to secondary cell walls (reviewed in Scheller and Ulvskov, 2010). Xylans are composed of a backbone of β-(1,4)-linked xylose mainly with substitution of glucuronic acid residues, known as glucuronoxylans in eudicots, while monocot xylans are structurally varied with glucuronoxylan in non-grass and glucuronoarabinoxylan in grass walls (Peña *et al.*, 2016). Mannans are the predominant hemicellulose of conifer secondary cell walls, and have β-(1,4)-linked backbones with all mannose, or with both mannose and glucose backbones (reviewed in Scheller and Ulvskov, 2010; Rodriguez-Gacio *et al.*, 2012). Different levels of xylan and mannan acetylation and/or methylation exist in the secondary cell wall and affect its integrity (Pawar *et al.*, 2013; Rennie and Scheller, 2014; Hao and Mohnen, 2014).

While mannan and xylan are both present in eudicot secondary cell walls, xylan is the most abundant (reviewed in Scheller and Ulvskov, 2010). Xylan biosynthesis requires a large number of enzymes such as glycosyltransferases, methyltransferases, acetyltransferases, and glycosyl hydrolases (reviewed in Rennie and Scheller, 2014), and the genes involved in xylan biosynthesis have been identified by numerous mutant studies (reviewed in Hao and Mohnen, 2014). For example, *IRX9*, *IRX10* and *IRX14* function redundantly with their homologs, *IRX9-L*, *IRX10-L* and *IRX14-L*, playing significant roles in xylan backbone synthesis (Brown *et al.*, 2009; Lee *et al.*, 2010; Wu *et al.*, 2010). Hemicellulose biosynthetic complexes in the Golgi have been proposed for producing hemicelluloses (reviewed in Meents *et al.*, 2018). IRX9, IRX10 and IRX14 in Asparagus were found to form a xylan biosynthesis complex in the Golgi by coimmunoprecipitation and bimolecular fluorescence complementation studies and the transient expression assay in tobacco leaves revealed that three proteins have to be co-expressed together to correctly locate at the Golgi or the ER localization would be observed (Zeng *et al.*, 2016).

Lignin is a polymer of cross-linked phenolic monolignols that impregnates the polysaccharide matrix to strengthen secondary cell walls. There are mainly three monolignols, p-coumary alcohol, coniferyl alcohol and sinapyl alcohol, which produce *p*-hydroxyphenyl (H), guaiacyl (G) and syringyl (S) units in the lignin, respectively. Lignin in gymnosperms is highly enriched with G units, but angiosperm lignin is made up of both G and S units, with abundant G units in vessel secondary cell walls and dominant S units in the cell walls of fibers (Donaldson, 2001). The monolignols are derived from phenylalanine, which enters the phenylpropanoid and monolignol biosynthetic pathways in the cytosol through a series of hydroxylation and methylation reactions of the phenyl ring and reduction of the terminal carbon of the propane side chain (Albersheim et al., 2010). Mutant studies in Arabidopsis, alfalfa, and poplar as well as *in vitro* enzyme characterizations have contributed to our understanding of monolignol biosynthesis (reviewed in Bonawitz and Chapple, 2010; Dixon *et al.*, 2014; Hao and Mohnen, 2014). For example, in the Arabidopsis *4-Coumarate: Coenzyme A Ligase* (*4CL*) suppression lines, the total lignin content and G/S lignin ratio was significantly decreased (Lee *et al.*, 1998). The *Cinnamoyl-CoA Reductase* (*CCR*) loss-of-function mutants has less than 50% of total lignin content compared with wild type, and display a stem phenotype with collapsed xylem vessels in Arabidopsis (Jones *et al.*, 2001). Downregulation of *Caffeic acid 3-O-methyltransferase* (*COMT*) in alfalfa and poplar plants result in significant reductions in both S lignin and total lignin contents (Guo *et al.*, 2001; Jouanin *et al.*, 2000).

Although the monolignol biosynthetic pathway has been well characterized, the revision of the pathway is still ongoing (reviewed in Zhao, 2016). Bouchaud *et al.* (2013) found the enzyme hydroxycinnamoyl CoA: shikimate/quinate hydroxycinnamoyltransferase (HCT) alone is not enough to produce metabolite caffeoyl shikimate, as the caffeate ester is highly accumulated in the *Caffeol Shikimate Esterase* (*CSE*) loss-of-function mutants. The *cse* mutant has a decreased lignin content, but possesses a high enrichment in H lignin, which suggest that the CSE enzyme is also involved in the lignin biosynthesis, providing a new

insight to the original model (Bouchaud *et al.*, 2013). After monolignols are produced by the cells undergoing lignification or possibly by other neighboring cells, they are exported to the cell wall. Secreted oxidative enzymes such as peroxidases and laccases catalyze monolignol oxidation, leading to randomly cross-coupling to generate the growing lignin polymer (reviewed in Zhao, 2016).

The lignin polymer is quite plastic, as it can adjust the composition of traditional three monomers and incorporate a variety of different unique units without affecting plant normal growth (reviewed in Mottiar *et al.*, 2016; Zhao, 2016). For instance, the *Ferulate-5-hydroxylase* (*F5H*) loss-of-function mutants have lost almost all the S lignin, but the total lignin content is not changed (Marita *et al.*, 1999). Overexpressing *F5H* in Arabidopsis *comt* mutants resulted in an enrichment of 5-hydroxyl-G units (Weng *et al.*, 2010). The catechyl (C) monomer was detected in the seed coats of vanilla orchid, which coexisted with G and S lignin in seed coats (Chen *et al.*, 2012; Tobimatsu *et al.*, 2013).

1.2 Xylem development and interfascicular fiber differentiation

Secondary cell walls are mainly deposited at the tracheary elements and fibers, where the vascular system is. Plant vascular systems include two main tissue types, phloem and xylem, which differentiate from two different meristematic tissues, the procambium and vascular cambium (Eames and MacDaniels, 1947). In herbaceous stems and the young stems of woody plants, the procambial initials form by the action of the apical meristems to produce primary xylem and primary phloem. When plants undergo secondary growth, vascular cambium initials, which originate from procambium and other parenchyma cells, give rise to secondary xylem known as wood and secondary phloem (Evert, 2006). Phloem tissues include fibers, parenchyma, sieve elements, and companion cells, and function to conduct organic compounds in a watery solution, and provide support. Xylem tissues from angiosperms include two tracheary element cell types, tracheids and vessel elements, which are able to facilitate water transport, as well as xylary fibers that function in physical support of the plant body.

Most xylem cells (e.g. tracheary elements) are dead at maturity, have secondary cell wall thickenings, and undergo a series of common developmental steps during their development, which is also defined as xylogenesis (reviewed in Fukuda, 1996). The first step in tracheary element or fiber differentiation is cell expansion, followed by secondary cell wall polysaccharide deposition and lignification (Samuels *et al.*, 2006). For vessels of angiosperms, expansion is strongly in the radial direction, while for angiosperm fibers, expansion is axial as the cells elongate by intrusive growth (reviewed by Mellerowicz *et al.*, 2001). The final stage of development for tracheary element cells is programmed cell death (PCD), which results in the cell becoming an empty tube to support water transport, such as the autolytic process in xylem fibers of the *Populus* stem (Courtois-Moreau *et al.*, 2009).

In many woody and herbaceous plants, the interfascicular cambium differentiates relatively early, and it may develop from cells of ground meristem. If it differentiates later, interfascicular development may result from dedifferentiation of mature interfascicular parenchyma. The cambial activity starts initially in the vascular bundles. Upon the establishment of continuity of the cambium, its mitotic activity results in continuous production of secondary xylem and secondary phloem.

1.3 Molecular mechanisms of vascular development

While these patterns of vascular differentiation have long been observed, we are just beginning to discover the molecular mechanisms underlying their development. Auxin has been well studied to be an important signal for vascular procambium development in embryos, the primary roots and leaf vein development (reviewed in Greco *et al.*, 2012; Ursache *et al.*, 2013). In Arabidopsis inflorescence stems, Mazur *et al.* (2014) observed a high accumulation of auxin in vascular bundles, as well as in the interfascicular parenchyma cells differentiating into interfascicular cambium, which contributes to the cambial ring formation within the stems. *PIN1* gene expression was always preceded by the high auxin

accumulation in differentiating cells, and polar PIN protein was observed in the basal plasma membrane of parenchyma cells and periclinal divisions (Mazur *et al.*, 2014). One of the Class III homeodomain leucin zipper (HD-ZIP III) genes, *AtHB8*, coordinates the procambium formation within and between leaf veins, which is induced by the auxin-response transcription factor MONOPTEROS (MP) directly (Donner *et al.*, 2009). In the auxin biosynthesis mutants, the expression of most of the HD-ZIP III genes, i.e., *PHABULOSA* (*PHB*), *PHAVOLUTA* (*PHV*), *REVOLUTA* (*REV*), *AtHB15* and *AtHB8*, was downregulated and metaxylem patterning was affected (Ursache *et al.*, 2014).

By analogy with other meristems, the balance between cell proliferation and differentiation is important for vascular development and controlled by secreted ligands, receptors, and HOMEOBOX transcription factors. Peptide ligands have been identified that lead to signals controlling xylem differentiation, regulating vascular cell division rate and determining the orientation of cell division (Zhang *et al.*, 2011). By using the xylogenic culture system, CLE41, CLE42 and CLE44, encoding the dodecapeptide tracheary element differentiation inhibitory factors (TDIF), were originally identified and demonstrated to play a unique role in xylem differentiation (Ito *et al.*, 2006). According to expression analysis, CLE41/44 peptide is mainly synthesized in the phloem and its neighboring cells, and then secreted from the phloem into the cambial tissue to suppress xylem differentiation by binding to the TDIF-receptor, which is the leucine-rich repeat receptor-like kinase PHLOEM INTERCALATED WITH XYLEM (PXY) (Fisher and Turner, 2007; Hirakawa *et al.*, 2008). A WUSCHEL-related HOMEOBOX gene, *WOX4*, is activated by the TDIF/TDR signaling pathways, and its expression was highly elevated by TDIF application (Hirakawa *et al.*, 2010). WOX14 functions redundantly with WOX4 in promoting vascular cell division, as *wox4 wox14* double mutants presented fewer cells in vascular bundles than wild type and single mutants (Etchells *et al.*, 2013). Disruption of *CLE41* expression results in disordered vascular development, while increasing phloem-specific expression of *CLE41* leads to well-ordered vascular tissue development, which reveals the function of CLE peptide in regulating the vascular tissue organization (Etchells and Turner, 2010).

BRASSINOSTEROID-INSENSITIVE 2 (BIN2) has been shown to be involved in the mechanism of mediating TDIF and TDIF RECEPTOR in the aspect of repressing xylem differentiation (Kondo *et al.*, 2014). BIN2, encoding a GSK3/SHAGGY-like kinase, was identified as a negative regulator to destabilize BES1 (BRI1-EMS-SUPPRESSOR 1) in controlling the steroid signaling pathway in plants (Li and Nam, 2002; Yin *et al.*, 2002). Kondo *et al.* (2014) found TDIF/TDR is directly associated with BIN2 at the plasma membrane in procambial cells, leading to the suppression of the transcription factor BES1, and subsequently inhibition of xylem differentiation. In the loss-of-function *BES1* mutant, the ectopic xylem cell differentiation in cotyledons induced by bikinin was barely visible, indicating BES1 is the main downstream transcription factor of TDIF-TDR-GSK3 (Kondo *et al.*, 2014; Kondo *et al.*, 2015).

1.4 Secondary cell wall transcriptional regulation network

Secondary cell wall deposition must be tightly coordinated with differentiation of tracheary elements and fibers. Therefore, regulatory mechanisms exist to control the different biosynthetic pathways of secondary wall components in different cell types (Zhong and Ye, 2007). The formation of secondary cell wall requires a very complex network of transcriptional regulation that includes at least three layers of regulators (Figure 1.2) (reviewed in Yang and Wang, 2016).

A set of NAC domain transcription factors has been identified as key transcriptional activators in regulating the biosynthesis of the three main secondary cell wall components (cellulose, hemicellulose and lignin) in Arabidopsis. These positive regulators include *VASCULAR-RELATED NAC-DOMAIN6* (*VND6*) and *VND7* which are responsible for secondary cell wall deposition in xylem vessel elements and the *NAC SECONDARY WALL THICKENING PROMOTING FACTOR1* (*NST1*), *NST2*, *NST3*/*SECONDARY WALL-ASSOCIATED NAC DOMAIN PROTEIN1* (*SND1*), that are associated with secondary cell wall formation in fibers (Kubo *et al.*, 2005; Ko *et al.*, 2007; Zhong *et al.*, 2006; Ruiqin

Zhong *et al.*, 2007; Mitsuda *et al.*, 2007; Zhong and Ye, 2015). In Arabidopsis, VND6 and VND7 have been reported to induce the differentiation of metaxylem- and protoxylem- like vessels respectively, and a dominant repression of VND6 and VND7 specifically inhibits metaxylem and proxylem formation in roots (Kubo *et al.*, 2005; M. Yamaguchi *et al.*, 2010). Global transcriptome analysis reveals that VND7 can regulate genes involved in a broad range of processes in xylem vessel differentiation directly, such as *XYLEM CYSTEINE PEPTIDASE 1* (*XCP1*), an enzyme involved in autolytic processing following cell death (Funk *et al.*, 2002; Yamaguchi *et al.*, 2011). The other five additional Arabidopsis *VND* genes, *VND1* to *VND5*, were also found to be able to regulate secondary cell wall biosynthesis in vessels (Zhou *et al.*, 2014). In Arabidopsis stems, loss-of-function both *SND1* and *NST1* results in the reduction of secondary wall formation in fibers, and overexpression of *SND1* or NST1 induces ectopic secondary wall thickenings in various tissues (Zhong *et al.*, 2006; Ruiqin Zhong *et al.*, 2007; Mitsuda *et al.*, 2007). Zhong and Ye (2015) found that NST2 functions together with SND1 and NST1 regulating secondary wall formation in fibers of stems, as triple mutants *snd1 nst1 nst2* caused a complete loss of secondary wall thickening in fibers.

The secondary wall NAC transcription factors directly activate the expression of MYB46 and MYB83, central regulators of secondary wall formation in both xylem vessels and fibers (Zhong *et al.*, 2007; McCarthy *et al.*, 2009; Zhong and Ye, 2012). It was reported that SND1 binds to MYB46 promoter and activates its transcription (Zhong *et al.*, 2007). Dominant repression of MYB46 results in a dramatic reduction in secondary cell wall thickening of both fibers and vessels (Zhong *et al.*, 2007). MYB83 functions redundantly with MYB46, promoting secondary cell wall biosynthesis in Arabidopsis (McCarthy *et al.*, 2009). Simultaneous downregulation of *MYB46* and *MYB83* leads to a more severe phenotype than *nst1 nst3* double mutants, with reduced growth, severe deformation of vessels and reduction in fiber secondary wall thickening (McCarthy *et al.*, 2009; Mitsuda *et al.*, 2007).

There are a lot of transcription factors functioning downstream of the NAC and MYB domain master switches (Zhong *et al.*, 2008a; Ko *et al.*, 2009; Zhong and Ye, 2012). SND2, SND3, MYB103, MYB85, MYB52 and MYN54 are positively regulated by SND1, and dominant repression of these genes leads to thinner secondary cell walls thickening in fibers (Zhong *et al.*, 2008a). Overexpressing *SND2*, *SND3* and *MYB103* upregulates the expression of cellulose synthase genes and results in thicker fiber secondary cell walls, while overexpression of MYB85 results in ectopic lignin deposition in epidermal and cortical cells in stems by specifically increasing *4CL1* expression (Zhong *et al.*, 2008). The promoters of most monolignol pathway genes contain AC-rich elements (Douglas, 1996; Zhao and Dixon, 2011). These AC-rich elements are binding sites for the transcription factors MYB58 and MYB63, which are specific activators of lignin during secondary wall formation (Zhou *et al.*, 2009). However, the lignin biosynthetic gene encoding *F5H* is an exception to this rule, as it lacks AC-rich elements and is not regulated by MYB58 and MYB63 (Zhou *et al.*, 2009). However, the fiber-specific transcription factor SND1/NST1 regulates *F5H* expression (Zhao *et al.*, 2010). Ohman *et al.* (2013) found that MYB103 is also required for *F5H* expression and S lignin biosynthesis, as the *myb103* mutant has very low transcript abundance of *F5H* gene and significant reduction in S lignin deposition in Arabidopsis.

Some transcription factors are characterized as repressors, fine-tuning the whole secondary cell wall regulatory network. KNAT7 was identified as a negative regulator of secondary cell wall formation, with thicker secondary cell walls in interfascicular fibers in the loss-of function *KNAT7* mutant (Li *et al.*, 2012). MYB75 and BLH6 interact with KNAT7, acting as transcriptional repressors to contribute to the regulation of secondary wall formation in interfascicular fibers, and the interaction between BLH6 and KNAT7 enhances the repression activity of BLH6 or KNAT7 alone (Bhargava *et al.*, 2010; Y., Liu *et al.*, 2014). The promoter activity of *REV*, one of the HD-ZIP III genes, is directly repressed by KNAT7 and BLH6, modulating interfascicular fiber secondary cell wall formation (Liu *et al.*, 2014). A large scale of yeast one-hybrid assay revealed that REV negatively regulates the lignin biosynthetic gene *PAL4* by binding to its promoter directly, and the PAL4 expression is

significantly increased in the *rev-5* loss-of-function mutants (Taylor-Teeples *et al.*, 2015). So KNAT7 can be a potential activator by repressing a repressor, such as *REV*. KNAT7 is a direct target of several NAC master switches and MYB 46 (Zhong *et al.*, 2008; Ko *et al.*, 2009). XYLEM NAC DOMAIN1 (XND1), a member of the NAC domain family, is highly expressed in the xylem and inhibits the secondary cell wall deposition and programmed cell death in xylem cells (Zhao *et al.*, 2008). MYB4, MYB7 and MYB32 are activated by MYB46, functioning as potential repressors to downregulate SND1 expression (Jin, 2000; Ko *et al.*, 2009; H., Wang *et al.*, 2011). VND-INTERACTING2 (VNI2) directly binds to VND7 and repress the expression of vessel-specific genes (Yamaguchi *et al.*, 2010). Overexpression of VNI2 results in an inhibition of the normal xylem vessel development in roots and aerial organs (Yamaguchi *et al.*, 2010). A WRKY transcription factor, WRKY12, has been reported to be a negative regulator, regulating secondary cell wall synthesis in pith cells by suppressing the expression of NST2 and C3H zinc finger transcription factors (H., Wang *et al.*, 2010). The negative regulators are important in maintaining the metabolic homeostasis with respect to metabolic commitment to secondary cell wall formation especially under undesirable growth conditions (Jin, 2000; Li *et al.*, 2012). A series of feed-forward loops are also involved in the secondary cell wall regulatory network to ensure regulation of the whole process under abiotic stress (Taylor-Teeples *et al.*, 2015). By testing protein-DNA interactions, E2Fc was identified as a key upstream repressor as well as activator to regulate VND7 expression, and it can bound to numerous gene promoters including those of VND6, VND7, MYB46 and cellulose-, hemicellulose- and lignin-associated genes (Taylor-Teeples *et al.*, 2015).

1.5 KNOTTED-like homeobox (KNOX) family proteins

As KNAT7 has a demonstrated role in negatively regulating interfascicular fiber secondary cell wall thickness, it is interesting to consider other potential roles in secondary cell wall biosynthesis for other KNOTTED-like homeobox transcription factors. The Homeobox class of proteins is defined by the homeodomain (HD), a 60 amino acid long DNA-binding domain. In the TALE (Three Amino acid Loop Extension) homeobox genes, three additional

residues are observed between helix 1 and 2 of the HD, and the TALE homeobox genes can be found in all eukaryotic lineages (Bürglin, 1997; Derelle *et al.*, 2007). Based on the sequence similarity, the TALE homeobox genes are classified into two different subfamilies, KNOTTED-like homeobox (KNOX) and BELL-like (BELL) (Mukherjee *et al.*, 2009). Based on gene duplication and diversification events in a common ancestor of land plants, KNOX genes are grouped into two classes, class I (KNOX1) and class II (KNOX2; Kerstetter et al., 1994; Mukherjee et al., 2009) (Figure 1.1a). A new class of KNOX genes, KNATM, which does not have a homeodomain, has been shown to regulate the leaf proximal-distal patterning and has only been identified in dicot species (Kimura et al., 2008; Magnani and Hake, 2008).

KNOTTED1, a maize *KNOX1* gene, was the first plant homeobox gene identified, and gain-of-function *KNOTTED1* plants have altered leaf phenotypes (Vollbrecht et al., 1991). In Arabidopsis, *KNOX1* genes include *SHOOTMERISTEMLESS (STM), BREVIPEDICELLUS (BP)/KNAT1, KNAT2* and *KNAT6*, which are involved in cell proliferation (Sakakibara et al., 2008) and required for development of shoot apical meristem (SAM; Long et al., 1996; Vollbrecht et al., 2000; Groover et al., 2006; Tsuda et al., 2011). The expression pattern of *STM* in Arabidopsis is very similar to that of *KNOTTED1* in maize, with the presence in all four types of SAMs: vegetative, axillary, inflorescence and floral (Long *et al.*, 1996). The *stm* mutants induced by ethylmethane sulphonate (EMS) fail to develop a SAM during embryogenesis (Long *et al.*, 1996). The *bp* mutants exhibit reduced internode and pedicel length, downward-pointing flowers and a compact inflorescence architecture, which indicates that BP acts in the differentiation of the inflorescence stem, pedicel, and style in Arabidopsis (Venglat *et al.*, 2002; Douglas *et al.*, 2002). *KNAT2* and *KNAT6* are required for floral organ abscission downstream of *BP*/*KNAT1*, as loss-of-function *KNAT2* and *KNAT6* rescues the *bp* floral abscission phenotype (Shi *et al.*, 2011).

Northern blot analysis in maize showed that *KNOX1* genes are highly expressed in meristem-enriched tissues, while *KNOX2* genes are broadly expressed in all tissues except the

meristematic regions (Kerstetter *et al.*, 1994). In Arabidopsis, there are four *KNOX2* genes, *KNAT3*, *KNAT4*, *KNAT5* and *KNAT7*, which have very similar broad expression profiles as maize *KNOX2* genes (Serikawa, 1997; Truernit *et al.*, 2006; Li *et al.*, 2012; Furumizu *et al.*, 2015). As mentioned previously, *KNAT7* expression is highly associated with the secondary cell wall formation and *knat7* mutants exhibit an irregular xylem vessel phenotype and increased secondary cell wall thickness in interfascicular fibers (Li *et al.*, 2012). Potential roles for KNAT3, KNAT4, and/or KNAT5 in secondary cell wall synthesis have not been explored.

Mutant analyses in Arabidopsis have demonstrated some functions of these additional members of the KNOX2 clade (Furumizu *et al.*, 2015). KNAT3 is reported to be not only involved in the embryo sac development, but also in ABA-mediated seed dormancy and early seedling development by interacting with BLH1 transcription factor (Pagnussat *et al.*, 2007; D., Kim *et al.*, 2013). *KNAT3*, *KNAT4* and *KNAT5* act redundantly in regulating plant development. The *knat3 knat4* and *knat3 knat5* double mutants have more deeply serrated leaves compared with *knat4 knat5* (Furumizu *et al.*, 2015). The *knat3 knat4* and *knat3 knat4/+ knat5* are female sterile with abnormal integument development while *knat3/+ knat4 knat5* plants are phenotypically wild-type with normal amount of seeds (Furumizu *et al.*, 2015). Interestingly, the loss-of-function *KNOX2* phenotypes resemble the gain-of-function *KNOX1* phenotypes, and visa versa (Hake *et al.*, 2004; Hay and Tsiantis, 2010). Furumizu *et al.* (2015) suggested that the way that KNOX2 can suppress meristem activity, while KNOX1 activates meristem activity is by acting oppositely on common downstream elements.

1.6 Ovate Family Proteins (OFPs)

KNAT7 was found to interact with both *Ovate Family Protein 1* (*OFP1*) and *OFP4* using yeast two-hybrid assays and bimolecular fluorescence complementation tests (Li *et al.*, 2011). The loss-of-function mutants are morphologically identical to Arabidopsis wild-type plants, but cross-sections taken from *ofp4* stems revealed an irregular xylem (irx) phenotype

similar to that found in *knat7* (Li *et al.*, 2011). OFP1 and OFP4 function also depends on KNAT7 at least partially, since their pleiotropic over-expression phenotypes are repressed in a *knat7* loss-of-function mutant (Li *et al.*, 2011). As such the researchers proposed that a functional complex of KNAT7-OFP negatively regulates secondary cell wall formation.

Both OFP1 and OFP4 belong to the plant-specific OVATE family, which was named after the first *OVATE* gene cloned in the tomato (Liu *et al.*, 2002). A premature stop codon of the *OVATE* gene in tomato caused a pear-shaped fruit phenotype (Liu *et al.*, 2002). It revealed a new class of proteins found throughout land plants, that have a conserved 70-aa C-terminal domain, which was defined as an OVATE domain (Hackbusch *et al.*, 2005; Wang *et al.*, 2011; Liu *et al.*, 2014). Through a large-scale yeast two-hybrid screen, nine members of OFPs were also found to interact with Arabidopsis TALE homeodomain proteins, and the subcellular localization of TALE proteins can be regulated by OFPs (Hackbusch *et al.*, 2005). Phylogenetic analysis revealed 19 OFPs in Arabidopsis with three major clades and 11 sub-groups (Liu *et al.*, 2014).

So far, there is little information regarding *OFP* function in Arabidopsis. In addition to participating in secondary cell wall development, OFP1 was reported to negatively regulate *GA20ox1*, inhibiting cell elongation through Gibberellic acid biosynthetic pathway in Arabidopsis (Wang *et al.*, 2007). By interacting with the protein Ku70, OFP1 is involved in DNA repair through the non-homologous end-joining (NHEJ) pathway (Wang *et al.*, 2010). Also, OFP1 interacts with BLH3 to regulate flowering time (Zhang *et al.*, 2016). These data suggest that OFP1 has different functions when interacting with different partners. Alternately, OFP5 was shown to regulate Arabidopsis embryo sac development by interacting with BLH1 and KNAT3 (Pagnussat *et al.*, 2007). According to *OFP* overexpression phenotypes, *OFP* genes in Arabidopsis were divided into three classes, and *OFP1*, *OFP2*, *OFP4*, *OFP5* and *OFP7* belong to class I, as their overexpression results in kidney-shaped cotyledons, round and curled leaves, small rosette size, later flowering, reduced fertilization and round seeds (Wang *et al.*, 2011). OFP1 and OFP4 negatively

regulate secondary cell wall development by interacting with KNAT7 (Li *et al.*, 2011), but it remains unclear if other OFPs are similarly involved in secondary wall development.

1.7 Research objectives and Significance of Findings

The main goal of my PhD thesis is to investigate the functions of Arabidopsis *KNOX2* and *OFP* genes focusing on those that may be involved in secondary wall development. To test the hypothesis that KNOX2 and OFP proteins are involved in the regulation of secondary wall formation through interaction with other partners, the following three objectives were addressed:

1. To determine the functions of *KNOX2* genes, *KNAT3*, *KNAT4* and *KNAT5,* in secondary cell wall development.
2. To identify the interaction partners of OFP4.
3. To explore the potential functions of *OFP2*, *OFP3*, and *OFP5* in the same phylogenetic clade as *OFP1* and *OFP4*.

Chapter 2 addresses the first research objective. By using combined molecular and genetic approaches, I concluded that other *KNOX2* genes are also playing an important role in secondary cell wall formation, especially *KNAT3*. It is the first time to discover the transcription factors in KNOX2 class may function antagonistically for secondary cell wall formation in interfascicular fibers. Also, all the differentially expressed genes regulated by KNAT3 and KNAT7 are revealed by mRNA sequencing.

Chapter 3 addresses research objective 2 and 3. Previous studies have shown that OFP4 is involved in secondary cell wall development, but a role for OFP4 secondary cell wall formation was not supported by my studies. To test what other proteins interact with OFP4, I performed a yeast two-hybrid screen. In this chapter, Nucleosome Assembly Protein 1 (NAP1) was identified as a new interaction partner of OFP4, and new roles for both NAP1 and OFPs in the regulation of cotyledon development in Arabidopsis were discovered.

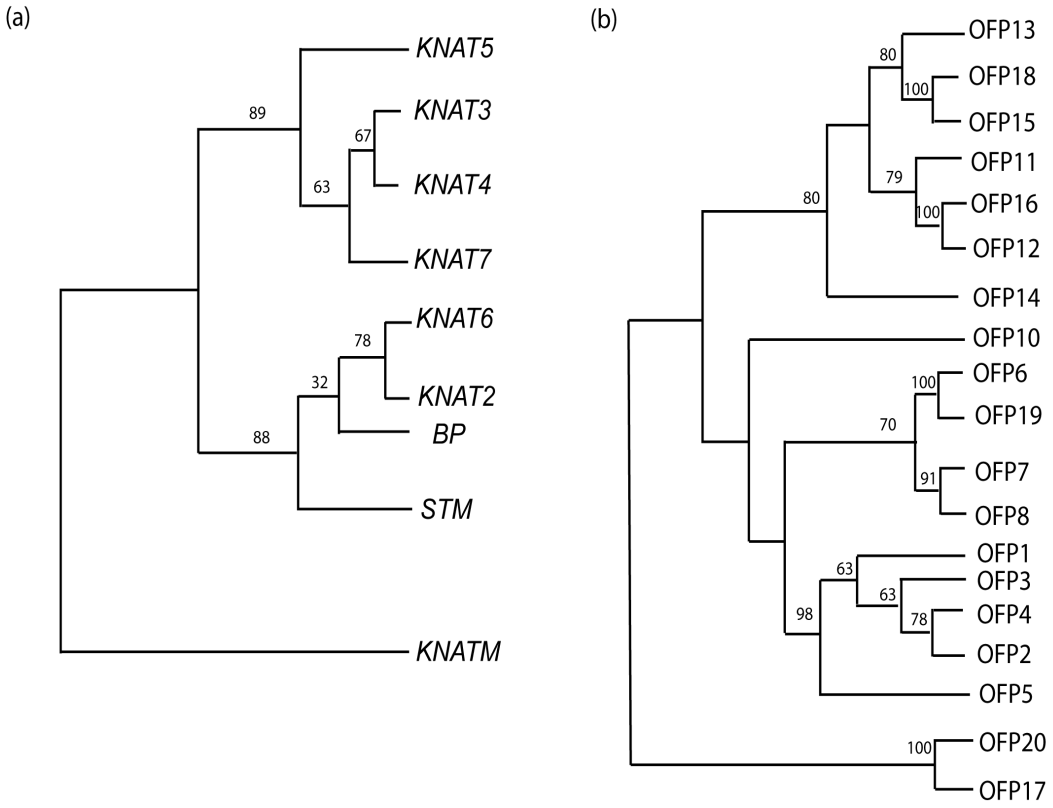

Figure 1.1 Phylogenetic analysis of Arabidopsis KNOX (a) and OFP (b) gene families

Bootstrap values are indicated above the branch. Figure is modified and reproduced from Figure 9 in Li *et al.* (2012) and Figure 1 in Liu *et al.* (2014). By permission from the publisher.

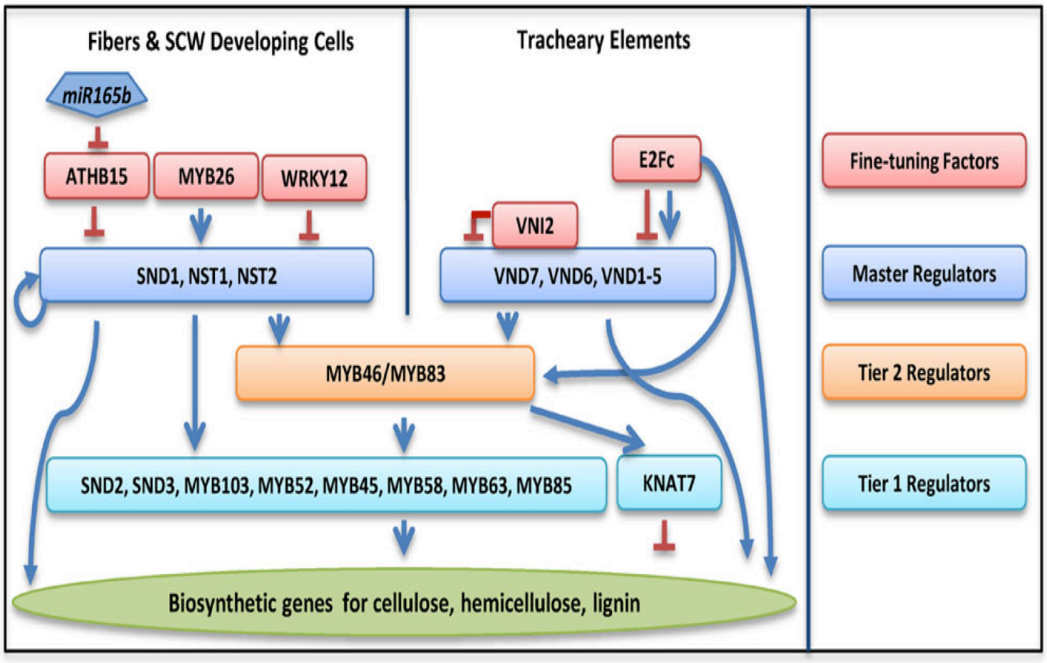

Figure 1.2 Transcriptional network of secondary cell wall development in Arabidopsis

The red line with blunt ends indicates negative regulation, and the blue arrow indicates positive regulation.

Figure is reproduced from Figure 2 in Yang and Wang (2016). By permission from the publisher.

Chapter 2: The Class II KNOX genes *KNAT3* and *KNAT7* work cooperatively to regulate secondary cell wall deposition and provide mechanical support to Arabidopsis stems

2.1 Introduction

Secondary cell walls confer the main structural components of mature tracheary elements and fibers, providing additional mechanical strength and stiffness to plant tissues (Cosgrove and Jarvis, 2012). The formation of secondary cell walls requires a complex network of transcriptional regulation in land plants, which includes at least three layers of regulators (reviewed in Nakano *et al.*, 2015; Yang and Wang, 2016). The VASCULAR-RELATED NAC-DOMAIN gene family (VND1-7) have been identified as key regulators of secondary cell wall deposition in vessel elements (Kubo *et al.*, 2005), while the SECONDARY WALL-ASSOCIATED NAC DOMAIN PROTEIN1 (SND1) and NAC SECONDARY WALL THICKENING PROMOTING FACTOR1 (NST1) gene families regulate secondary cell wall deposition in interfascicular fibers (Zhong *et al.*, 2006; Mitsuda *et al.*, 2007). The second-layer master switches are MYB-type transcription factors, such as *MYB46* and *MYB83*, which are directly regulated by the NAC transcription factors, and act as regulators of secondary wall formation in both xylem vessels and fibers (Zhong *et al.*, 2007; McCarthy *et al.*, 2009; Ohashi-Ito *et al.*, 2010; Wang *et al.*, 2011; Zhong and Ye, 2012). Many other transcription factors also function downstream of the NAC and MYB domain master switches, forming a feed forward regulatory network for secondary wall deposition (Zhong *et al.*, 2008a; Ko *et al.*, 2009; Taylor-Teeples *et al.*, 2014a).

One of the Arabidopsis Knotted-like homeobox (KNOX) genes, *KNOTTED ARABIDOPSIS THALIANA7* (*KNAT7)*, has been shown as a direct target of both *SND1* (Zhong *et al.*, 2008a) and *MYB46* (Ko *et al.*, 2009). Unlike the NAC and MYB domain transcription factors that activate secondary cell wall deposition, KNAT7 was reported to act as a negative regulator

of secondary cell wall formation in interfascicular fibers, with thicker fiber walls observed in loss-of-function *KNAT7* mutants (Li *et al.*, 2012). However, Zhong *et al.* (2008) found that transgenic plants with dominant repression of *KNAT7* had a reduction in secondary wall thickness. Paradoxically, *knat7* mutants also had an irregular xylem (*irx*) phenotype (Li *et al.*, 2012), as reported previously in the original *irregular xylem* studies (Brown *et al.*, 2005). Based on the identification of KNAT7 interactors, such as OVATE FAMILY PROTEIN4 (OFP4), BELL-LIKE HOMEODOMAIN6 (BLH6), and MYB75 (Hackbusch *et al.*, 2005; Bhargava *et al.*, 2010; Li *et al.*, 2011; Y., Liu *et al.*, 2014), KNAT7 may have defined functions in secondary wall formation, depending on specific cell type and interaction partners, however, the specificities of the mechanism of *KNAT7* regulation of secondary cell wall biosynthesis are still poorly understood.

Including *KNAT7*, there are in total nine *KNOX* genes in Arabidopsis, which belong to the plant-specific THREE AMINO ACID LOOP EXTENSION (TALE) homeodomain superfamily (Hake *et al.*, 2004; Hay and Tsiantis, 2010). Based on gene duplication and diversification events in a common ancestor of land plants, *KNOX* genes were grouped into two classes, class I (*KNOX1*) and class II (*KNOX2*; Kerstetter *et al.*, 1994; Mukherjee *et al.*, 2009). A new class of *KNOX* genes, *KNATM*, which does not have a homeodomain, has been shown to regulates the leaf proximal-distal patterning and has only been identified in dicot species thus far (Kimura *et al.*, 2008; Magnani and Hake, 2008). *KNOX1* genes include *SHOOTMERISTEMLESS* (*STM*), *BREVIPEDICELLUS* (*BP*), *KNAT2* and *KNAT6*, which are involved in cell proliferation (Sakakibara *et al.*, 2008) and required for development of shoot apical meristem(Long *et al.*, 1996; Vollbrecht *et al.*, 2000; Groover *et al.*, 2006; Tsuda *et al.*, 2011). *KNOX2* genes *KNAT3*, *KNAT4*, *KNAT5* function redundantly to regulate lateral organ differentiation in Arabidopsis (Furumizu *et al.*, 2015). *KNAT3* was also reported to modulate abscisic acid (ABA) responses during germination and early seedling development (Kim *et al.*, 2013). *KNAT7* also belongs to the *KNOX2* clade, and since it plays diverse roles in secondary wall formation, the question arises whether the other three *KNOX2* genes, *KNAT3*, *KNAT4* and *KNAT5*, may play a role in secondary wall formation.

In this chapter, I report the secondary cell wall characteristics of *knat3*, *knat4* and *knat5* mutants in Arabidopsis stems. I found that all *KNOX2* genes are expressed in the inflorescence stems, and loss-of-function analysis show *knat3knat7* double mutants exhibit an enhanced irregular xylem (*irx*) phenotype, typified by weak inflorescence stems. In addition, the interfascicular fiber wall thickness is reduced and cell wall compositions are modified in *knat3knat7* double mutants. Constitutive overexpression of *KNAT3* led to thicker interfascicular fiber walls. Whole-genome expression profiling of *knat3knat7* double mutants showed differential gene expression associated with cell wall and secondary metabolism genes. My results suggest that *KNAT3* plays a positive role in interfascicular fiber secondary wall formation, and may work cooperatively with *KNAT7* to contribute to plant stem strength by affecting the cell wall deposition and the integrity of the cell-wall matrix. Together, the KNOX2 proteins appear to form a complex network of positive and negative regulators of secondary cell wall formation.

2.2 Materials and methods

2.2.1 Plant material and growth condition

Arabidopsis thaliana ecotype Columbia was used as wild type in all experiments, and all the transgenic lines and mutants are also in the Columbia background. T-DNA insertion lines for *knat3* (SALK_136464), *knat4-1* (SALK_020216) and *knat5* (SALK_000339C) were obtained from the Arabidopsis Biological Resource Center (ABRC). The *knat7-1* allele described in Li *et al*. (2012) was used for all *knat7* phenotypic analyses. Homozygous T-DNA insertion lines were screened by PCR using gene-specific primers (Table 2.1). *knat3*, *knat4-1*, *knat5*, and *knat7* alleles were used to generate *knat3knat7*, *knat4-1knat7*, *knat5knat7*, *knat3knat4-1knat7* and *knat3knat5knat7* double and triple mutants. The other double and triple mutants, *knat3knat4-2*, *knat3knat5*, *knat4-2knat5* and *knat3knat4-2knat5* were kindly gifted from Dr. John Bowman (Furumizu *et al.*, 2015). For the overexpression

analysis of *KNAT3*, homozygous lines for *35S:KNAT3* (Furumizu *et al.*, 2015a) were employed for all experiments.

In all experiments, seeds were sterilized with 70% ethanol and sown on Murashige and Skoog (MS) medium with 1% sucrose, then cold-treated at 4°C for 48 hours in the dark, and grown at 20°C under a 16/8 h (light/dark) photoperiod at about 120 μmol m^{-2} s^{-1} light for 7 to 10 days. Seedlings were transferred to soil and grown under long-day conditions (16/8 h light/dark cycle) at ~100 μmol m^{-2} s^{-1} light, 20°C in growth chambers for further analysis.

2.2.2 Cloning and plant transformation

To generate Pro_{KNAT3}*:GUS*, Pro_{KNAT4}*:GUS*, Pro_{KNAT5}*:GUS,* and Pro_{KNAT7}*:GUS* constructs, the fragment upstream of the ATG start codons of *KNAT3* (3207 bp), *KNAT4* (3290 bp), *KNAT5* (1119 bp) and *KNAT7* (2591 bp) respectively, were sub-cloned into the pCR8/GW/TOPO entry vectors, and then subsequently cloned into the binary vector PMDC163. For complementation experiments, the genomic fragments of *KNAT3* and *KNAT7* containing the 5' promoter and 3' untranslated regions were amplified from Col-0 genomic DNA, respectively. Following verifification of the nucleotide sequences of the amplified fragments, each fragment was cloned into the binary vector PMDC107 containing the hygromycin resistance genes to generate the Pro_{KNAT3}*:KNAT3-GFP* and Pro_{KNAT7}*:KNAT7-GFP* constructs. Gene-specific oligonucleotides used for cloning and construct generation are shown in Table 2.1.

All the constructs were introduced into *Agrobacterium tumefaciens* strain GV3101 for plant transformation. Wild-type Columbia was transformed for expression pattern analysis, while the complementation constructs were transformed into *knat3knat7* double mutant lines via the floral dip method (Clough and Bent, 1998) to generate transgenic plants.

2.2.3 GUS expression assay

GUS activity was assayed on hand-sections of 8-week-old inflorescence stems by incubating tissues in a solution containing 0.1M sodium phosphate buffer (PH 7.0), 1mM substrate 5-bromo-4-chloro-3-indolyl-β-D-glucuronide (X-Gluc), 0.5mM potassium ferricyanide and 0.01%(v/v) Triton X-100 at 37°C for 1 h to overnight. The resulting stained tissues were fixed with FAA (50 [v/v] ethanol, 5% [v/v] acetic acid and 10% [v/v] formaldehyde), and observed with an Olympus AX70 light microscope.

2.2.4 Microscopy

Freshly harvested 8-week-old inflorescence stems were hand-sectioned, stained with aqueous 0.05% toluidine blue O for 1-2 min and mounted with water, or stained with 2% (v/v) phloroglucinol for 30 sec and mounted with concentrated HCl. Mäule staining was performed by treating hand sections for 5 min with 0.5% $KMnO_4$, rinsing in water, and treating with 30% HCl until the brown colour disappeared. Samples were mounted in concentrated NH_4OH and viewed using an Olympus AX70 light microscope. ImageJ was used to measure the thickness of interfascicular fibers. For each cell, three measurements were taken, and the average used as the value of that cell. Statistical analysis was performed by Student's T-test and one-way ANOVA followed by Tukey's post hoc test.

Roots of Pro_{KNAT3}*:KNAT3-GFP* and Pro_{KNAT7}*:KNAT7-GFP* plants in the *knat3knat7* background were counterstained with propidium iodide and observed on a Perkin-Elmer UltraView VoX spinning disk confocal mounted on a Leica DMI6000 inverted microscope with a Hamamatsu 9100-02 CCD camera. The microscope used for all live-cell imaging was fit with the following excitation/emission filters: GFP (488 and 525) and propidium iodide (620/720). ImageJ software was used for image processing.

2.2.5 Physical tests

Tensile and three-point flexural tests were carried out using a 5565 model Instron universal testing machine according to the detailed methods describe by MacMillan *et al.* (2010). 60mm basal stems samples were harvested and used for all tensile tests. The 20mm basal segments were attached to paper tabs by moisture-activated cyanoacrylated Loctite 454 gel (Henkel, Dusseldorf, Germany). The instron testing machine was fit with a 5kN load cell, and employed a cross-head speed of 10 mm/min. Flexural bending strength was estimated on a specimen 15mm from the stem base, using the Instron fitted with a 10N load cell and a cross head speed of 10mm/min. A digital caliper was used to measure the diameter of each stem. BlueHill software was employed to capture and calculate the force and modulus of elasticity for each sample. Statistical analysis was performed by one-way ANOVA followed by Tukey's post hoc test.

2.2.6 Cell-wall analysis

All the cell-wall analyses were performed on dried stems harvested 0-11cm from the base. Lignin content was determined by the modified Klason method described previously (Coleman *et al.*, 2008), in which 100mg of ground, hot acetone-extracted Arabidopsis stem tissue was incubated with 72% H_2SO_4 for 2 hours with regular stirring and then diluted to 3% H_2SO_4 and autoclaved to completely hydrolyze cell wall polysaccharides. The monosaccharides were quantified by HPLC (DX-500; Dionex) equipped with a CarboPac PA1 column (Thermofisher) and a pulsed amperometric detector with a gold electrode. Acid-insoluble lignin was quantified gravimetrically, while the acid-soluble lignin content was measured spectrophotometrically at 205 nm.

α-cellulose content was estimated according to the method of Porth *et al.* (2013). 100 mg of ground, extract-free stem tissue was mixed with 3.5 ml buffer (60ml of glacial acetic acid, 1.3g NaOH/L) and 1.5 ml of 20% sodium chlorite, and then gently mixed at 50 °C for 16 hours. The reaction was repeated again and the residual sample was transferred to crucible to

determine holocellulose gravimetrically. α-cellulose content was then quantified by reacting 30 mg of holocellulose with 2.5ml of 17.5% NaOH for 30 min, followed by a second 8.75% NaOH for an additional 30 min. Then α-cellulose was finally determined gravimetrically.

Lignin monomer composition was estimated by thioacidolysis as described by Robinson and Mansfield (2009). Statistical analysis was performed by one-way ANOVA followed by Tukey's post hoc test, using three biological replicates and two technical replicates.

2.2.7 Total RNA isolation and quantitative RT-PCR

The basal 0-11cm of 8-week-old inflorescence stems were frozen and homogenized. Total RNA isolation and subsequent cDNA synthesis was completed as per Liu *et al.*, (2014). For qRT-PCR analysis of the basal stem segments, PCR amplification was performed using a CFX Connect™ real-time system (Bio-Rad), using 40 quantitative PCR cycles that were run under the following parameters: denaturation step, 95°C for 20 sec; annealing step, 55°C for 30 sec; elongation step, 72°C for 1 min. *ACTIN2* was used as the reference housekeeping gene. All primers are listed in Table 2.1. The calculation of differences in gene expression was according to Bhargava *et al.* (2010). Three biological replicates consisting of three technical replicates were used for each analysis.

2.2.8 RNA-seq analysis

Total RNA was extracted from wild type, *knat3*, *knat7*, and *knat3knat7* inflorescence stems (1-15cm from the top) using TRIZOL reagent (Invitrogen, Life Technologies) following the manufacturer's protocol. In total, 12 samples were sent to UBC-Djavad Mowafaghian Centre for Brain Health (DMCBH) Next Generation Sequencing Centre for library preparation and Ion Proton™ semiconductor-based transcriptome sequencing (4 genotypes times 3 biological replicates).

The sequencing quality of the RNAseq reads was evaluated by FastQC software (http://www.bioinformatics.babraham.ac.uk/projects/fastqc), and clean reads were mapped to the *A. thaliana* TAIR 10 reference genome using STAR (https://github.com/alexdobin/STAR). FPKM (fragments per kilobase of exon per million fragments mapped) was used to estimate the gene transcript abundance. Cuffdiff (Trapnell *et al.*, 2012) was used to calculate FPKM and identify differentially expressed genes across genotypes. GO functional enrichment analysis was performed using PANTHER (https://www.arabidopsis.org/tools/go_term_enrichment.jsp) with a significance level of $P < 0.05$ (Mi *et al.*, 2013). The metabolism overview of DEGs between mutants and wild type was detected by MAPMAN software (http://mapman.gabipd.org/).

2.3 Results

2.3.1 KNOX2 genes are expressed in the inflorescence stems

In Arabidopsis, there are four genes encoding KNOX2 proteins, *KNAT3*, *KNAT4*, *KNAT5* and *KNAT7* (Furumizu *et al.*, 2015a). To investigate if these KNOX2 genes are expressed in cells undergoing secondary wall deposition, and overlapping with that of KNAT7, lines containing Pro_{KNAT3}*:GUS*, Pro_{KNAT4}*:GUS*, Pro_{KNAT5}*:GUS,* and Pro_{KNAT7}*:GUS* were generated, and similar stem expression patterns were observed among all independent transformants (Figure 2.1). The *KNOX2* promoter directed *GUS* expression in cortical cells and developing vascular bundles near the apex of the stems (Figure 2.1a-d). This expression pattern was retained in the more mature stem regions, where GUS staining was also detected in the differentiating interfascicular fibers (Figure 2.1e-h). Interestingly, the expression of all four *KNOX2* genes was absent in fully differentiated interfascicular fibers and metaxylem vessels in the lower regions of mature inflorescence stems, but was still apparent in cortical cells, phloem, and protoxylem cells (Figure 2.1i-l). These findings suggest that *KNAT3*, *KNAT4* and *KNAT5* share similar expression patterns as *KNAT7* in the different developmental stages of inflorescence stems, and they are expressed in differentiating interfascicular fibers and xylem cells where secondary cell walls are actively being deposited.

2.3.2 *knat3knat7* double knock-out mutants have enhanced irregular xylem (irx) phenotype

To test the potential role of *KNOX2* genes in xylem development, their null alleles were obtained, which included SALK_136464 (*knat3*), SALK_020216 (*knat4-1*), N759461 (*knat4-2*), SALK_000339C (*knat5*), and SALK_002098 (*knat7*) (Kim *et al.*, 2013; Furumizu *et al.*, 2015a; Li *et al.*, 2012). Stem cross-sections were examined at the base of mature inflorescence stems for each genotype to determine xylem morphology. *knat3, knat4, and knat5* single mutants exhibited normal vessels morphology (Figure 2.2b-d). As previously reported (Brown *et al.*, 2005; Li *et al.*, 2012; Y., Liu *et al.*, 2014a), *knat7* single mutant exhibited an irregular xylem (*irx*) phenotype (Figure 2.2e). Due to their overlapping expression patterns, gene redundancy may potentially mask these observations, so different combinations of double and triple mutants were generated (*knat3knat7, knat4-1knat7, knat5knat7, knat3knat4-1knat7, knat3knat5knat7*) or generously obtained from Dr. John Bowman (*knat3knat4-2, knat3knat5, knat4-2knat5, knat3knat4-2knat5*).

Interestingly, the vessels of *knat3knat7* double mutants were more frequently irregular and collapsed compared to wild-type plants and the associated single mutants (Figure 2.2f). The enhanced *irx* phenotype of *knat3knat7* was obvious in all vascular bundles of plants examined. *knat4-1knat7* and *knat5knat7* showed a mild *irx* phenotype (Figure 2.3d,e), which appeared to vary in severity between vascular bundles and plants. Their mild *irx* phenotype was similar to that commonly observed in *knat7* single mutants (Y., Liu *et al.*, 2014a). The other double mutants did not show any obvious changes in xylem morphology compared to wild-type plants (Figure 2.3f-h). Cross-sections of triple mutant plants revealed that *knat3knat4-1knat7* and *knat3knat5knat7* had severe *irx* phenotypes, mimicking that of *knat3 knat7* double mutants, while *knat3knat4knat5* vessels appeared similar to that of wild-type plants (Figure 2.3i-k). These results indicate that in addition to *KNAT7*, *KNAT3* may also play a role in the xylem vessel development.

2.3.3 Knockout of *KNAT3* and *KNAT7* affects stem mechanical properties and fiber wall thickness

The *knat3knat7* double mutants exhibited a pendent stem phenotype following 7 weeks growth, while the other single and double mutants showed no apparent stem morphological differences compared to wild-type plants (Figure 2.4a, 2.5). Often the double mutants of *knat3knat7* displayed shorter inflorescence stems than wild type, but this was not consistent across all generations and experiments. The obvious weak stem phenotype implies that the mechanical properties of *knat3knat7* inflorescence stems may have been impaired, so both uniaxial tensile tests and three-point flexural tests of stems were performed. As described previously (Turner, 1997; MacMillan *et al.*, 2010), the stem strength is measured as the maximum stress at yield for breaking the sample, and the stem stiffness (as defined by modulus of elasticity) is a measure of the force required to deform the sample. The bases of *knat3knat7* fresh stems were considerably weaker than wild-type plants, displaying an approximately 80% reduction in the tensile strength and 60% reduction in the tensile stiffness compared to wild type (Figure 2.4b,c). In comparison, *knat3* and *knat7* single mutants do not possess weaker tensile strength and stiffness than wild type (Figure 2.4b,c). However, the flexural strength of the base of *knat7* fresh stems showed a significant increase compared to wild-type stems (Figure 2.4d). Unlike tensile strength, *knat3knat7* fresh stems had no change in flexural strength (Figure 2.4d). When it comes to the bases of dried stems, the trends in flexural strength were similar to tensile strength, with a pronounced decrease in *knat3knat7* double mutants, and no considerable changes in the corresponding single mutants (Figure 2.4d). The differences in flexural strength between fresh and dried stems may be a function of the turgor pressure coming from stem water contents. Furthermore, the *knat3knat7* stems had reduced flexural stiffness compared to wild type and single mutants, for both fresh and dried stems (Figure 2.4e). The reduction in flexural stiffness in *knat3knat7* stem bases was particularly remarkable in dried stems (82%), whereas fresh stems showed a 56% reduction compared to wild-type plants (Figure 2.4e).

Arabidopsis interfascicular fibers are particularly important for providing the necessary mechanical strength to inflorescence stems, as demonstrated in a significant number of mutants, including *rev* and *fra8* (Zhong, 1997; Zhong, 2005), to mention only a few. To determine whether the striking stem phenotype in *knat3knat7* double mutants was caused by defects in interfascicular fibers, the fiber wall thickness was examined. Cross-sections of stem bases stained with phloroglucinol-HCL revealed that the interfascicular fiber wall thickness of *knat3 knat7* double mutant was smaller compared (decreased by 37%; Figure 2.6e) with that of wild type (Figure 2.6a-d), as well as *knat3*, and *knat7* mutant plants. In contrast, *knat7* had a significant increase in interfascicular fiber wall thickness, as previously reported (Li *et al.*, 2011; Li *et al.*, 2012; Y., Liu *et al.*, 2014a), while *knat3* did not show differences compared to that of wild-type (Figure 2.6e). .

2.3.4 *KNAT3* and *KNAT7* expression affect secondary cell wall composition

Secondary cell wall is the major constituent of xylem vessels and fiber cells in Arabidopsis stems. The enhanced *irx* and decreased fiber wall thickness phenotypes predict an alteration in secondary cell wall composition in *knat3knat7* double mutants. Monosaccharide compositional analysis was performed on the basal segments of inflorescence stems. Single mutants had no significant or mild changes in the concentrations of sugars derived from cell wall carbohydrates, while the changes in the double mutants *knat3knat7* were significant (Table 2.2). The glucose, xylose and mannose content in the double mutants was significantly reduced by 22%, 43% and 40% respectively, but considerable increases were also observed in arabinose, rhamnose and galactose of the double mutants, displaying 75%, 41% and 41% more than wild-type (Table 2.2). Given cellulose is a polymer of β(1,4)-linked glucose, the decreased glucose content maybe attributed to a reduction in cellulose deposition in stems, so cellulose content was further investigated. The α-cellulose content in *knat3knat7* stem bases was approximately 20% lower than in wild type, and no significant difference were observed in *knat3* and *knat7* single mutants (Table 2.3). Lignin, another important composition of secondary cell wall, was also quantified. There was no discernible

change in the lignin content of *knat3* single mutant relative to the wild-type control (Table 2.3). However, a different trend was observed between *knat7* and the double mutants relative to the wild type (Table 2.3). *knat7* had an approximate 11% increase in acid-insoluble lignin and 19% decrease in soluble lignin, while *knat3knat7* displayed a 4% decrease in acid-insoluble lignin and 26% increase in soluble lignin (Table 2.3). It is quite interesting that *knat7* single mutant had increased total lignin content as previously reported (Li *et al.*, 2012; Liu *et al.*, 2014), while the double knockout mutant *knat3knat7* did not have a significant change in total lignin (Table 2.3).

The lignin monomer composition, as determined by thioacidolysis, was further characterized in single and double mutant stems (Figure 2.7), and revealed that *knat3* and *knat7* single mutants had lower S/G lignin ratio than the wild-type control plants. However, the ratio was much lower in the *knat3knat7* double mutant stems (around 84% lower than the wild-type S/G lignin; Figure 2.7a). Mäule staining of stem cross-sections was concurrently conducted in attempts to selectively localize syringyl (S) lignin in single and double mutants (Figure 2.7b). The vascular elements and interfascicular fibers displayed the classical the red coloration in wild type and single mutants, which is indicative of syringyl-derived lignin (Figure 2.7b), while the same cells in the *knat3knat7* double mutants were much lighter (Figure 2.7b). The decreased S lignin in the double mutant stems is consistent with the chemical determinatin of S/G monomer ratio.

2.3.5 *knat3knat7* phenotypes are complemented by Pro_{KNAT3}:KNAT3-GFP and Pro_{KNAT7}:KNAT7-GFP

To investigate whether the *knat3knat7* phenotypes were caused by loss of function of *KNAT3* and *KNAT7*, complementation experiments were performed. *knat3knat7* was transformed with two different constructs, Pro_{KNAT3}*:KNAT3-GFP* and Pro_{KNAT7}*:KNAT7-GFP*. Expression of *KNAT3* under the control of its native promoter partially rescued the severe *irx* phenotype consistently observed in *knat3knat7*, manifesting in a phenotype similar to *knat7* (Figure

2.8a). Plants transformed with *Pro$_{KNAT7}$:KNAT7-GFP* in the *knat3knat7* background fully rescued the *irx* phenotypes of *knat3knat7* (Figure 2.8a). The pendent phenotype of *knat3knat7* was also complemented in both transformants (Figure 2.8b). The interfascicular fiber wall thickness was quantified in inflorescence stems of the complementation lines (Figure 2.8c,d), and shown to be restored to a level relative to the wild type by expressing *KNAT3-GFP* under the control of its native promoter in *knat3knat7* background (Figure 2.8c), mimicking the *knat7* single mutant. As with *knat3* single mutants, the interfascicular fiber cell wall thickness was not different than wild type when *KNAT7-GFP was expressed* in *knat3knat7* mutants (Figure 2.8c).

KNAT3 and *KNAT7* were also confirmed to have overlapping expression patterns during secondary cell wall deposition, as reflected in the GFP signals using the complemented lines, since both lines were under the control of their native promoters (Figure 2.9). *KNAT3* had a broader expression pattern compared with *KNAT7*, but both were detected in the protoxylem and metaxylem vessel precursors in the roots, and in the interfascicular fiber cells in inflorescence stems of the complemented lines (Figure 2.9).

2.3.6 Overexpression of *KNAT3* increases interfascicular fiber wall thickness of stems

The contrasting phenotypes of *knat3knat7* double mutants having decreased interfascicular fiber wall thickness, while *knat7* single mutants had increased fiber wall thickness, suggested that *KNAT3*, along with *KNAT7,* plays a regulatory role in the development of interfascicular fibers. In an attempt to enhance the levels of *KNAT3*, plant lines overexpressing *KNAT3* under the control of *35S* promoter were generated. Cross-sections of the basal inflorescence stems were examined by Toluidine Blue staining (Figure 2.10) and compared to wild type, and the overexpression lines appeared to have thicker interfascicular fibers secondary cell walls (Figure 2.10a). Measurements taken via high-magnification light microscopy images confirmed that constitutive expression of *KNAT3* (*Pro$_{35S}$:KNAT3*) significantly increased interfascicular fiber wall thickness (Figure 2.10b), suggesting that *KNAT3* may play a role in the positive regulation of secondary wall formation in interfascicular fibers.

2.3.7 Genome-wide transcript profiling shows altered expression of secondary cell wall related genes in *knat3knat7* plants

In an attempt to uncover the mechanistic role of *KNAT3* and *KNAT7* in secondary cell wall development, the transcript abundance of known cellulose, hemicellulose and lignin biosynthetic genes was profiled by qRT-PCR in cDNA isolated from basal stems of *knat3*, *knat7* and *knat3knat7* mutants. It was clearly shown that the expression levels of secondary cell wall specific *CELLULOSE SYNTHASE* (*CESA*) genes (*CESA4*, *CESA7*, *CESA8*), and one of xylan biosynthetic genes (*IRX9*) were dramatically increased in the double mutants compared with wild-type and the individual single mutants (Figure 2.11a). Another xylan synthetic gene, *IRX10*, was significantly down regulated in *knat7* and *knat3knat7* plants, and *knat3* showed a slightly increase in *IRX10* expression (Figure 2.11a). Loss of *KNAT3* and *KNAT7* functions together also resulted in both up-regulation and down-regulation of several phenylpropanoid biosynthetic genes (Figure 2.11b). Specifically, the expression of *C4H*, *C3H1*, *CCoAMT1* and *CCR1*, was elevated 1.5- to 2-fold in the basal segments of *knat3knat7* inflorescence stems, while the abundance of *FERULATE-5-HYDROXYLASE* (*F5H*), a key enzyme for S lignin biosynthesis, was considerably decreased (about 50%) in *knat3knat7* mutants (Figure 2.11b). This latter finding is consistent with the reduced S lignin deposition observed in our biochemical and histochemical assessment of the *knat3knat7* stems.

To gain further insights into *KNAT3* and *KNAT7* function, mRNA sequencing was carried out to identify all the genes showing significant changes in expression among wild-type, *knat3*, *knat7* and *knat3knat7* stems. Compared with wild type, *knat3knat7* had a total of 959 up-regulated and 1001 down-regulated genes, whereas *knat3* and *knat7* had 484 and 367 down-regulated, respectively (Figure 2.12a,c). Comparative analyses revealed that of all the mis-regulated genes, 32 and 117 genes were found in common in *knat3*, *knat7* and *knat3knat7* plants (Figure 2.12a,c). To determine the identities of these differentially expressed genes (DEGs), GO ontology classifications were performed based on their known functions. In *knat7*, genes involved in cell wall organizational processes were significantly

up-regulated and over-represented compared to wild-type plants (Figure 2.12b), which is consistent with a repressor-type function in secondary cell wall formation (Li *et al.*, 2012). Compared with *knat3* and *knat7*, a significant number of up-regulated genes in *knat3knat7* were related to glucuronoxylan biosynthesis, plant-type secondary cell wall biogenesis, nucleotide-sugar biosynthetic processes, microtubule-based processes and pectin metabolic processes (Figure 2.12b). Additionally, a few biological processes were over-represented in the down-regulated DEGs found in *knat3knat7* plants, such as aromatic amino acid family catabolic process, phloem transport, and response to red light, to mention only a few (Figure 2.12d). MapMan was further used to visualize the differentially expressed genes in various metabolic pathways (Figure 2.13, 2.14). Generally consistent with the qRT-PCR data, *knat3knat7* exhibited both increased and decreased transcript levels of phenylpropanoid biosynthetic genes (Figure 2.13, 2.14, Table 2.4). The weak stem and enhanced *irx* phenotypes of *knat3knat7* may be caused by the mis-regulation of a number of secondary cell wall related genes, representing all major biochemical pathways (lignin, cellulose and hemicellulose).

2.4 Discussion

KNAT7, one of the four *KNOX2* genes in Arabidopsis, has been proposed to function as a transcriptional repressor regulating secondary cell wall formation in interfascicular fibers (Li *et al.*, 2011; Li *et al.*, 2012). Three other Arabidopsis *KNOX2* genes, *KNAT3*, *KNAT4*, and *KNAT5*, were found to act redundantly in regulating plant development, with serrated leaves apparent on *knat3knat4*, *knat3knat5* and *knat3knat4knat5* plants (Furumizu *et al.*, 2015), however, little is known about their exact biological role(s), if any, in secondary cell wall formation. In this study, beyond the developmental roles of KNOX2 in leaf development, we focused on their putative roles in secondary cell wall formation. *KNAT3* was identified as a potential transcriptional activator, working antagonistically with *KNAT7* to regulate secondary wall formation in interfascicular fibers, while in xylem vessels, *KNAT3* and *KNAT7* may function together to activate secondary cell wall deposition.

Expression data shows that all four *KNOX2* genes are co-expressed in the same cell types of inflorescence stems (Figure 2.1, 2.9), suggesting *KNAT3*, *KNAT4* and *KNAT5* may also play a role(s) in secondary cell wall formation (Li *et al.*, 2012; Y., Liu *et al.*, 2014a). Interestingly, Pro_{KNAT3}*:KNAT3-GFP* has an expanded expression pattern compared with Pro_{KNAT7}*:KNAT7-GFP* in the roots, with expression apparent throughout other root cell layers, other than protoxylem and metaxylem vessel precursors (Figures 2.9). This suggests that KNAT3 may play multiple roles in plant development, which is consistent with previous findings that KNAT3 can modulate ABA responses (Kim *et al.*, 2013) and regulate lateral organ development (Furumizu *et al.*, 2015a).

The collapsed xylem vessel phenotype, *irx*, has been widely used to isolate Arabidopsis mutants defective in the secondary cell wall biosynthesis (Turner, 1997; Jones *et al.*, 2001; Brown *et al.*, 2005). Analysis of *knat4knat7*, *knat5knat7* mutants revealed an *irx* phenotype, which phenocopied *knat7* (Li *et al.*, 2012), while *knat3knat7* afforded an enhanced *irx* phenotype (Figure 2.2, 2.3). The synergistic effect of the xylem vessel phenotype in double mutants indicates that KNAT3 and KNAT7 may function redundantly in modulating vessel secondary cell wall development, although KNAT7 likely plays the dominant role, as the single mutant *knat7* displays the *irx* phenotype, while *knat3* has no obvious xylem vessel phenotypes (Figure 2.2).

A striking effect of loss-of-function *KNAT3* and *KNAT7* was the weak inflorescence stem with reduced tensile and flexural strength and stiffness (Figure 2.4). Thinner interfascicular fiber cell walls in the *knat3knat7* double mutants is undoubtedly the reason for the pendent stem phenotype, as interfascicular fibers are important for the mechanical strength of Arabidopsis inflorescence stems (Zhong, 2005; Zhong *et al.*, 2007). Although the thicker secondary cell walls phenotype in interfascicular fibers in *knat7* mutants was observed here, as well as in previous studies (Li *et al.*, 2012), the double mutants *knat3knat7* displayed an opposing trend with thinner interfascicular fiber wall thickness (Figure 2.6). Thus, the thicker secondary cell wall phenotype in *knat7* appears to be associated with a functional KNAT3.

KNAT3 may be able to activate secondary cell wall formation in fibers, as ectopic expression of *KNAT*3 manifested in thicker interfascicular fiber secondary cell walls (Figure 2.10). However, *knat3* single mutants do not show an obvious interfascicular fiber secondary cell wall development phenotype (Figure 2.6), which suggests *KNAT3* has some redundancy with other genes in plants to regulate secondary wall formation. KNAT7 may have distinct roles by interacting with different partners, such as the helix-loop-helix leucine zipper domain (bHLHZip) transcription factor family proteins demonstrated in animals (reviewed in Lüscher, 2001; Amoutzias *et al.*, 2008). Zhong *et al.* (2008) found dominant transcriptional repression of *KNAT7* caused reduction in secondary cell wall thickening in interfascicular fibers, which is similar to *knat3knat7* double mutants. Since the dominant repression approach may not only inhibit the function of targeted transcription factor, but also their homologs (Hiratsu *et al.*, 2004), it is possible that the thinner fibers phenotype emanates from the repression of both *KNAT3* and *KNAT7*.

The cellulose polymer is the major load bearing component affecting stem tensile and flexural strength, as demonstrated in Arabidopsis and rice mutants (Turner and Somerville, 1997; Li *et al.*, 2003). The lower cellulose content of *knat3knat7* stem cell walls (Table 2.3) can easily explain the decreasing tensile and flexural strength of *knat3knat7* stems. In addition, the lignin composition was modified in the *knat3knat7* double mutants, with significant reductions in both S lignin and S/G lignin ratio in inflorescence stems (Table 2.3). Secondary cell walls are the main structural component of xylem vessels and interfascicular fibers in Arabidopsis inflorescence stems, and therefore the altered cell wall chemical composition in *knat3knat7* mutants may account for the *irx* and thinner interfascicular fiber wall phenotypes. The complementation tests in our study confirmed the involvement of *KNAT3* and *KNAT7* in the regulation of secondary cell wall development in Arabidopsis stems (Figure 2.8).

The impact of *KNAT3* and *KNAT7* on cell wall development was also assessed by qRT-PCR and messenger RNA sequencing. Both techniques clearly showed increasing expression of

the secondary cell wall-specific cellulose biosynthetic genes (*CESA4*, *CESA7* and *CESA8*) in the basal stems of *knat3knat7* mutants (Figure 2.11), which was unexpected as the *knat3knat7* mutants had lower cellulose contents (Table 2.3). We reasoned that the observed up-regulation of cellulose synthase genes may reflect a feedback mechanism where that plant is attempting to over compensate for impaired secondary cell wall development in *knat3knat7* stems. The key enzyme for syringyl monomer biosynthesis and integration into the lignin polymer, F5H, was significantly down regulated in the *knat3knat7* tissue (Figure 2.11), which is consistent with the observed reduction in both S lignin and the associated S/G lignin ratio (Figure 2.7). RNA-seq experiments provided an overview of the effects of the various mutation on the global stem transcriptomes. The down-regulation of *F5H* was again apparent in the transcriptome analysis, and was one of the most highly down-regulated genes in *knat3knat7* stems. In addition, a number of secondary cell wall-related transcription factors and biosynthetic genes were only differentially expressed in the *knat3knat7* double mutants. Among the down-regulated cell wall-related genes were *MAP70-5*, which encodes a plant-specific microtubule-associated protein that is important for secondary cell wall patterning (Pesquet *et al.*, 2010; Oda and Fukuda, 2012), *VND-INTERACTING2* (*VIN2)*, which is a transcriptional repressor regulating xylem cell specification (Yamaguchi *et al.*, 2010), and *PECTIN METHYLESTERASE35* (*PME35*), which has been shown to have a pendent stem phenotype and an increased deformation rate of stem in the loss-of-function mutant (Hongo *et al.*, 2012). GO classification analysis clearly showed the cell wall organization process was overrepresented in *knat7* DEGs (Figure 2.12b), which may explain the thicker interfascicular fibers and higher lignin phenotypes in *knat7* mutants. The mRNAseq also highlighted a number of up-regulated genes in the *knat3knat7* plants involved in secondary cell wall biogenesis process, which is consistent with qRT-PCR results. This specific up-regulation in *knat3knat7* may represent a negative feedback mechanism to fine-tune secondary cell wall development. MAPMAN analysis revealed a number of cell wall and secondary metabolism-related genes that were uniquely mis-regulated in the *knat3knat7* mutants (Figure 2.13, 2.14), which may explain their weak stem and heighten *irx* phenotypes.

Liu *et al.* (2014) showed that the expression of *REV* was negatively regulated by KNAT7, resulting in thicker interfascicular fibers in *knat7* mutants. However, the *REV* transcript level was not significantly changed in *knat3knat7* mutants in my RNA-seq analysis, suggesting the thinner interfascicular fiber phenotype of *knat3knat7* may not be caused by REV functions (Table 2.4). Taken together, we found that the *knat3* mutation could enhance *knat7* xylem vessel and S lignin secondary cell wall phenotypes (Figure 2.2,2.7), while concurrently repressing the *knat7* interfascicular fiber phenotype (Figure 2.6). KNAT3 may be a potential activator of xylem vessel secondary cell wall formation, acting together with KNAT7, while it may act antagonistically with KNAT7 for secondary wall formation in interfascicular fiber wall biosynthesis. KNAT3 and KNAT7 appear to work cooperatively to activate S lignin biosynthesis and regulate secondary cell wall composition and integrity.

Table 2.1 Oligonucleotides used in Chapter 2

Gene name	Application	Primer sequence (5' to 3')
KNAT3	genotyping	salk_136464-L: TCTCCTTCAATCATTTCACCG
		salk_136464-R: ACATCTAATCCCCCATCGAAC
		LBb1.3: ATTTTGCCGATTTCGGAAC
KNAT4	genotyping	salk_020216-L: AACTTTAGAAGCCGCTCAAGG
		salk_020216-R: TGACAAGTTCTTGGTTGATTGG
		N759461-L: GATCACCAAAAAGCTGGTACTC
		N759461-R: CATGAAGTGGTCAAGCTCCTTGTC
KNAT5	genotyping	salk_000339-L: CTCTTCTCCGATCCCAAAAAC
		salk_000339-R: AACGTGGTGTTGGAGTTGTTC
KNAT7	genotyping	salk_002098-L: AAGTTTGGGCTTGGGCTTGAC
		salk_002098-R: TTGCCTTGTCATCTTCCTGTTCA
KNAT3	cloning ProKNAT3:GUS	ProKNAT3-L: CAACATTTACGGGGGTTGTTACGT
		ProKNAT3-R: CGCGAACCGCTCTCTTCCGCTATT
KNAT4	cloning ProKNAT4:GUS	ProKNAT4-L: CGCGGTGAACATGAAAAACTCT
		ProKNAT4-R: CGTTTTCGTGTTGAATTTGTTTTTG
KNAT5	cloning ProKNAT5:GUS	ProKNAT5-L: AAACTGGCCTATATGAAGAT
		ProKNAT5-R: TGTTTTCCTGCGTTTTTGGG
KNAT7	cloning ProKNAT7:GUS	ProKNAT7-L: TCTTTTGTAAAAACGGTTTTAA
		ProKNAT7-R: AACCTTGACACAAGACCGGA

Gene name	Application	Primer sequence (5' to 3')
KNAT3	cloning ProKNAT3: KNAT3-GFP	ProKNAT3-L: CAACATTTACGGGGGTTGTTACGT KNAT3-R: CGCGAACCGCTCTCTTCCGCTATT
KNAT7	cloning ProKNAT7: KNAT7-GFP	ProKNAT7-L: TCTTTTGTAAAAACGGTTTTAA KNAT7-R: GTGTTTGCGCTTGGACTTCAA
ACTIN2	qRT-PCR	ACTIN2-L: CCAGAAGGATGCATATGTTGGTGA ACTIN2-R: GAGGAGCCTCGGTAAGAAGA
CESA4	qRT-PCR	CesA4-L: GGATCAGCTCCGATCAATTT CesA4-R: ACCACAAAGGACAATGACGA
CESA7	qRT-PCR	CesA7-L: CAGGCGTACTCACAAATGCT CesA7-R: TGTCAATGCCATCAAACCTT
CESA8	qRT-PCR	CesA8-L: ACGGAGAGTTCTTTGTGGCT CesA8-R: GGTCTGTGTTGGAACAATGG
IRX9	qRT-PCR	IRX9-L: TTTGCGGGACTAAACAACAT IRX9-R: ATCGGAGGCTTTGTCTCTGT
IRX10	qRT-PCR	IRX10-L:AATTGGCCTTATTGGAATCG IRX10-R: TTCGTCCAAACAGACATGG
PAL1	qRT-PCR	PAL1-L: AAGATTGGAGCTTTCGAGGA PAL1-R: TCTGTTCCAAGCTCTTCCCT
PAL2	qRT-PCR	PAL2-L: GAGGCAGCGTTAAGGTTGAG PAL2-R: TTCTCGGTTAGCGATTCACC
C4H	qRT-PCR	C4H-L: ACTGGCTTCAAGTCGGAGAT C4H-R: ACACGACGTTTCTCGTTCTG
4CL1	qRT-PCR	4CL1-L: TCAACCCGGTGAGATTTGTA 4CL1-R: TCGTCATCGATCAATCCAAT

Gene name	Application	Primer sequence (5' to 3')
C3H1	qRT-PCR	C3H1-L: GTTGGACTTGACCGGATCTT C3H1-R: ATTAGAGGCGTTGGAGGATG
HCT	qRT-PCR	HCT-L: GCCTGCACCAAGTATGAAGA HCT-R: GACAGTGTTCCCATCCTCCT
CCoAOMT1	qRT-PCR	CCoAMOMT1-L: CTCAGGGAAGTGACAGCAAA CCoAMOMT1-R: GTGGCGAGAAGAGAGTAGCC
CCR1	qRT-PCR	CCR1-L: GTGCAAAGCAGATCTTCAGG CCR1-R: GCCGCAGCATTAATTACAAA
F5H1	qRT-PCR	F5H-L: CTTCAACGTAGCGGATTTCA F5H-R: AGATCATTACGGGCCTTCAC
COMT1	qRT-PCR	COMT1-L: TTCCATTGCTGCTCTTTGTC COMT1-R: CATGGTGATTGTGGAATGGT
CAD5	qRT-PCR	CAD5-L: TTGGCTGATTCGTTGGATTA CDA5-R: ATCACTTTCCTCCCAAGCAT

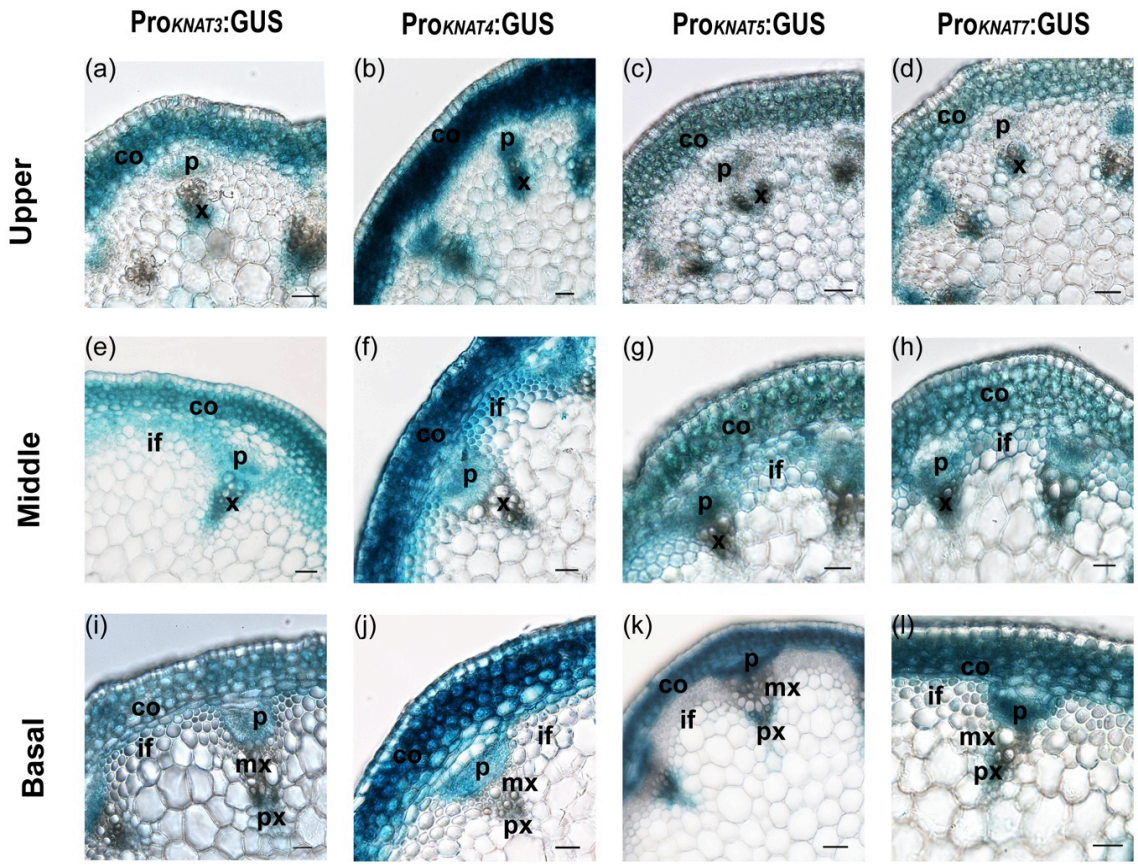

Figure 2.1 The expression patterns of *KNOX2* genes in Arabidopsis stems.

Histochemical localization of *Pro$_{KNAT}$:β-GLUCURONIDASE* (GUS) activity in 8 week-old inflorescence stems of Pro$_{KNAT3}$:GUS (a, e, i), Pro$_{KNAT4}$:GUS (b, f, j), Pro$_{KNAT5}$:GUS (c, g, k), and Pro$_{KNAT7}$:GUS (d, h, l) transgenic plants. Results shown are representative of more than 3 independent lines. (a-d) hand cross-sections from young upper inflorescence stems, and GUS signals were found in the cortex and vascular bundles. (e-h) hand cross-sections from the middle of inflorescence stems, showing GUS expression in cortex, interfascicular fibers and vascular bundles. (i-l) hand cross-sections from basal inflorescence stems. The promoter activities at the basal stems were detected in cortex, phloem and protoxylem, but not in the fiber cells. co, cortex; if, interfascicular fibers; p, phloem; x, xylem. px, protoxylem; mx, metaxylem. Scale bars = 30μm.

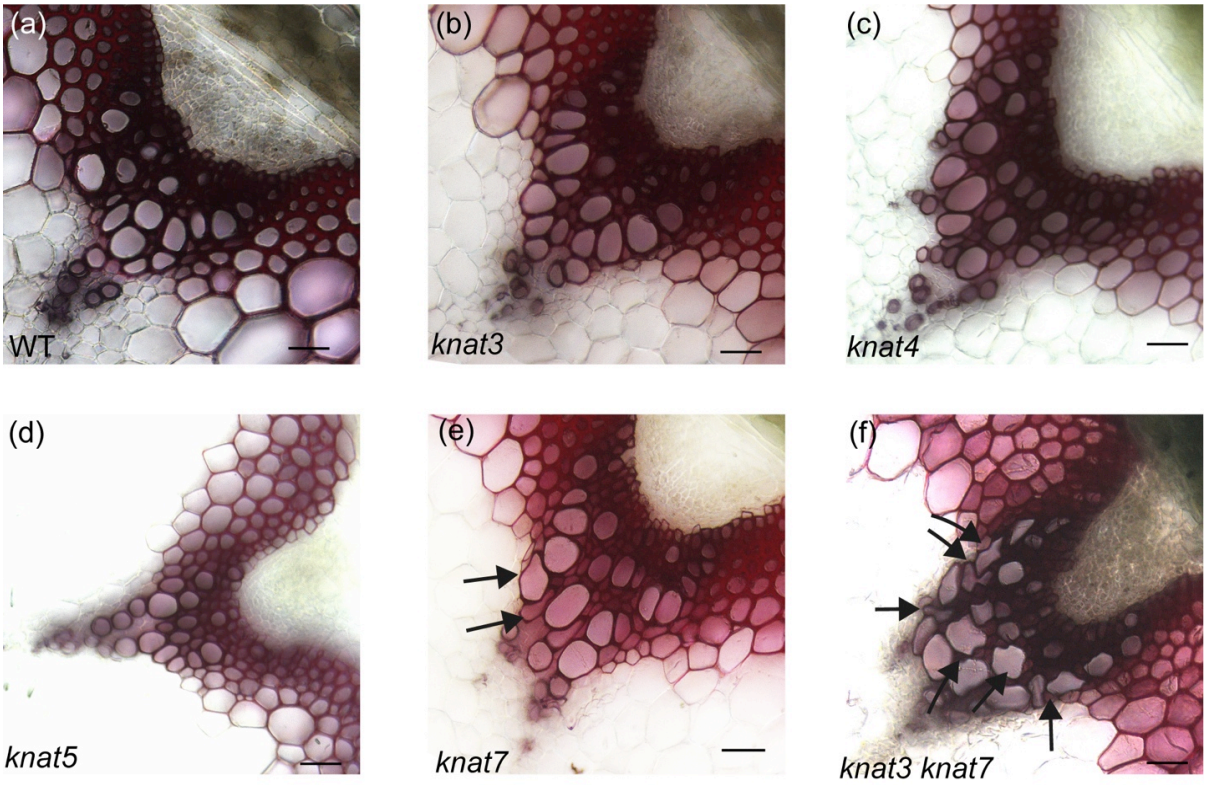

Figure 2.2 Xylem vessel morphology of wild-type (WT) and *KNOX2* mutant plants.

Cross-sections of basal stem vascular bundles stained with phloroglucinol from 8-week-old WT (a), *knat3* (b), *knat4* (c), *knat5* (d), *knat7* (e), and *knat3knat7* (f) plants; Arrows indicate collapsed xylem vessels. Scale bars = 30μm.

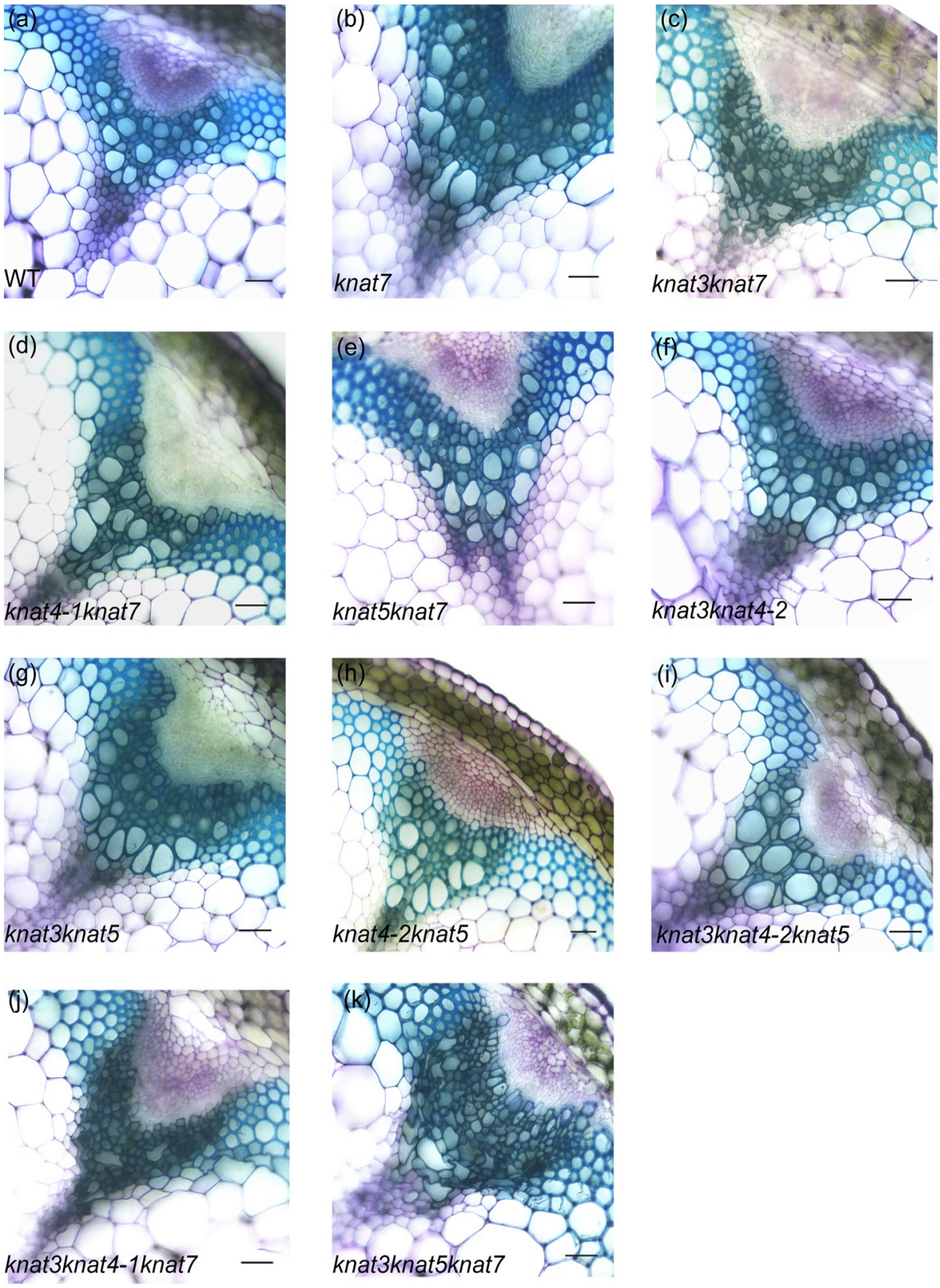
(a)
WT
(b)
knat7
(c)
knat3knat7
(d)
knat4-1knat7
(e)
knat5knat7
(f)
knat3knat4-2
(g)
knat3knat5
(h)
knat4-2knat5
(i)
knat3knat4-2knat5
(j)
knat3knat4-1knat7
(k)
knat3knat5knat7

Figure 2.3 Cross-sections of stem vascular bundles in wild-type (WT) and different combinations of *knox2* mutants.

Stem sections stained with toluidine blue. A single representative vascular bundle is shown from each mutant. (a) WT; (b) *knat7*; (c) *knat3knat7*; (d) *knat4-1knat7*; (e) *knat5knat7*; (f) *knat3knat4-2*; (g) *knat3knat5*; (h) *knat4-2knat5*; (i) *knat3knat4-2knat5*; (j) *knat3knat4-1knat7*; (k) *knat3knat5knat7*. Scale bars = 30μm.

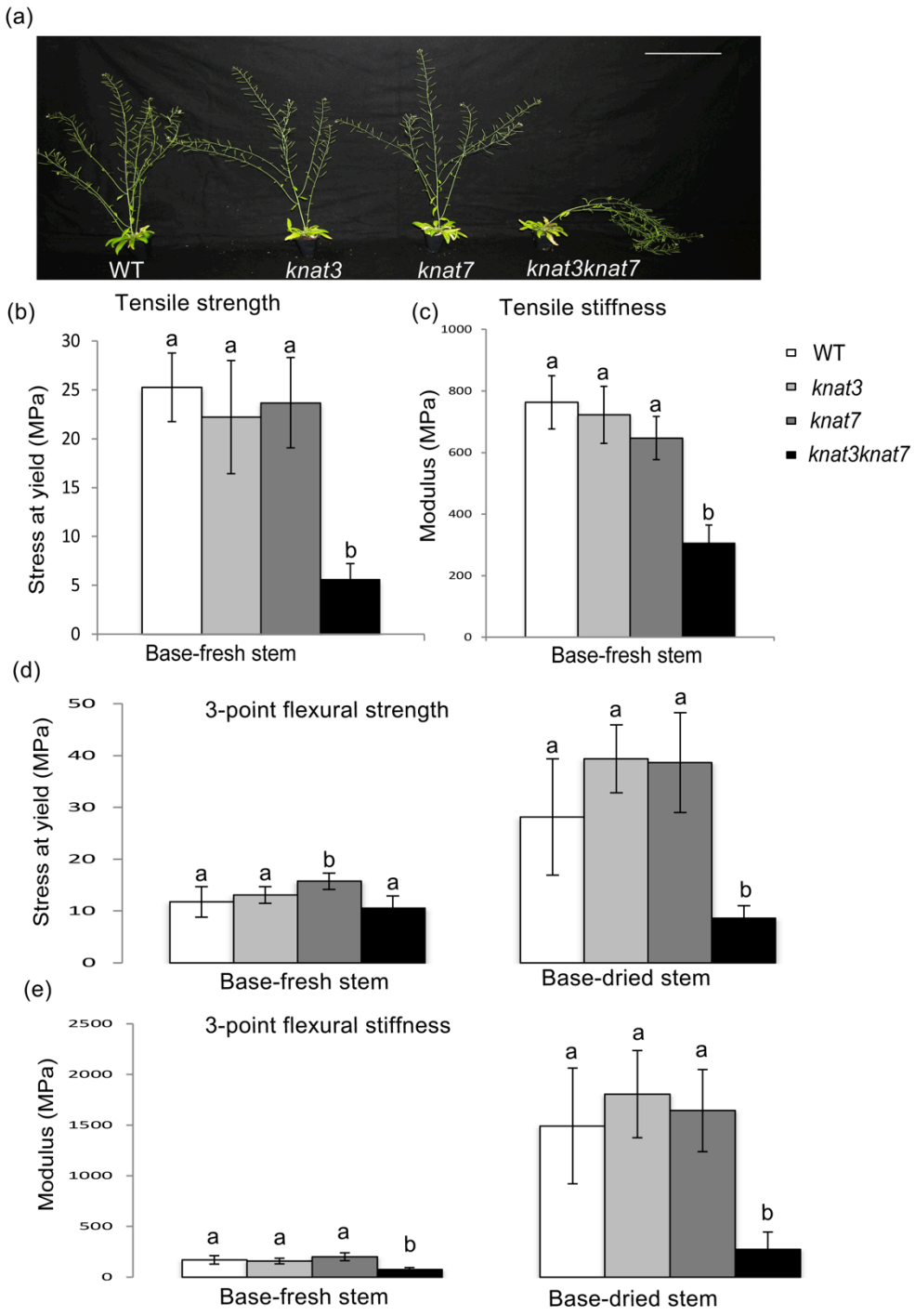

Figure 2.4 Plant morphology and stem biomechanical properties of WT, *knat3*, *knat7* and *knat3knat7*.

Figure 2.4 Plant morphology and stem biomechanical properties of WT, *knat3*, *knat7* and *knat3knat7*.

(a) Fifty-day-old *knat3knat7* plants had a pendant stem phenotype compared with WT, *knat3* and *knat7* single mutants. Bar = 10cm. Tensile strength (b) and tensile stiffness (c) tests show that the bases of fresh stems (0-60mm from the base) of *knat3knat7* had reduced tensile strength and tensile stiffness compared to WT or single mutants. 3-point flexural tests measured the stress at yield (d) and the modulus of elasticity (e) of both fresh and dried stems at 15mm from the base. White bars, WT; light-grey bars, *knat3*; dark-grey bars, *knat7*; black bars, *knat3knat7*. The error bars reperesent means ± SD. Statistical differences among the samples are labeled with different letters (n=5-10; $P<0.05$, one-way ANOVA followed by Turkey's post hoc test).

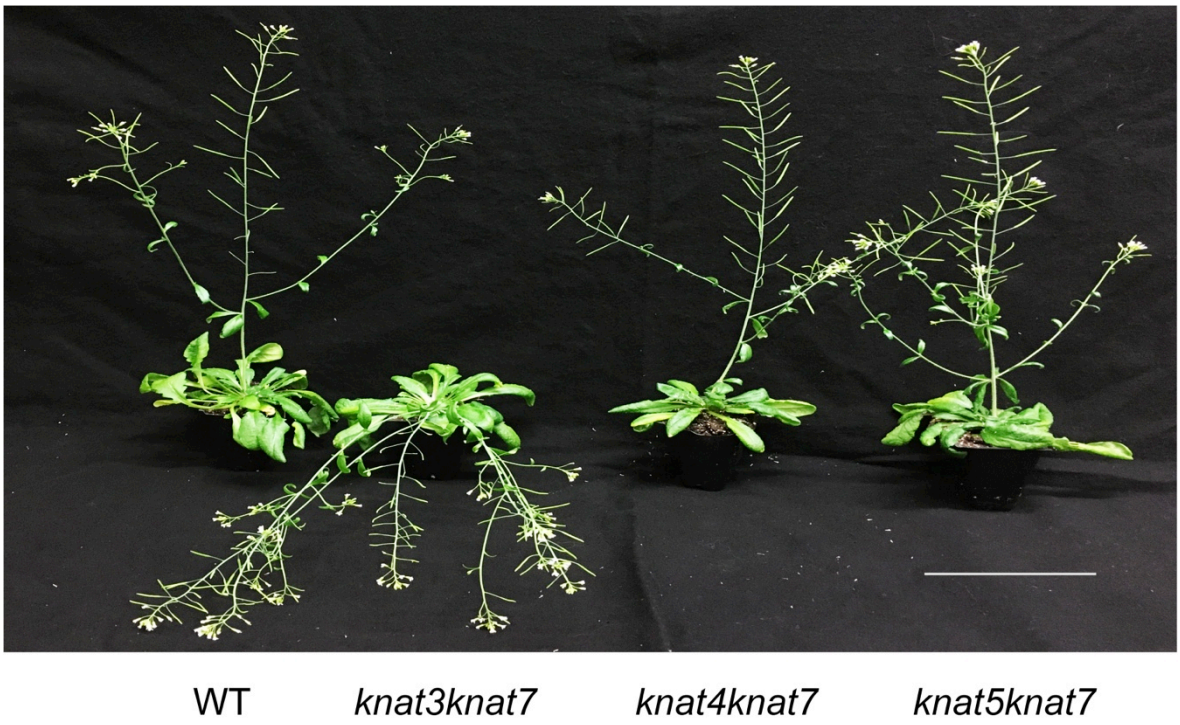

Figure 2.5 Plant morphology of WT, *knat3knat7*, *knat4knat7*, *knat5knat7*.

Forty-day-old plants of *knat3knat7* have a pendent stem phenotype compared with WT, *knat4knat7* and *knat5knat7*. Bar = 10cm.

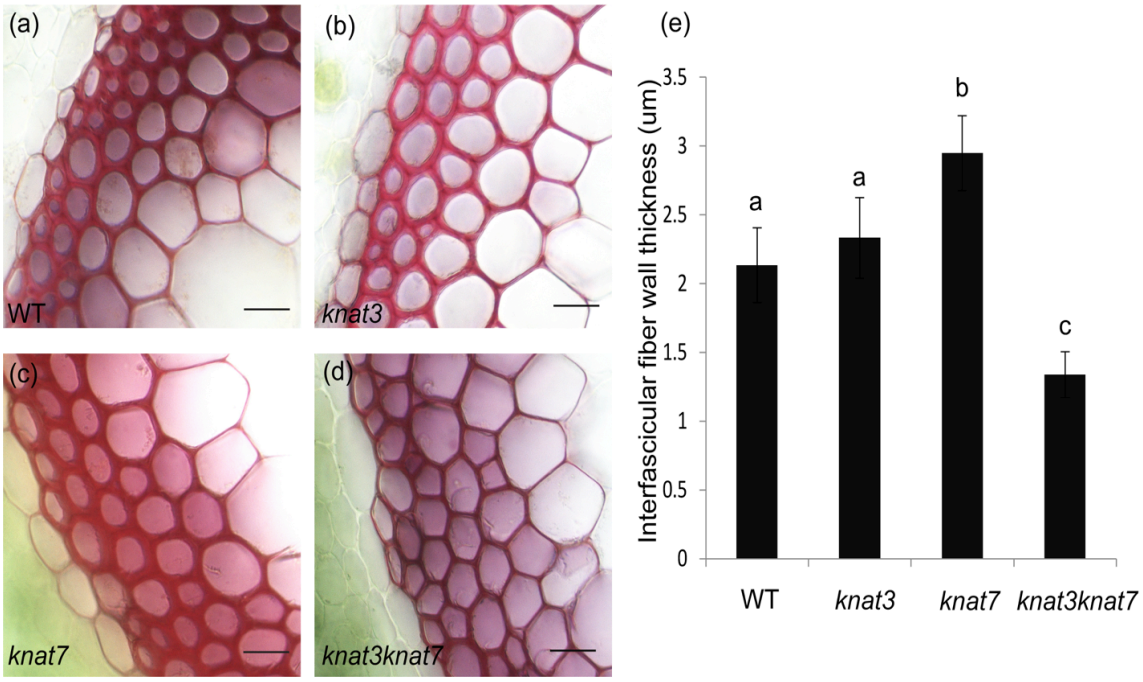

Figure 2.6 Interfascicular fibers of WT, *knat3*, *knat7* and *knat3knat7* inflorescence stems.

Cross-sections from the bases of stems of 8-week-old WT (a), *knat3* (b), *knat7* (c), and *knat3knat7* (d) plants stained with phloroglucinol. Bars = 20μm. (e) Quantification of fiber wall thickness in WT, single and double mutants. *knat7* had a significant increase in interfascicular fiber wall thickness, while the double mutants *knat3knat7* had a dramatic decrease in interfascicular fiber wall thickness. Statistical differences among the samples are labeled with different letters ($P<0.01$, one-way ANOVA followed by Turkey's post hoc test). Error bars = 2 × SD. n= 30-50.

Table 2.2 Cell-wall monosaccharide content of WT, *knat3*, *knat7* and *knat3knat7* stems

Sample	Glucose	Xylose	Mannose	Arabinose	Rhamnose	Galactose
WT	352.4±3.2^{a}	120.6±1.2^{a}	17.9±0.9^{a}	9.6±0.3^{a}	7.2±0.2^{a}	15.8±0.3^{a}
knat3	330.2±7.2^{b}	112.9±2.9^{b}	15.4±0.8^{a}	8.8±0.2^{b}	6.7±0.5^{a}	14.1±0.8^{a}
knat7	324.8±2.9^{b}	121.2±0.9^{a}	11.3±0.7^{b}	9.5±0.2^{ab}	7.2±0.2^{a}	14.1±0.1^{a}
knat3knat7	274.4±2.4^{c}	69.0±2.4^{c}	10.8±0.4^{b}	16.8±0.1^{c}	10.2±0.4^{b}	22.3±0.8^{b}

Cell-wall monosaccharide contents were determined by HPLC following secondary acid hydrolysis and are represented as μg per mg basal stem dry weight (0-11 cm from the base). The *knat3knat7* double mutants had significantly reduced glucose, xylose and mannose, but considerably increased arabinose, rhamnose and galactose contents compared with WT. Data are means ± SD values from three technical replicates for a single experiment, and were able to be repeated by three times with three different biological experiments. Statistical differences among the samples are labeled with different letters ($P<0.01$, one-way ANOVA followed by Turkey's post hoc test).

Table 2.3 Cellulose and lignin contents of WT, *knat3*, *knat7* and *knat3knat7* stem bases

Sample	Cellulose content (mg/100 mg ± SD)	Acid-insoluble lignin (mg/100 mg ± SD)	Acid-soluble lignin (mg/100 mg ± SD)	Total lignin (mg/100 mg ± SD)
WT	27.16±0.26[a]	18.59±0.38	2.3±0.01	20.89±0.38[a]
knat3	27.58±1.07[a]	18.45±0.40	2.22±0.06	20.67±0.35[a]
knat7	26.47±1.20[a]	20.61±0.20	1.86±0.04	22.48±0.23[b]
knat3knat7	21.84±0.65[b]	17.89±0.09	2.89±0.05	20.79±0.06[a]

Cellulose and lignin contents were measured from the bases of inflorescence stems (0-11cm from the base). *knat3knat7* had lower cellulose content and acid-insoluble lignin, but more acid-soluble lignin compared with wild-type plants. No change in total lignin was detected in double mutant stems. Statistical differences among the samples are labeled with different letters ($P<0.01$, one-way ANOVA followed by Turkey's post hoc test). Values are means ± SD for three technical replicates. The data was repeated by three times with three different biological experiments.

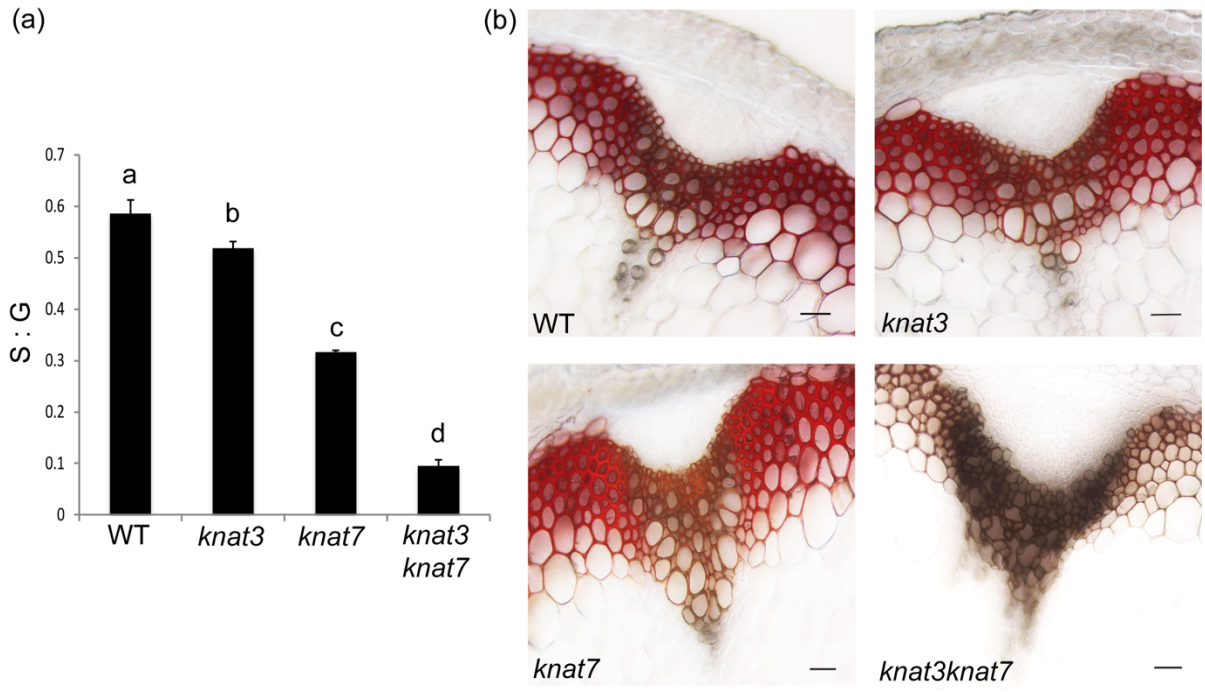

Figure 2.7 Lignin composition of WT, *knat3*, *knat7* and *knat3knat7* stem cell walls.

(a) Syringyl to guaiacyl (S/G) lignin monomer ratio of dried stem bases (0-11cm from the base), as determined by thioacidolysis and histochemical staining with Mäules reagent. *knat3knat7* stem had significantly lower S/G lignin ratio. Error bars represent the standard deviations; Statistical differences among the samples are labeled with different letters ($P<0.01$, one-way ANOVA followed by Turkey's post hoc test). n = 3.

(b) Mäule stain produces red colour in syringyl lignin-rich cell walls. Cross-sections from the bases of stems of 8-week-old WT, *knat3*, *knat7*, and *knat3knat7* plants. The double mutant *knat3knat7* had less S lignin deposition. Scale bars = 30 μm.

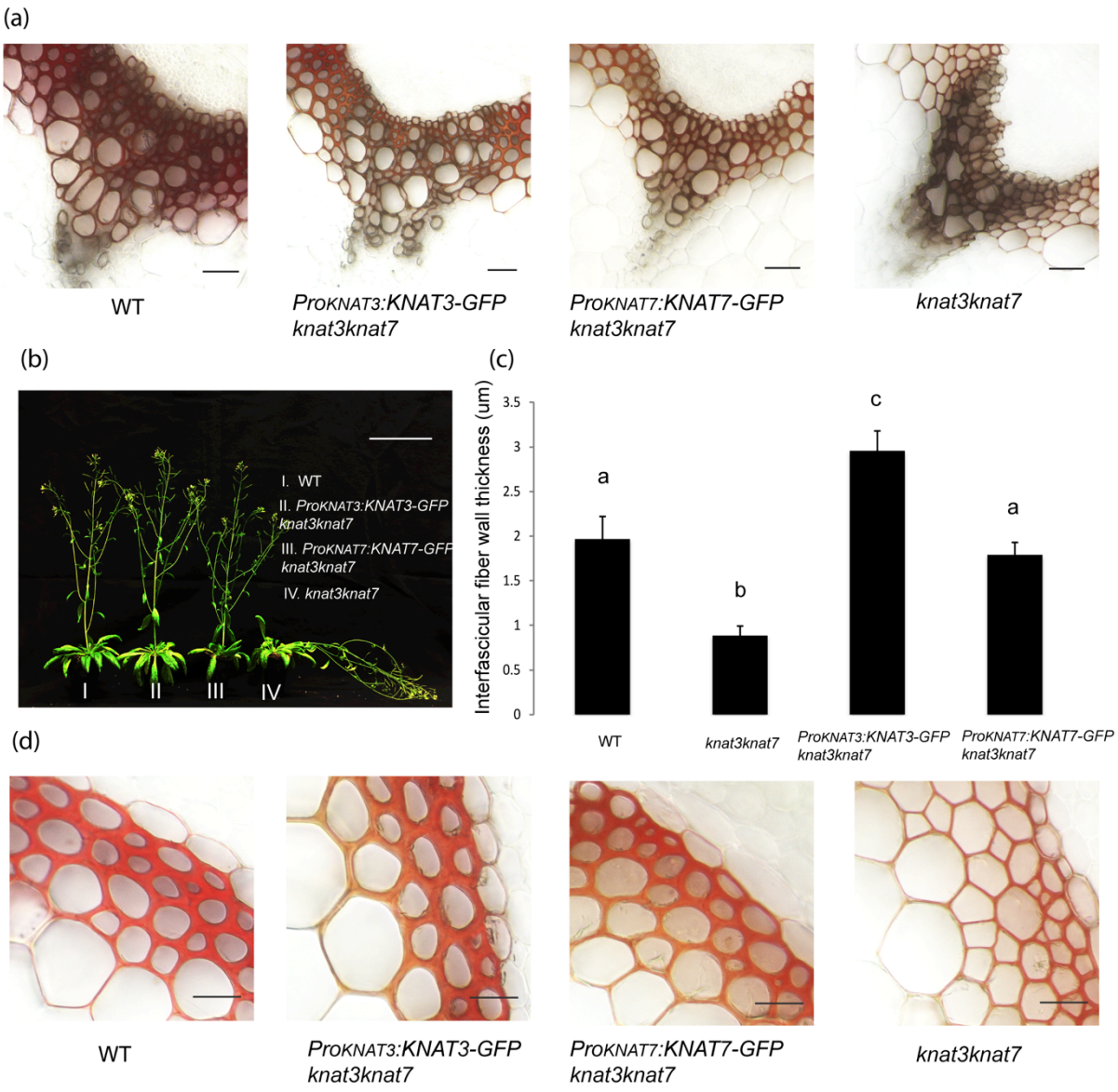

Figure 2.8 Complementation of *knat3knat7* phenotypes with *Pro$_{KNAT3}$:KNAT3-GFP* and *Pro$_{KNAT7}$:KNAT7-GFP*.

(a) Xylem vessel morphology of WT, *knat3knat7* and complemented lines. Cross-sections of basal stem vascular bundles with Mäule staining from 8-week-old plants show that the *irx* phenotype of *knat3knat7* was complemented. Scale bars = 30μm.

Figure 2.8 Complementation of *knat3knat7* phenotypes with Pro_{KNAT3}:*KNAT3-GFP* and Pro_{KNAT7}:*KNAT7-GFP*.

(b) Fifty-day-old plants showing the pendent phenotype of *knat3knat7* was complemented in both transformants. Bar = 10cm.
(c) and (d) showing the interfascicular fibers in WT, *knat3knat7* and complementation lines. The reduced wall thickness in *knat3knat7* was restored to an increased level relative to the wild-type by expressing *KNAT3* under the control of its native promoter at *knat3knat7* background, while the thickness was fully recovered to wild-type by expressing *KNAT7* back to *knat3knat7* mutants. Error bars represent the standard deviations. Statistical differences among the samples are labeled with different letters ($P<0.01$, one-way ANOVA followed by Turkey's post hoc test). Scale bars = 20μm. n= 30-50.

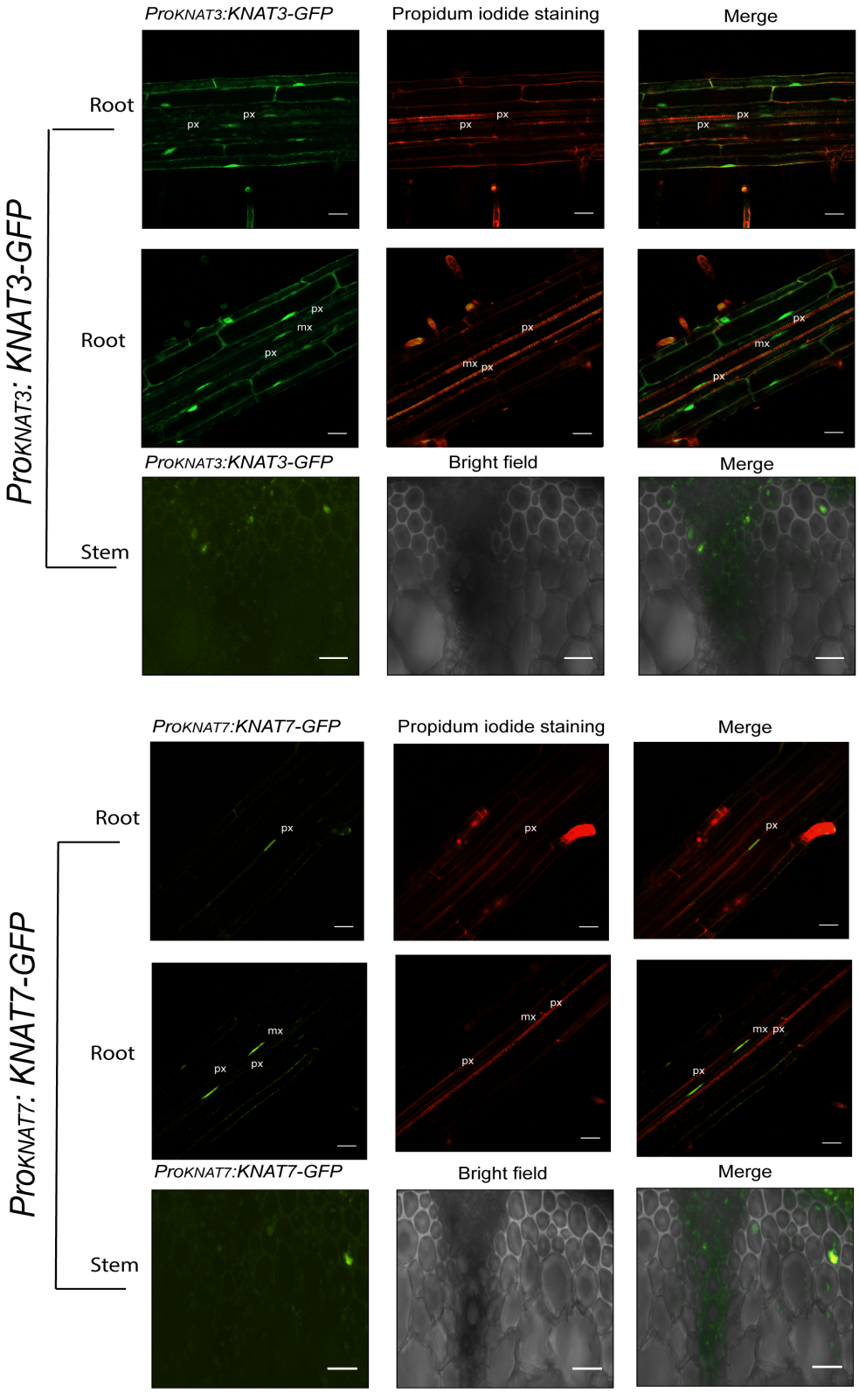
ProKNAT3: KNAT3-GFP
ProKNAT3:KNAT3-GFP
Propidum iodide staining
Merge
Root
Root
ProKNAT3:KNAT3-GFP
Bright field
Merge
Stem
ProKNAT7: KNAT7-GFP
ProKNAT7:KNAT7-GFP
Propidum iodide staining
Merge
Root
Root
ProKNAT7:KNAT7-GFP
Bright field
Merge
Stem
px
mx

Figure 2.9 Expression patterns of *KNAT3* and *KNAT7* in the root and stem.

Expression of Pro_{KNAT3}*:KNAT3-GFP* and Pro_{KNAT7}*:KNAT7-GFP* were detected in the protoxylem and metaxylem, and in the interfascicular fiber cells in 6-week-old inflorescence stems. Confocal laser scanning microscopy images of roots counterstained with propidium iodile. px, protoxylem; mx, metaxylem. Scale bars = 30μm.

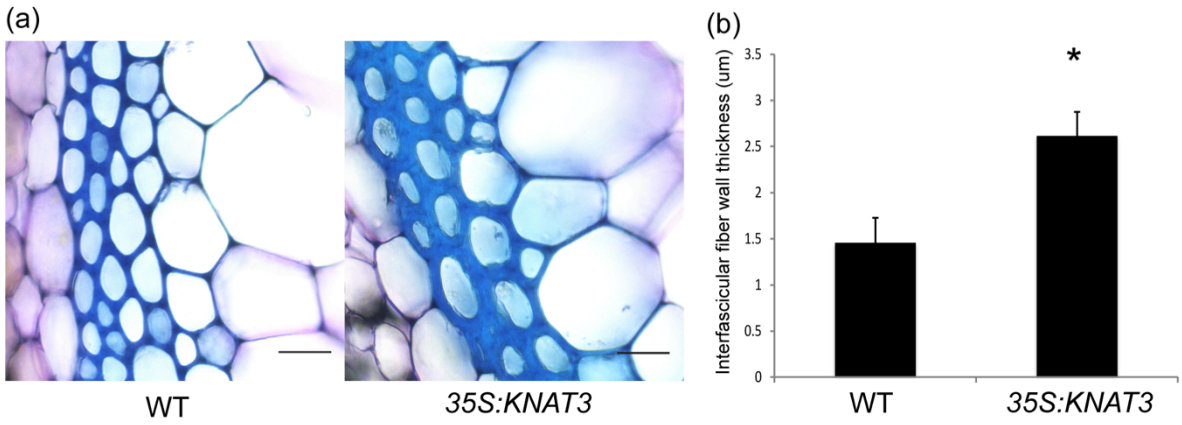

Figure 2.10 Interfascicular fibers have thicker secondary cell walls in *35S:KNAT3* basal stems.

(a) Cross-sections of the bases of 8-week-old inflorescence stems of WT and *35S:KNAT3* plants stained with Toluidine Blue. Bars = 20μm.
(b) Quantification of interfascicular fiber wall thickness in WT and *KNAT3* overexpression lines. The results shown are representative of two independent overexpression lines. Compared to wild-type, the overexpression lines appeared to have thicker secondary cell walls of interfascicular fibers. Asterisk (*) indicates the sample is significantly different from WT at $P < 0.01$ determined by Student's T-test. Error bars represent the standard deviations. n= 30-50.

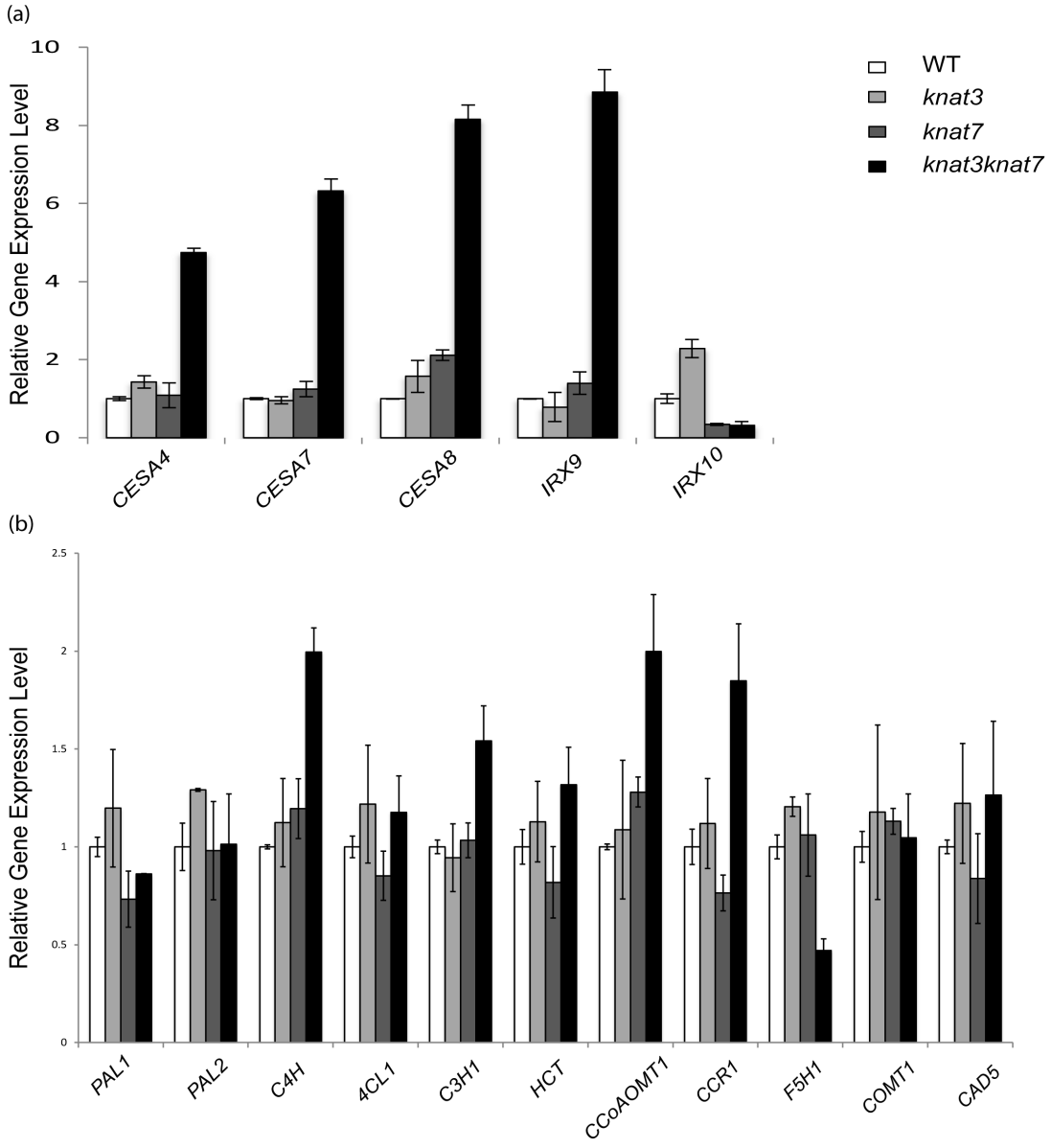

Figure 2.11 Expression of secondary cell wall-related genes in lower stems of WT, *knat3*, *knat7* and *knat3knat7* double mutants.

RNA was extracted from the basal segment of inflorescence stems (0-11cm) of 8-week-old WT, *knat3*, *knat7* and *knat3knat7* plants for qRT-PCR analysis. Error bars represent the standard deviations of three biological replicates.

Figure 2.11 Expression of secondary cell wall-related genes in lower stems of WT, *knat3*, *knat7* and *knat3knat7* double mutants.

(a) Expression of *CELLULOSE SYNTHASE* (*CESA*) genes (*CESA4*, *CESA7*, *CESA8*) and hemicellulose (*IRREGULAR XYLEM 9*, *IRX9*; *IRX10*) biosynthetic genes. *CESA4*, *CESA7*, *CESA8,* and *IRX9* were dramatically up-regulated in *knat3knat7* double mutants, while *IRX10* was significantly down-regulated compared with WT as determined by Student's T-test ($P<0.01$).

(b) Expression of lignin biosynthetic genes. *PHENYLALANINE AMMONIA LYASE 1* (*PAL1*), *PAL2*; *CINNAMATE-4-HYDROXYLASE* (*C4H*); *4-COUMARATE-COA LIGASE 1* (*4CL1*); *COUMARATE 3-HYDROXYLASE 1* (*C3H1*); *HYDROXYCINNAMOYL-COA:SHIKIMATE HYDROXYCINNAMOYL TRANSFERASE* (*HCT*); *CAEEROYL-COA 3-O-METHYLTRANSFERASE 1* (*CCoAOMT1*); *CINNAMOYL-COA REDUCTASE 1* (*CCR1*); *FERULATE-5-HYDROXYLASE* (*F5H*); *CAFFEIC ACID O-METHYLTRANSFERASE 1* (*COMT1*); *CINNAMYL ALCOHOL REDUCTASE 5* (*CAD5*). *C4H*, *C3H1*, *CCoAMT1,* and *CCR1*, were elevated 1.5- to 2-fold in the basal segments of *knat3knat7* inflorescence stems, but the transcript abundance of *F5H*, a key enzyme for S lignin biosynthesis, was considerably decreased in *knat3knat7* mutants compared with WT at $P<0.01$ as determined by Student's T-test.

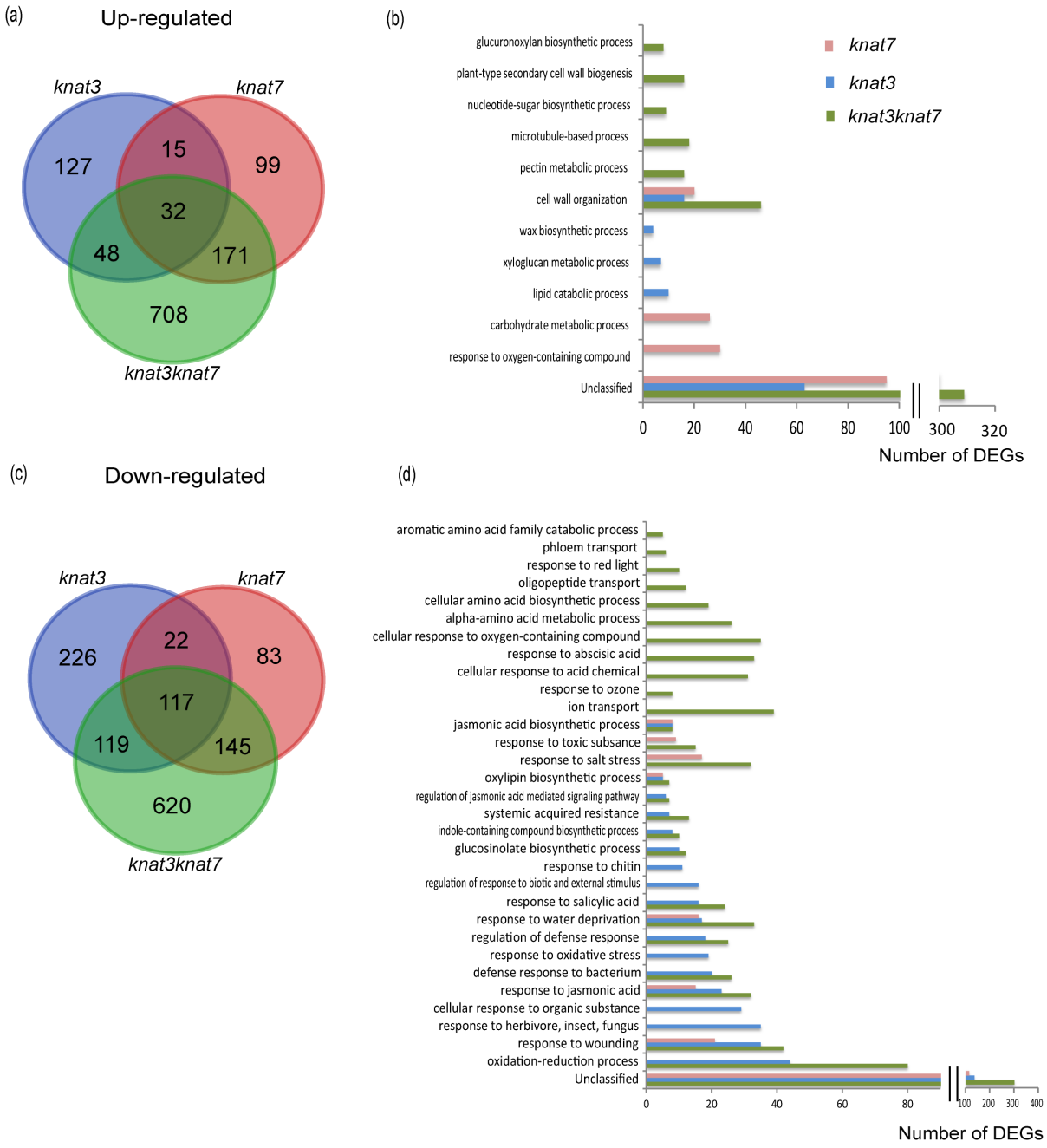

Figure 2.12 Venn diagram and GO term enrichment analysis of differentially expressed genes (DEGs) of *knat3* versus WT, *knat7* versus WT, and *knat3knat7* versus WT.

Figure 2.12 Venn diagram and GO term enrichment analysis of differentially expressed genes (DEGs) of *knat3* versus WT, *knat7* versus WT, and *knat3knat7* versus WT.

(a and b) Venn diagram (a) and GO biological processes (b) of genes with increased expression in *knat3* versus WT, *knat7* versus WT and *knat3knat7* versus WT.
(c and d) Venn diagram (c) and GO biological processes (b) of genes with decreased expression in *knat3* versus WT, *knat7* versus WT and *knat3knat7* versus WT
Go terms were identified using PANTHER (https://www.arabidopsis.org/tools/go_term_enrichment.jsp) with default significant level ($P<0.05$).

WT vs *knat3knat7*

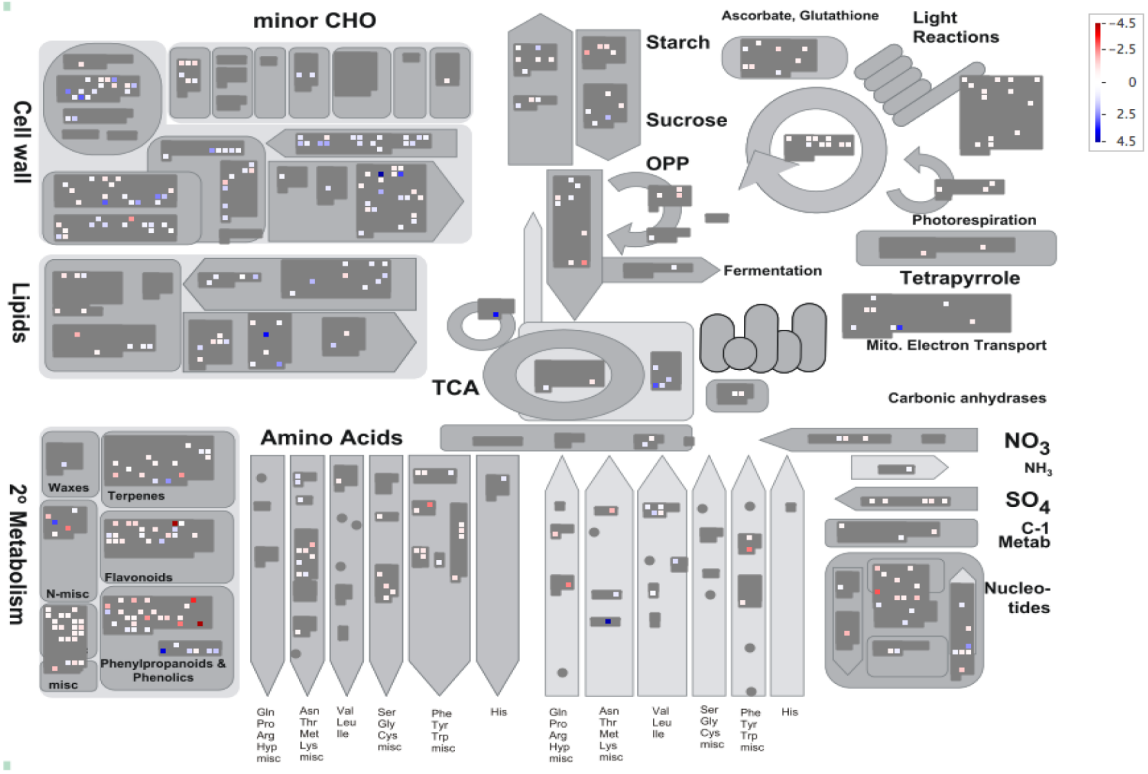

Figure 2.13 MAPMAN schematic providing a metabolic overview of the differential gene expression between WT and *knat3knat7* stems.

The different colors represent the $\log_2$ (FC) values of the gene expression levels in *knat3knat7* versus wild-type stems: red, down-regulation; white, no change; blue, up-regulation.

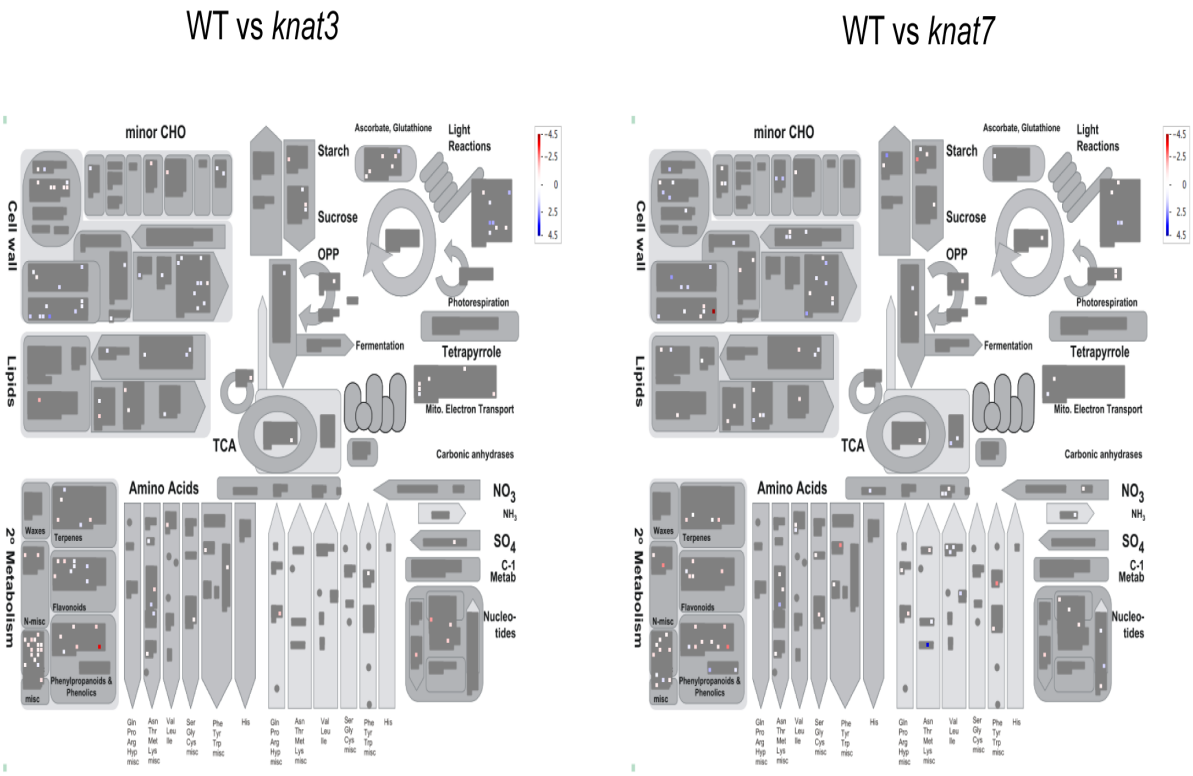

Figure 2.14 MAPMAN schematic providing a metabolic overview of the differential gene expression levels in *knat3* and *knat7* stems compared with WT.

The different colors represent the $\log_2$ (FC) values of the gene expression levels in *knat3* and *knat7* versus wild-type stems: red, down-regulation; white, no change; blue, up-regulation.

Table 2.4 Expression changes of secondary cell wall-related genes in *knat3knat7* stems

Gene Name	Gene ID	*knat3knat7* VS WT RNA-seq FPKM log2(fold_change)	RNA-seq Sig.	*knat3knat7* VS WT qRT-PCR log2(fold_change)
CESA4	AT5G44030	0.13	no	2.25
CESA7	AT5G17420	1.39	yes	2.66
CESA8	AT4G18780	1.51	yes	3.03
IRX9	AG2G37090	2.32	yes	3.15
IRX10	AT1G27440	-2.93	yes	-1.65
REV	AT5G60690	0.56	no	0.66
PAL1	AT2G37040	-0.76	yes	-0.21
PAL2	AT3G53260	-0.56	yes	0.02
C4H	AT2G30490	-0.04	no	1.00
4CL1	AT1G51680	-0.84	yes	0.23
C3H1	AT2G40890	0.12	no	0.62
HCT	AT5G48930	-0.44	no	0.40
CCoAOMT	AT4G34050	0.61	yes	1.00
CCR1	AT1G15950	0.00	no	0.89
F5H1	AT4G36220	-2.65	yes	-1.09
COMT1	AT5G54160	0.15	no	0.21
CAD5	AT4G34230	0.19	no	0.34

RNA-seq experiments were carried out using the top 1-15cm of inflorescence stems of *knat3knat7*. qRT-PCR analysis was done using the basal stems of *knat3knat7* double mutants. FPKM (fragments per kilobase of exon per million fragments mapped) was used to estimate the abundance of gene transcripts. The significance (Signi.) for RNA-Seq was determined by the q value ($q<0.01$).

Chapter 3: Ovate Family Proteins are associated with Brassinosteroid homeostasis and function in cotyledon development by interacting with Nucleosome Assembly Protein 1 in Arabidopsis

3.1 Introduction

The ovate family of transcription factors is named after a tomato *ovate* mutant that has elongated fruit (Liu et al., 2002). In Arabidopsis, Ovate Family Proteins (OFP) interact with a number of TALE homeodomain proteins and regulate their subcellular localization in plant cells to control plant development (Hackbusch *et al.*, 2005). More specifically, nine ovate family proteins were found to be involved in the interaction network of TALE proteins and OFP1 could change the nucleus localization of KNAT1 or BLH1 to the cytoplasm by protein-protein interactions (Hackbusch *et al.*, 2005). OFPs were defined by their conserved C-terminal 60-70 amino acid ovate domain, and they are only found in land plants so far (Hackbusch *et al.*, 2005; Wang *et al.*, 2007, 2011, 2016; Liu *et al.*, 2014).

In Arabidopsis, there are 19 OFP genes, which were classified into 3 clades and 8 sub-groups according to the phylogenetic analysis (Liu *et al.*, 2014). Among them, *OFP1*, *OFP2*, *OFP3*, *OFP4* and *OFP5* are close homologs. OFP1 has been reported to have multiple functions in plants, such as inhibiting cell elongation through repressing *GA20ox* (Wang *et al.*, 2007), facilitating DNA repair by interacting with the Ku protein (Wang *et al.*, 2010) and forming a complex with BLH3 to regulate the flowering time (Zhang *et al.*, 2016). OFP1 and OFP4 were also shown to interact with KNAT7, negatively regulating secondary cell wall formation, and *ofp4* mutants phenocopied *knat7*, with *irx* and increased fiber cell wall thickness (Li *et al.*, 2011; Liu and Douglas, 2015). OFP5 was found to regulate the embryo development, by interacting with KNAT3 and BLH1 (Pagnussat *et al.*, 2007). The previous chapter has demonstrated the roles of *KNAT3* and *KNAT7* in secondary cell wall development, and the goal of this chapter was to test if the uncharacterized OFP family

members, *OFP5* and its homologs*, OFP2* and *OFP3,* also play a role in secondary wall formation.

In this study, I took the reverse genetics approach to identify the secondary cell wall phenotypes in *ofp* single mutants. However, all of the *ofp* single mutants did not show any distinguishable phenotype from wild type, even for the *ofp4*, which was previously described as a secondary cell wall mutant (Li *et al.*, 2011). Instead, I confirmed OFP overexpression phenotypes with kidney-shaped cotyledons (Wang *et al.*, 2011). I also found the hypocotyls of *OFP1*, *OFP2*, *OFP4* and *OFP5* overexpression plants had cell swelling, disordered microtubules, and dark-grown de-etiolated phenotypes, resembling brassinosteroid (BR) deficient mutants. Exogenous BR treatment partially rescued the hypocotyl phenotypes of *OFP* overexpressing plants, which provided new insights into OFP functions in maintaining BR homeostasis in Arabidopsis.

To identify novel OFP4 interaction partners, I used yeast two-hybrid and bimolecular fluorescence complementation assays to identify Nucleosome Assembly Protein 1 (NAP1) family proteins. NAP1;1 and NAP1;2, were shown to interact with OFP4 *in vitro* and *in vivo*. Both YFP-NAP1;1 and YFP-NAP1;2 fusion proteins were localized abundantly in the cytoplasm, associated with the ER. By phenotypic analysis of higher-order loss-of-function mutants, I found that *nap1;1nap1;2nap1;3* triple mutant; the *ofp4nap1;1nap1;2nap1;3* quadruple mutant; and the *ofp1ofp2ofp3ofp4ofp5* quintuple mutant exhibited similar phenotypes, with altered cotyledon shapes and reduced cotyledon width/length ratio. In addition, the kidney-shaped cotyledon phenotype of *OFP4* overexpressing plants was suppressed in the *nap1;1nap1;2nap1;3* triple mutant background, suggesting OFP4 functions in cotyledon development at least partially depend on NAP1 proteins. All together, these data indicate that the complex of OFP and NAP1 plays a significant role in the cotyledon development in Arabidopsis seedlings.

3.2 Materials and methods

3.2.1 Plant materials and growth condition

Arabidopsis thaliana ecotype Columbia was used as wild type in all experiments, and all the transgenic lines and mutants are also in the Columbia background. T-DNA insertion lines for *ofp2* (SALK_122550), *ofp3* (GABI_167F01) and *ofp5* (SALK_203823) were obtained from the Arabidopsis Biological Resource Center (ABRC). The *ofp1* (SM_3_21689)*, ofp4* (SALK_022396) described in (Wang *et al.*, 2007; Li *et al.*, 2011) were used for *ofp1, ofp4* phenotypic analyses. Homozygous T-DNA insertion lines were screened by PCR using gene-specific primers (Table 3.1). The *nap1;1* (SALK_013610), *nap1;2* (SAIL_84_B01), *nap1;3* (SALK_131746) and *nap1;1nap1;2nap1;3* were kindly obtained from Dr. Aiwu Dong's group (Liu *et al.*, 2009) and the homozygous transgenic plants *pUBQ1: mRFP-TUB6* were kindly obtained from Dr. Chris Ambrose (2011). Quadruple and quintuple mutants of *ofp4nap1;1nap1;2nap1;3* and *ofp1ofp2ofp3ofp4ofp5* were generated by genetic crossing, and the genotypes confirmed with PCR.

In all experiments, Arabidopsis seeds were sterilized with 70% ethanol and sown on half Murashige and Skoog (MS) medium with 1% sucrose, then cold-treated at 4°C for 48 hours in the dark. For normal growth conditions, after cold treatment, seeds were grown at 20°C under a 16/8 h (light/dark) photoperiod at about 120 μmol m^{-2} s^{-1} light for 7 to 10 days. For dark growth conditions, plates were wrapped with aluminum foil and placed vertically in the growth chamber for 7 days. For whole plant growth, seedlings were transferred to soil and grown under long-day conditions (16/8 h light/dark cycle) at ~100 μmol m^{-2} s^{-1} light, 20°C in growth chambers for further analysis.

3.2.2 RNA isolation and quantitative RT-PCR

Total RNA was extracted from tissues using Qiagen RNeasy columns following the manufacturer's instructions, and treated with DNase I (Qiagen). 2 μg RNA was transcribed into cDNA using the Omniscript RT kit (Qiagen) according to the manufacturer's

instructions. For qRT-PCR of the basal stem segments, PCR amplification was performed using a CFX Connect™ real-time system (Bio-Rad), using 40 quantitative PCR cycles that were run under the following parameters: denaturation step, 95°C for 20 sec; annealing step, 55°C for 30 sec; elongation step, 72°C for 1 min. *ACTIN2* was used as the reference housekeeping gene. All primers are listed in Table 3.1. The calculation of differences in gene expression was used as described by Bhargava *et al.* (2010). Three biological replicates were performed and each measurement consisted of three technical replicates.

3.2.3 Cloning and plant transformation

To generate the overexpression constructs, the full-length open-reading frames of *OFP1*, *OFP2*, *OFP3*, *OFP4*, *OFP5*, *NAP1;1*, and *NAP1;2* were amplified by PCR from the cDNA of Col-0 ecotype prepared as previously described, and sub-cloned into the pCR8/GW/TOPO entry vectors, respectively. After verifying the nucleotide sequences of the amplified fragments, they were cloned into the binary vector pEarlyGate 101, pEarlyGate 104 and PMDC43 for generating the *35S: OFP1-YFP*, *35S: OFP2-YFP*, *35S: OFP3-YFP*, *35S: OFP4-YFP*, *35S: OFP5-YFP*, *35S: YFP-NAP1;1*, *35S: YFP-NAP1;2* and *2 x 35S: GFP-OFP4* constructs, respectively. For generating BiFC constructs, the clone of *OFP4* was transferred to the Gateway destination vector pSAT4-DEST-nYFP-C1 and *NAP1;1/NAP1;2* were cloned into pSAT5-DEST-cYFP-C1 (Citovsky *et al.*, 2006), to generate OFP4 fusions to the N-terminal half of YFP, and NAP1;1/NAP1;2 fusions to the C-terminal half of YFP. To generate Pro_{OFP2}*:OFP2-GUS*, Pro_{OFP3}*: GUS*, and Pro_{OFP5}*: GUS* constructs, the full genome sequence including the promoter region of *OFP2* (2462bp), or only the promoter region of *OFP3* (2143bp), and *OFP5* (2156bp) were cloned into the binary vector PMDC163. Gene-specific oligonucleotides used for cloning and construct generation are shown in Table 3.1.

All the binary constructs were introduced into *Agrobacterium tumefaciens* strain GV3101 for plant transformation. The wild-type Columbia was transformed for expression pattern and overexpression analysis. The *2 x 35S: GFP-OFP4* construct was transformed to Col-0 and

nap1;1nap1;2nap1;3 mutants. The *35S:OFP-YFP* constructs were also transformed to *pUBQ1: mRFP-TUB6* for microtubule analysis. The floral dip method (Clough and Bent, 1998) was used for generating transgenic plants. T1 plants for *35S:OFP-YFP* were selected with Basta resistance while the other transformants were selected with hygromycin resistance.

3.2.4 GUS expression assay

The GUS activity was assayed using 10-day-old seedlings, which were incubated with 90% acetone by vacuum infiltration, then moved to an ice bath for 30 min, followed by washing with 0.1M sodium phosphate buffer three times and incubating tissues in a solution containing 0.1M sodium phosphate buffer (PH 7.0), 1mM substrate 5-bromo-4-chloro-3-indolyl-β-D-glucuronide (X-Gluc), 0.5mM potassium ferricyanide and 0.01%(v/v) Triton X-100 at 37°C for 1 h to overnight. The resulting stained tissues were fixed with FAA (50 [v/v] ethanol, 5% [v/v] acetic acid and 10% [v/v] formaldehyde), and observed with an Olympus AX70 light microscope.

3.2.5 Transient expression in *N. benthamiana* and BiFC assay

To determine the subcellular localization, the leaves of 4-week-old *Nicotiana benthamiana* plants were agroinfiltrated with *OFP* and *NAP1* overexpression constructs respectively using a syringe (1mL) without needle, and then the infiltrated tobacco plants were placed in the growth chamber for 72 to 96 h. For co-expression and BiFC assays, the Agrobacterium cultures with different expression constructs were mixed in the infiltration medium to a final OD_{600} of 0.05, and the infiltration in tobacco leaves was carried out as described previously (Velasquez *et al.*, 2011).

3.2.6 Light and confocal microscopy

For observing secondary cell wall phenotypes, the base of freshly harvested 8-week-old inflorescence stems were hand-sectioned, stained with aqueous 0.05% toluidine blue O for 1-

2 min, mounted with water and viewed using an Olympus AX70 light microscope. To observe the cotyledon vascular pattern, one-week-old seedlings were cleared with 90% acetone, washed with phosphate buffer and mounted with chloral hydrate solution. All the cotyledon phenotypes were viewed using the dissecting microscope (Zeiss), and the one-week-old hypocotyls grown in the dark were viewed using the Olympus AX70 light microscope. Image J was used to measure the dark-grown hypocotyl length, and the cotyledon width and length. Statistical analysis was performed by one-way ANOVA followed by Tukey's post hoc test and Student's T-test.

YFP-fusion, GFP-fusion and mRFP-marker proteins were observed on a Perkin-Elmer UltraView VoX spinning disk confocal mounted on a Leica DMI6000 inverted microscope with a Hamamatsu 9100-02 CCD camera. The microscope used for all live-cell imaging was fit with the following excitation filters: YFP (514nm), GFP (488nm), and RFP (561nm). Image J software was used for image processing.

3.2.7 BR treatment

To test the responses of *OFP OX* seedlings to exogenous BR, plants were germinated and grown on one-half-strength MS medium with different concentrations of epibrassinolide (epiBL, Sigma). 2 mg epiBL was dissolved in 1ml 80% EtOH as a stock. And the plates were placed vertically in the growth chamber equipped with light for one week before photographing. Image J software was used for hypocotyl length measurements. Statistical analysis was performed by Student's T-test and one-way ANOVA followed by Tukey's post hoc test.

3.2.8 Yeast two-hybrid assays

The yeast two-hybrid screen was performed using the DUALhybrid Kit (Dualsystems Biotech) following the manufacturer's instructions. The full-length of *OFP4* cDNA was cloned into pLexA-N vector as the bait and the prey used an Arabidopsis cDNA library in the

pGAD-HA vector obtained from the Dualsystems Biotech. The yeast NMY51 strains were co-transformed with DBD-OFP4 and the empty cDNA library, and spread on selection media lacking Trptophan (Trp), Leucine (Leu), and Histidine (His) and supplemented with different concentrations of 3-Amino-1,2,4-triazole (3-AT) (SD/-Trp/-Leu/-His/3-AT), to determine the conditions of the screen according to the self-activation level of the bait. Then the cDNA library (Dualsystems Biotech) was transformed into NMY51 expressing the DBD-OFP4 bait and interactors were selected on plates that contained the concentration of 3-AT determined in the pilot screen. Plasmids from cells growing under selection and expressing both the reporter genes were isolated and all positive interactors were confirmed by the bait-dependency test.

To confirm the interactions, the ProQuest yeast two-hybrid system (Invitrogen) was performed as described previously (Guo *et al.*, 2009). OFP4 was cloned into the pDEST32 as a bait vector and NAP1;1/NAP1;2 were cloned into pDEST22 as the prey vector. The positive control used the known interactors MYB75 and TT8 (Zimmermann *et al.*, 2004) and the negative control was the interaction between OFP4 and the empty prey vector. Positive interaction was determined by the yeast growth on the triple selective SD medium lacking leucine, tryptophan and histidine but supplemented with 40mM 3-AT, or the selective SD medium lacking leucine, tryptophan and uracil.

3.3 Results

3.3.1 *OFP* loss-of-function mutants have no secondary cell wall defects

OFP1, *OFP2*, *OFP3*, *OFP4*, and *OFP5* are close homologs in the same class in Arabidopsis. To investigate the potential roles of *OFP2*, *OFP3* and *OFP5* in regulating secondary cell wall formation, and to confirm the secondary cell wall functions of *OFP1* and *OFP4*, the T-DNA insertion alleles of *ofp2* (salk_122550), *ofp3* (GABI_167F01) and *ofp5* (salk_203823) were obtained from the Arabidopsis Biological Resources Centre (ABRC) and the null alleles of *ofp1* and *ofp4* were obtained from Liu and Douglas (2015). PCR-based genotyping

was carried out to identify homozygous mutants and loss-of-function mutant alleles were confirmed by RT-PCR. Stem cross-sections were examined at the bases of mature inflorescence stems for each genotype to determine the xylem or interfascicular fiber morphology.

Previous studies have shown that *OFP4* loss-of-function mutants phenocopy that of *knat7*, with irregular xylem (*irx*) and thicker fiber cell wall phenotypes (Li *et al.*, 2011; Liu and Douglas, 2015). However, in my study, there were no phenotypic differences in the vascular bundles detected between *ofp4* mutants and wild type (Figure 3.1a, e) after testing at least three trials. *ofp1*, *ofp2*, *ofp3* and *ofp5* single mutants were similar to *ofp4*, exhibiting normal xylem vessels and no obvious changes in interfascicular fibers compared with that in wild type (Figure 3.1). Also, I did not observe other significant morphological defects in the stems of *OFP* loss-of function mutants.

3.3.2 *OFP* genes are expressed in Arabidopsis seedlings

As there were no secondary cell wall phenotypes in loss-of-function mutants, I turned my attention to *OFP* gain-of-function phenotypes, focusing on *OFP1*, *OFP2*, *OFP3*, *OFP4* and *OFP5*. The overexpression plants of each *OFP* were generated respectively, by transforming Col-0 plants with a binary vector containing *OFP-YFP* transgene driven by the strong CaMV *35S* promoter. Plants overexpressing *OFP1*, *OFP2*, *OFP4* and *OFP5* presented kidney shaped cotyledons, while *OFP3* overexpression plants did not display any significant difference compared with wild type (Figure 3.2). The *OFP* overexpression phenotypes are consistent with previous findings (Wang *et al.*, 2011; Li *et al.*, 2011).

Since the transgenic plants of *35S:OFP* have cotyledon phenotypes, and both *OFP1* and *OFP4* are expressed in the veins and other tissues in cotyledons (Wang *et al.*, 2007; Li *et al.*, 2011), the expression pattern of the other three *OFP* genes, *OFP2*, *OFP3* and *OFP5*, in cotyledons were tested. By generating the transgenic lines containing Pro_{OFP2}*: OFP2-GUS*, Pro_{OFP3}*: GUS* and Pro_{OFP5}*: GUS*, respectively, I found that *OFP2*, *OFP3* and *OFP5* had

similar expression patterns in 10-day-old seedlings, and they were detected in the cotyledon tips, veins, leaf trichomes and the shoot apex (Figure 3.3a-f). They were also expressed in the vascular cylinder in the seedling roots (Figure 3.3g-i).

3.3.3 OFP proteins are localized to the nucleus and cytoplasm

To determine the localization of OFP proteins in plant cells, *35S:OFP-YFP* constructs were generated and expressed in the leaf lamina of tobacco plants transiently. The YFP fluorescence of OFP1 and OFP5 accumulated in the nucleus and labeled structures reminiscent of the cortical cytoskeleton in cytoplasm (Figure 3.4a, e), which is consistent with previous findings (Hackbusch *et al.*, 2005). OFP2-YFP and OFP4-YFP proteins were localized in the nucleus and distributed throughout the cytoplasm (Figure 3.4b, d). Interestingly, OFP3-YFP was exclusively located in the nucleus (Figure 3.4c). All the YFP signals of OFP proteins were highly concentrated in the nucleolus (Figure 3.4).

3.3.4 *OFP* overexpression plants have cell swelling and de-etiolated phenotypes in hypocotyls

In the four-day-old seedlings, overexpressing OFP proteins did not only affect the cotyledon leaf phenotype, but also the cell elongation and expansion in hypocotyl epidermal cells (Figure 3.5). Overexpression of *OFP1*, *OFP2*, *OFP4* and *OFP5* caused epidermal cells to swell in the hypocotyls (Figure 3.5), which led to the hypothesis that microtubule function could be impaired in these cells. To check if the microtubule organization has been changed in the epidermal cells, the binary vector of *35S:OFP-YFP* was transformed into the RFP-βTubulin6 (*pUBQ1: mRFP-TUB6*) homozygous transgenic plants (Ambrose *et al.*, 2011). Confocal observations showed that most cortical microtubules in wild type exhibited transverse and oblique orientations in the hypocotyl epidermal cells (Figure3.5c), while after overexpressing *OFP1*, *OFP2*, *OFP4* and *OFP5*, the microtubule orientation was changed to predominantly longitudinal and oblique (Figure3.5f, i, l, o). The changes in the cortical

microtubule orientation may explain the hypocotyl cell swelling phenotype in Arabidopsis seedlings.

In dark growth conditions, the overexpression seedlings of *OFP1*, *OFP2*, *OFP4* and *OFP5* exhibited de-etiolated hypocotyl phenotypes (Figure 3.6a, b). The hypocotyl length was considerably shortened in the *OFP* overexpression plants compared with that of wild-type plants in one-week-old dark-grown seedlings (Figure 3.6b). Taken together, the hypocotyl elongation and epidermal cell expansion were significantly affected by overexpressing OFP proteins in Arabidopsis seedlings.

3.3.5 *OFP* overexpression plants show responses to exogenous BR treatment in hypocotyls

In the *OFP* overexpression plants, the microtubule disorganization and de-etiolation phenotypes in the dark mimic brassinosteroid (BR)-deficient or BR–signalling mutants. To test if these phenotypes are the result of BR-deficiency or BR-signalling, exogenous BR was added to overexpressing *OFP* plants. Without any synthetic BR (epiBL) treatment, the hypocotyl lengths of light-grown *OFP2* overexpression seedlings were significantly shorter than those of wild type (Figure3.6c, d). When germinated on ½ MS medium containing epiBL, both wild type and *OFP2* overexpression (*OFP2 OX*) seedlings showed a considerable increase in hypocotyl lengths with the increasing concentrations of epiBL (Figure 3.6c, d). Compared with the hypocotyl length of wild type seedlings growing on normal ½ MS medium, hypocotyl lengths of *OFP2 OX* were significantly shorter at 0.2 μM epiBL, but there was a sign of the rescue when epiBL concentration was increased to 0.5 μM (Figure 3.6d). The hypocotyl lengths of *OFP2 OX* at 0.5 μM epiBL were comparable with those of the wild type without any treatment (Figure 3.6d). The same rescue responses were found in the other *OFP1*, *OFP4* and *OFP5* overexpression plants upon treating with various concentrations of epiBL (Figure 3.7). However, the kidney-shaped cotyledon phenotypes of *OFP* overexpression plants were not changed by exogenously applied epiBL. These data

indicate that the BR signaling pathway was not blocked in the hypocotyls of *OFP* overexpression plants, and their hypocotyl phenotypes may be associated with BR deficiency.

3.3.6 OFP4 interacts with Nucleosome Assembly Protein 1

OFP4 has been reported to form different complexes with KNAT7 and BLH6, to regulate secondary cell wall formation (Li *et al.*, 2011; Liu *et al.*, 2014). In this study, *OFP4* overexpressing plants exhibited pleiotropic phenotypes (Figure 3.2, 3.5, 3.6). To identify other possible components in complexes including OFP4 in regulating different aspects of plant development, a yeast two-hybrid screen was performed. Arabidopsis *OFP4* cDNA was cloned into pLexA-N vector as the bait and an cDNA library made from leaves, inflorescence stems and roots of Arabidopsis, in the pGAD-HA vector as the prey (obtained from Dualsystems Biotech). The DBD-bait and AD-prey were co-transformed into yeast NMY51 strains and spread on selection media lacking Trp, Leu, and His and supplemented with 1mM 3-Amino-1,2,4-triazole (3-AT) (SD/-Trp/-Leu/-His/3-AT). Approximately 3 x 10^6 transformants were screened and 95 positive clones were isolated and sequenced, which could activate the reporter genes upon co-expression with the DBD-OFP4 bait but not with the negative controls. Sequence alignments were performed and five different genes, *Nucleosome Assembly Protein 1;1* (*NAP1;1*), *Nucleosome Assembly Protein 1;2* (*NAP1;2*), *TON1 Recruiting Motif 20* (*TRM20*), *Bromodomain and Extraterminal Domain Protein 9* (*BET9*) and *Spiral 2* (*SPR2*) were identified (Table 3.2). Among them, *NAP1;2* was found the most times with 87 positive clones (Table 3.2). *NAP1;1* and *NAP1;2* genes encode proteins that belong to the same Nucleosome Assembly Protein 1 (NAP1) family in Arabidopsis, although *NAP1;1* was only identified once in my experiment (Table 3.2). So I subsequently focused my work on interactions between OFP4 and NAP1 proteins.

To confirm the interactions between OFP4 and full-length NAP1 proteins encoded by *NAP1;1* or *NAP1;2* cDNA, a yeast two-hybrid assay was carried out using another yeast strain MaV203. An *OFP4* cDNA was cloned into a bait vector and the full-length *NAP1;1*

and *NAP1;2* cDNAs were cloned into the prey vector. Figure 3.8(a) shows that the yeast cells expressing an OFP4-DBD fusion and a NAP1;1-AD fusion or a NAP1;2-AD fusion interacted well in the system, as judged by growth on both His^- and Ura^- selective media, which confirms the yeast two-hybrid screen result using the strain NMY51.

To test OFP4-NAP1 protein-protein interactions in plant cells, the Bimolecular Fluorescence Complementation (BiFC) was used (Hu *et al.*, 2002). OFP4 and NAP1 were fused to N- and C-terminal fragments of enhanced Yellow Fluorescent Protein (OFP4-nYFP and NAP1;1/NAP1;2-cYFP), respectively. Different combinations of fusion constructs were transformed into *Nicotiana benthamiana* leaves and the complete Yellow Fluorescent protein (YFP) would be generated only when two proteins are able to interact with each other. The fluorescence was detected in the cytoplasm when OFP4-nYFP and NAP1;1 or NAP1;2-cYFP were co-transformed into tobacco leaves, while no fluorescence was observed when OFP4-nYFP was co-expressed with empty-cYFP that served as a negative control (Figure 3.8b). These results indicated that OFP4 interacted with NAP1;1 and NAP1;2 *in vitro* and *in vivo*.

3.3.7 NAP1;1 and NAP1;2 proteins are localized to the ER membrane in epidermal cells of *N. benthamiana* leaves

The BiFC analysis indicates that OFP4 interacted with NAP1;1 and NAP1;2 in cytoplasm, with a structure reminiscent of the endoplasmic reticulum (ER) membrane adjacent to the cell nucleus (Figure 3.8b). To test the localization of NAP1;1 and NAP1;2 proteins in plant cells, and to determine if NAP1;1 and NAP1;2 are associated with the ER membrane, *35S:YFP-NAP1;1* or *35S:YFP-NAP1;2* constructs were generated, and co-transformed with the ER-marker HDEL-RFP (Napier *et al.*, 1992) into epidermal cells of tobacco leaves. YFP-NAP1;1 and YFP-NAP1;2 fused proteins gave strong fluorescence labeling a reticulate structure in the epidermal cells (Figure 3.9 a,d), and the yellow fluorescence colocalized with the red fluorescence signals coming from the ER maker, which indicated NAP1;1 and

NAP1;2 were localized to the ER membrane in epidermal cells of tobacco leaves (Figure 3.9c,f).

3.3.8 *NAP1* and *OFP4* loss-of-function mutants have altered cotyledon shapes

To investigate the roles of NAP1 in plant development, all the homozygous *NAP1* loss-of-function mutants were obtained from Dr. Aiwu Dong's group, which have been confirmed to be null alleles (Liu *et al.*, 2009). As OFP4 had been reported to interact with KNAT7 to regulate secondary cell wall development, and *knat7* mutants displayed wall phenotypes (Li *et al.*, 2011; Li *et al.*, 2012), I tested the potential secondary cell wall roles of our identified OFP4 interactors, NAP1;1 and NAP1;2. Stem cross-sections were taken from the bases of *nap1;1* and *nap1;2* mutants, and no secondary cell wall defects were observed in their stems compared with that of wild-type plants (Figure 3.10a-c). There are four *NAP1* genes in Arabidopsis, and *NAP1;1*, *NAP1;2* and *NAP1;3* genes have previously been shown to be expressed ubiquitously, while the *NAP1;4* gene was tissue-specifically expressed only in root segments and pollen grains (Zhu *et al.*, 2006; Liu *et al.*, 2009). Because of the gene redundancy, we focused on investigating the phenotypes of obtained triple mutants *nap1;1nap1;2nap1;3*. The xylem or interfascicular fiber morphology in triple mutants was still indistinguishable from wild type (Figure 3.10d), which was similar to *ofp4* mutants. These data suggest that OFP4 and NAP1 may not be involved in secondary cell wall development.

Interestingly, we observed some changes in cotyledons of the triple mutants, *nap1;1nap1;2nap1;3*, which presented the oblong shape compared with the round ones in wild type seedlings (Figure 3.11a). All the other *nap1* single and double mutants did not show any significant phenotypes compared with wild type in our experiments, although *nap1;1* was previously reported to have enlarged size in early development (Galichet and Gruissem, 2006). The distal part (leaf tip) of cotyledons in *nap1* triple mutants was narrower than that of wild type, and the cotyledon width to length ratio was significantly reduced in the triple mutants *nap1;1nap1;2nap1;3* (Figure 3.11).

To further test the potential roles of the complex of NAP1 and OFP4 in cotyledon development, I generated the quadruple mutants *ofp4nap1;1nap1;2nap1;3* by crossing *ofp4* with the *nap1* triple mutants. The cotyledons in the quadruple mutants exhibited similar phenotypes to the *nap1* triple mutants, with narrower distal part, reduced width/length ratio and oblong shapes (Figure 3.11), which indicates that NAP1 and OFP4 may function in the same pathway. However, I did not detect any obvious cotyledon phenotype in *ofp4* single mutants. Because of the functional redundancy of OFP proteins (Wang *et al.*, 2011), the quintuple mutants *ofp1ofp2ofp3ofp4ofp5* were generated. The cotyledon phenotypes of the *ofp* quintuple mutants had a more oblong shaped cotyledon and a higher degree of reduction in cotyledon width/length ratio compared to *nap1;1nap1;2nap1;3* and *ofp4nap1;1nap1;2nap1;3* mutants (Figure 3.11). Among these mutants, except the cotyledon phenotypes, I did not observe other morphological differences compared with wild type. All the findings confirmed that the complex of NAP1 and OFP proteins function in cotyledon development in Arabidopsis seedlings.

A number of cotyledon mutants, such as *cvp1*, *cvp2*, *wox2* and *stpl*, to mention a few, presented disordered patterns of vascularization (Carland *et al.*, 1999; Lie *et al.*, 2012). Therefore I further tested the cotyledon vasculature development in the triple mutants *nap1;1nap1;2nap1;3*, quadruple mutants *ofp4nap1;1nap1;2nap1;3*, and quintuple mutants *ofp1ofp2ofp3ofp4ofp5*, to better understand the causes of observed changes in their cotyledons. However, in seedlings of wild type and all the mutants, there were no significant differences in the cotyledon vasculature forms, and all of them had a similar pattern with two to four closed loops around a single main vein (Figure 3.12). This suggests that the cotyledon vascular patterning may not be the reason for their shape changes in the *nap1* and *ofp* mutants.

3.3.9 Genetic interactions between OFP4 and NAP1

To investigate the genetic interactions between OFP4 and NAP1 and to see whether the functions of OFP4 in cotyledon development depend on NAP1 proteins, the *OFP4* constitutive construct *2 x 35S:GFP-OFP4* was generated and transformed to wild type and the triple mutants *nap1;1 nap1;2 nap1;3*. By screening T1 transformants on MS medium with hygromycin resistance, the majority of surviving seedlings in the wild type background were found to have kidney-shaped cotyledons (Figure 3.13b), which represented the *OFP4* gain-of-function phenotypes, while all the surviving seedlings at the *nap1* triple mutant background presented normal round shape cotyledons (Figure 3.13c). I further investigated the GFP-OFP4 expression in the survival of T1 seedlings in the triple mutant background by confocal microscopy. GFP-OFP4 fluorescence was detected in the cytoplasm in most of cotyledon epidermal cells (Figure 3.14c), and its nucleus localization was only detected in a few cells in most of transgenic seedlings (Figure 3.14b), which suggested that the normal wild-type look of cotyledons in transgenic plants at *nap1* triple mutant background was not caused by silencing. All together, these data indicate that the functions of OFP4 in cotyledon development may require NAP1 proteins.

3.4 Discussion

A previous study suggested, based on qualitative evidence, that *ofp4* mutants exhibited *irx* and thicker fiber cell wall phenotypes, and KNAT7 could form complexes with OFP1 and OFP4, regulating secondary wall development (Li *et al.*, 2011). However, I did not find the *ofp4* phenotypes in secondary cell wall development (Figure 3.1). Liu and Douglas (2015) found similar phenotypes as mine, although they described the *ofp4* mutants as having a mild *irx* phenotype, from the quantification of *irx* and fiber cell wall thickness in Liu and Douglas (2015), the ratio of *ofp4* xylem bundles with *irx* to total xylem bundles, the number of *irx* per bundle, and the fiber wall thickness in *ofp4* stems were indistinguishable from wild type, suggesting *ofp4* mutants had no secondary cell wall defects. Statistically 'mild' *irx* phenotype was not significantly different than wild type. The reason that Li *et al.* (2011)

detected the *irx* phenotype, but it was not found in Liu and Douglas (2015) or my study, may be that their plants were stressed in some uncontrolled manner. I have observed that when plants are stressed, even wild-type plants may display some mild irregular xylem vessels. In addition, Li *et al.* (2011) presented that *OFP1* and *OFP4* functions partially depend on *KNAT7*, as their pleiotropic overexpression phenotypes were suppressed in the *knat7* mutants. In my studies, by transforming the OFP1 and OFP4 overexpression constructs into *knat7* mutants, the typical *OFP* overexpression phenotypes were still observed (data not shown). Dr. John Bowman's group found the same results when they were studying the genetic interactions between *OFP* and *KNOX* genes (unpublished data). Therefore, it appears that OFP4 does not function in secondary cell wall development, and that the earlier claims must be reassessed in light of this new data.

The importance of critically evaluating previously reported phenotypes is also highlighted by my work on *ofp5* mutants. The *ofp5* mutants was reported that the T-DNA insertion line (SALK_010386) of *OFP5* had collapsed ovules during embryo development (Pagnussat *et al.*, 2007), but the T-DNA in this line was actually inserted in the 3'-UTR as described in the T-DNA Express database (Signal.salk.edu., 2018). I ordered a true *OFP5* loss-of-function mutant (SALK_203823) with the T-DNA insertion in the exon, and found that the embryo development in the new line was normal and the homozygous plants were successfully obtained. All the *ofp* single mutants that I tested did not show any obvious defects, which suggested that OFP proteins have high functional redundancy for plant growth and development.

By *OFP* overexpression analysis, I confirmed the previous finding that overexpressing *OFP1*, *OFP2*, *OFP4* and *OFP5* resulted in kidney-shaped cotyledons (Wang *et al.*, 2011), but overexpressing *OFP3* had no obvious phenotypes (Figure 3.2). Interestingly, in the subcellular localization analysis, only OFP3-YFP was expressed in the nucleus, the other OFPs-YFP fluorescence was found in both nucleus and cytoplasm (Figure 3.4). OFP proteins were reported previously to be able to regulate the subcellular localization of TALE proteins

from nucleus to cytoplasm (Hackbusch *et al.*, 2005). My data suggests the hypothesis that the cytoplasmic localization of OFPs may be contributing to their kidney-shaped cotyledon phenotypes in overexpression plants.

Recently, a couple of ovate family proteins in rice have been well studied. OsOFP8 can be phosphorylated by the signaling kinase OsGSK2 and then transported to the cytoplasm, playing a positive role in the brassinosteroid (BR) signaling pathway (Yang *et al.*, 2016). OsOFP1 protein was localized to both nucleus and cytoplasm and the expression of OsOFP1 was highly induced by BR (Xiao *et al.*, 2017). *OsOFP19* was also involved in BR signaling pathway (Yang *et al.*, 2018). In Arabidopsis, I found *OFP* overexpression plants demonstrated some phenotypes resembling the BR-deficient mutants, such as dwarfism described previously (Wang *et al.*, 2011), disorganized microtubules in hypocotyl epidermal cells (Figure 3.5), and de-etiolated phenotypes grown in the dark (Figure 3.6). However, in the present study, exogenous BR treatment rescued the short hypocotyl phenotype in *OFP* overexpression seedlings (Figure 3.6), indicating the BR signaling pathway was not affected in Arabidopsis overexpression plants, which is different from the OsOFP8 findings in rice. An area of future work could test if the hypocotyl phenotypes of *OFP* overexpression plants in Arabidopsis may be associated with BR biosynthesis instead of signaling.

In Arabidopsis, OFP proteins have been reported to interact with TALE proteins regulating different aspects of plant development (Hackbusch *et al.*, 2005; Pagnussat *et al.*, 2007; Li *et al.*, 2011; Liu *et al.*, 2014; Zhang *et al.*, 2016). Interestingly, by performing the yeast two-hybrid screen using OFP4 as bait, we did not identify any TALE transcription factors, which is consistent with the previous finding of yeast two-hybrid screen using Tomato *OVATE* gene as the bait (van der Knaap *et al.*, 2014). More than 90% of interacting clones were identified as NAP1;1 and NAP1;2, which belong to the same Nucleosome Assembly Protein 1 family (Table 3.2). By the BiFC assay, the interactions between OFP4 and NAP1 were found to be in the cytoplasm in the epidermal cells of tobacco leaves (Figure 3.8). Subcellular localization of NAP1 revealed that NAP1;1 and NAP1;2 proteins were abundant in the

cytoplasm, associated with ER membrane (Figure 3.9). OFP4 was previously shown to localize to both the cytoplasm and nucleus (Figure 3.4). The complete YFP signal adjacent to the cell nucleus detected in the BiFC assay (Figure 3.8) indicated that OFP4 and NAP1 protein may interact with each other on the surface of the ER membrane in epidermal cells of tobacco leaves. Previous findings suggested that NAP1 proteins are primarily localized in the cytoplasm in Arabidopsis, and both *NAP1;1* and *NAP1;2* are expressed ubiquitously in plants (Liu *et al.*, 2009), which is consistent with the model that OFP4 may form functional complexes with NAP1 proteins in Arabidopsis.

By checking the secondary cell wall phenotypes of *NAP1* loss-of-function mutants, I found similar results as *ofp4* mutants, with no distinguishable cell wall defects, which confirmed my previous work that OFP does not function in secondary cell wall development. In contrast, I found the triple mutants of *nap1;1 nap1;2 nap1;3* had altered cotyledon shapes, which are consistent with the *OFP* overexpression lines. The phenotype in the triple mutants was mild but it was significantly different from wild type, according to the quantification of cotyledon width/length ratios (Figure 3.11). Because of functional redundancy of OFP proteins, the higher order *OFP* loss-of-function mutants were generated. We also observed the altered cotyledon shape in the *ofp1 ofp2 ofp3 ofp4 ofp5* quintuple mutants, which was even more severe than the *nap1;1 nap1;2 nap1;3* triple mutants (Figure 3.11). *OFP* overexpression plants had kidney-shaped cotyledons (Figure 3.2), but loss-of-function mutants had oblong shaped cotyledons (Figure 3.11), and all *OFP* genes were expressed in the seedlings (Figure 3.3). All these revealed that OFP and NAP1 proteins are functioning in the cotyledon development. In addition, the *ofp4 nap1;1 nap1;2 nap1;3* cotyledon phenotypes were similar to that of *nap1;1 nap1;2 nap1;3* triple mutants, rather than showing an additive phenotype, which suggested that OFP4 and NAP1 proteins may function in a common pathway. Overexpressing *OFP4* in the *nap1;1 nap1;2 nap1;3* background failed to show the kidney-shaped cotyledons, indicating OFP4 requires NAP1 proteins to function in the cotyledon development. All the evidence are consistent with the model that OFP and NAP1 regulate the cotyledon development by forming functional complexes.

Although the cotyledon shapes were changed in the *OFP* and *NAP1* high-ordered loss-of-function mutants, their vascular patterning did not differ from wild type, suggesting the patterns of vascularization in cotyledons may not contribute to their shape modification. NAP1;1 and NAP1;2 proteins have been reported to have responses to BR treatment, with a significant decrease in NAP1;1 and a considerable increase in NAP1;2 in BL-treated cells (Shigeta *et al.*, 2011). Our present work also suggests that OFP proteins may be associated with BR biosynthesis. It would be interesting to further investigate if the altered cotyledon phenotypes were caused by BR induced cell elongation and cell expansion in the future.

Overall, my data suggest that OFP proteins may be involved in maintaining BR homeostasis, and OFP4 interacts with NAP1;1 and NAP1;2, playing significant roles in the cotyledon development in Arabidopsis seedlings. The mechanism of OFP-NAP1 regulatory model in the cotyledon development requires further investigations.

Table 3.1 Oligonucleotides used in Chapter 3

Gene name	Application	Primer sequence (5' to 3')
ofp1	genotyping	SM_3_21689-L: ATGGGTAATAACTATCGGTTTAAG SM_3_21689-R: TTATTTGGAATGGGGTGGTGGAA Tran-element: TACGAATAAGAGCGTCCATTTTAGAGTGA
ofp2	genotyping	SALK_122550-L: ACCAAATTCAAAGAAGCATCG SALK_122550-R: TGGTGAGTTATGGTGAGGAGG LBb1.3: ATTTTGCCGATTTCGGAAC
ofp3	genotyping	GABI_167F01-L: CAGAAAATGGGGACTCACAAG GABI_167F01-R: TGACTTTGAGAAAGAGGACGG GK T-DNA: ATATTGACCATCATACTCATTGC
ofp4	genotyping	SALK_022396-L: ATGAGGAACTATAAGTTAAGATTG SALK_022396-R: CTACTTCGATGCAAATGTAGAG
ofp5	genotyping	SALK_203823-L: GACAACATCTTCATCTCCCTCC SALK_203823-R: ATTATGCACCTGCTGGAACAC
nap1;1	genotyping	SALK_013610-L: TCTGTAAACTGTCCCGTGAGC SALK_013610-R: CATAGCCTTCTCAAGCAGTGG
nap1;2	genotyping	SAIL_84_B01-L: GTCATCTGCCTCAACAGCTTC SAIL_84_B01-R: TTTCTGCATTCGTGATTG LB2 SAIL: GCTTCCTATTATATCTTCCCAAATTACCAATACA

Gene name	Application	Primer sequence (5' to 3')
nap1;3	genotyping	SALK_131746-L: TAATTGGCTTGGCATTCTTTG SALK_131746-R: TTCAGGTTTGGGAAAACTTCC
OFP2	cloning *ProOFP2: OFP2-GUS*	ProOFP2-L: GAAGCTTTTTTGGTGATGATG OFP2-R: CTTTGTTTTTGTAAGTTGAAGC
OFP3	cloning *ProOFP3: OFP3-GUS*	ProOFP3-L: TGAGAGGCGGCGAGAGAATTAG OFP3-R: CTCTCAAATATTTTATGAGCTC
OFP5	cloning *ProOFP5: OFP5-GUS*	ProOFP5-L: CTAACGTACTAACTCTATAA OFP5-R: TCCAAGAATCTGAAGAAGTT
OFP1	cloning *35S: OFP1-YFP*	OFP1-L: ATGGGTAATAACTATCGGTTTA OFP1-R: TTTGGAATGGGGTGGTGGAAGA
OFP2	cloning *35S: OFP2-YFP*	OFP2-L: ATGGGGAATTACAAGTTCAGAA OFP2-R: CTTTGTTTTTGTAAGTTGAAGC
OFP3	cloning *35S: OFP3-YFP*	OFP3-L: ATGAAACAGAAAATGGGGAC OFP3-R: GAGAGAGATAGAGAGTCCTTGA
OFP4	cloning *35S: OFP4-YFP*	OFP4-L: ATGAGGAACTATAAGTTAAGA OFP4-R: CTTCGATGCAAATGTAGAGT
OFP5	cloning *35S: OFP5-YFP*	OFP5-L: ATGATGAGATGGGGAAGAAAGA OFP5-R: ATGAAAATTAAAATCATTATGC
NAP1;1	cloning *35S: YFP-NAP1;1*	NAP1;1-L: ATGAGCAACGACAAGGATAGCT NAP1;1-R: TTACTGTTGCTTGCATTCGGGT

Gene name	Application	Primer sequence (5' to 3')
NAP1;2	cloning *35S: YFP-NAP1;2*	NAP1;2-L: ATGAGCAACGACAAGGACAGCA NAP1;2-R: TCACTGCTGCTTACATTCCGGT
OFP4	cloning *2 x 35S: GFP-OFP4*	OFP4-L: ATGAGGAACTATAAGTTAAGA OFP4-R: CTACTTCGATGCAAATGTAGA
OFP1	qRT-PCR	OFP1-L: ATGGGTAATAACTATCGGTTTA OFP1-R: GCTATTTGGTTGGCTCTGAAGATTCT
OFP2	qRT-PCR	OFP2-L: AGAGCAAACAAGATGTTCTA OFP2-R: TTTGTAAGTTGAAGCCAGAT
OFP3	qRT-PCR	OFP3-L: ATGAAACAGAAAATGGGGAC OFP3-R: TTGGGAGAAGAAAGATGGTG
OFP4	qRT-PCR	OFP4-L: ATGAGGAACTATAAGTTAAGA OFP4-R: TATGGAGTAAAGAGGAAGAGA
OFP5	qRT-PCR	OFP5-L: GATGGAGGAATGGAGAACGA OFP5-R: TTATGCACCTGCTGGAACAC
ACTIN2	qRT-PCR	ACTIN2-L: CCAGAAGGATGCATATGTTGGTGA ACTIN2-R: GAGGAGCCTCGGTAAGAAGA

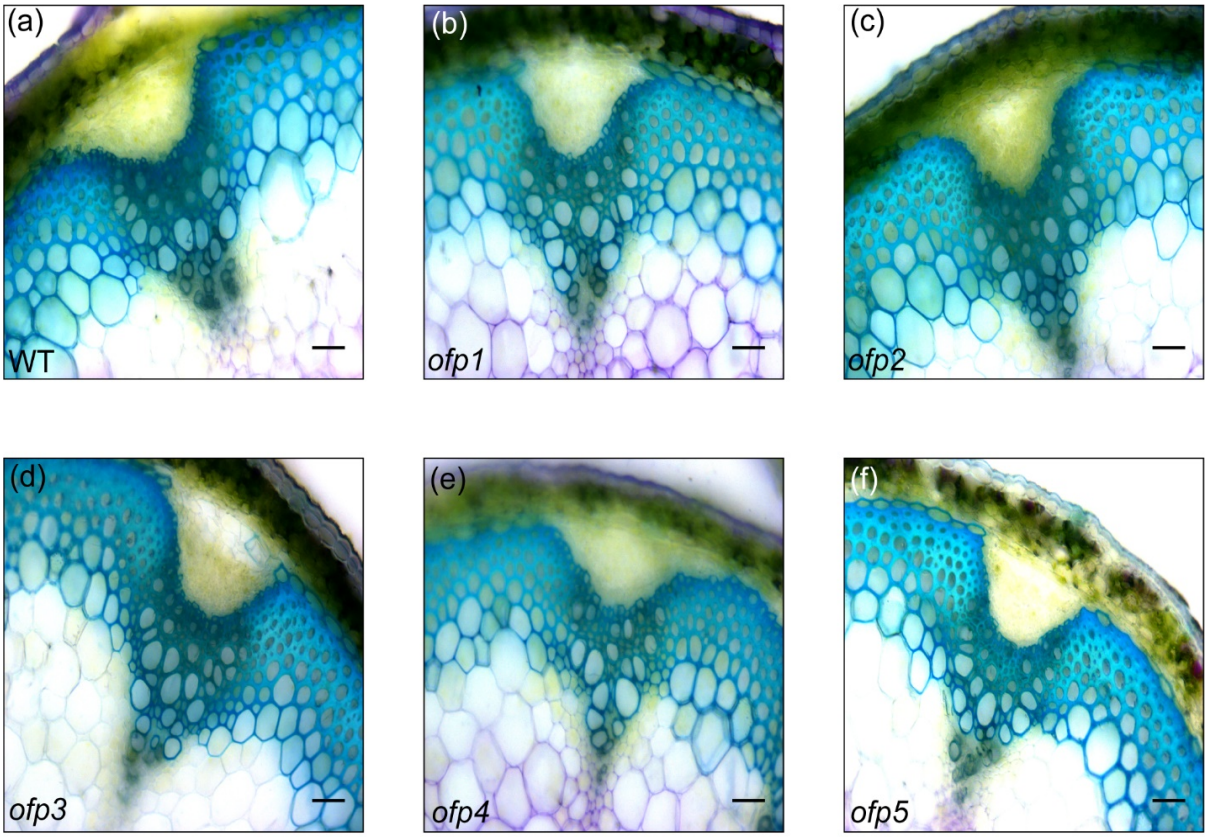

Figure 3.1 Cross-sections of stem vascular bundles in wild type (WT) and *ofp* single mutants.

Stem sections from the base of 8-week old Arabidopsis plants, stained with toluidine blue. A single representative vascular bundle is shown from each mutant. (a) WT; (b) *ofp1*; (c) *ofp2*; (d) *ofp3*; (e) *ofp4*; (f) *ofp5*. No obvious differences are shown in xylem or interfascicular fiber morphology between *ofp* single mutants and wild type. Say how many batches of plants you tested. Scale bars = 20μm.

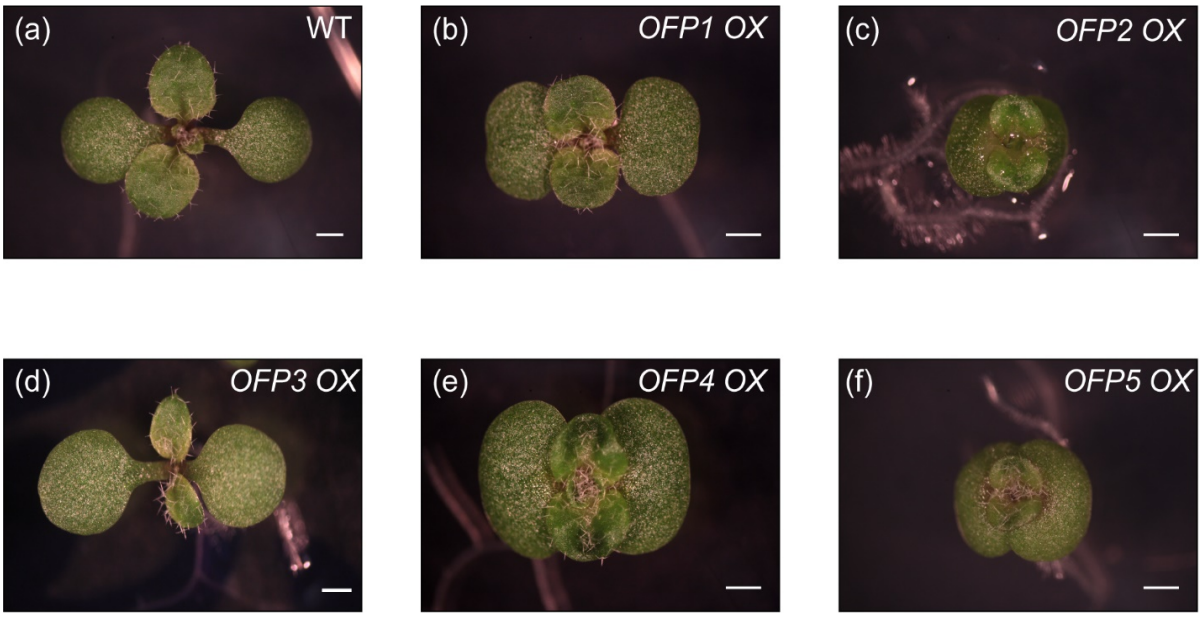

Figure 3.2 Phenotypes of wild type (WT) and *OFP* overexpression (OX) seedlings.

Ten-day-old wild type (WT) (a), *35S:OFP1-YFP* (*OFP1 OX*) (b), *35S:OFP2-YFP* (*OFP2 OX*) (c), *35S:OFP3-YFP* (*OFP3 OX*) (d), *35S:OFP4-YFP* (*OFP4 OX*) (e), and *35S:OFP5-YFP* (*OFP5 OX*) (f) seedlings

Plants overexpressing *OFP1*, *OFP2*, *OFP4* and *OFP5* presented kidney shaped cotyledons, while *OFP3* overexpression plants did not display any significant difference compared with wild type. Scale bars = 5mm.

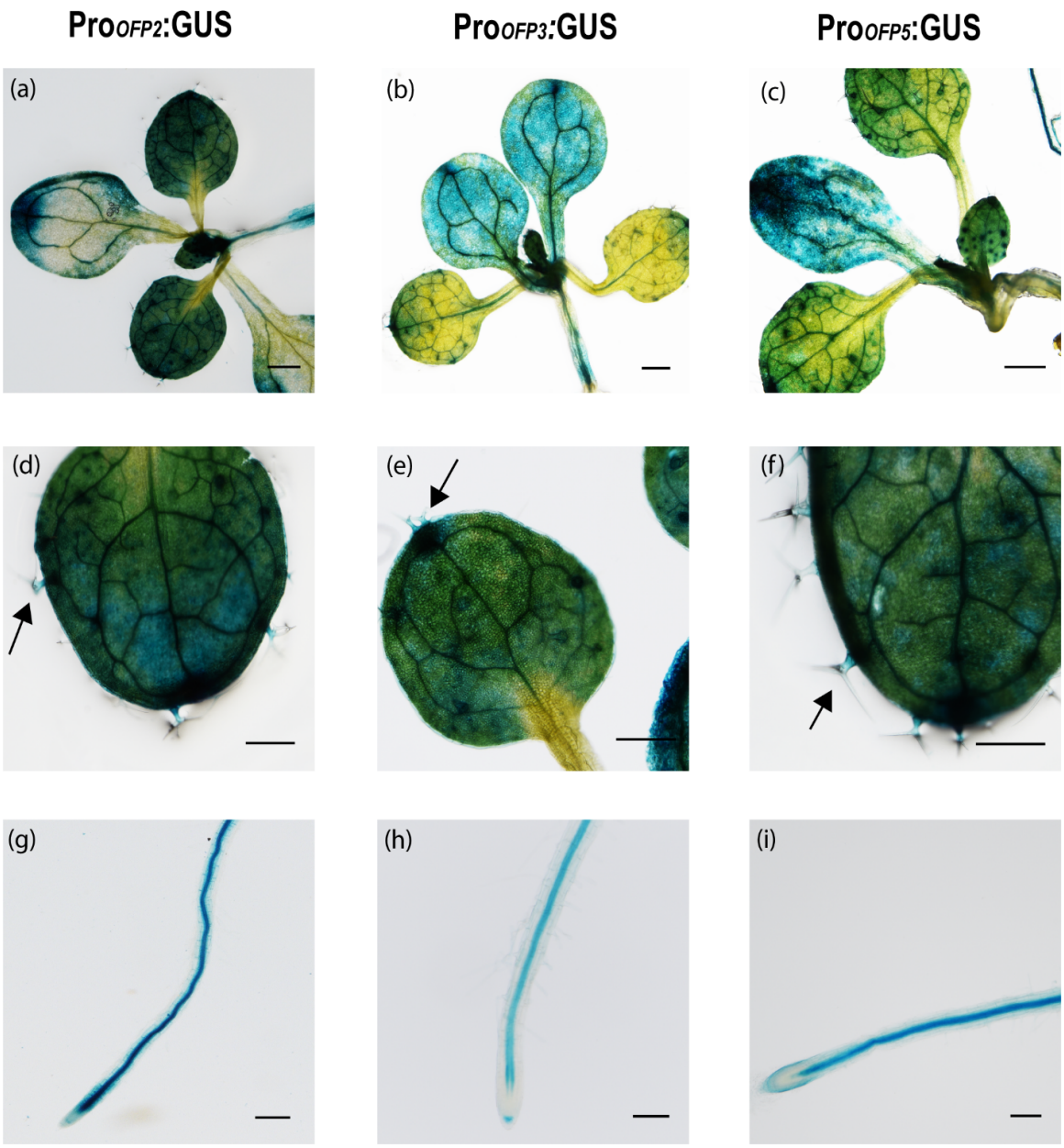

Figure 3.3 The expression patterns of *OFP2*, *OFP3* and *OFP5* in Arabidopsis seedlings.

Histochemical localization of Pro$_{OFP}$:GUS activity in 10-day-old seedlings of Pro$_{OFP2}$:GUS (a, d, g), Pro$_{OFP3}$:GUS (b, e, h), and Pro$_{OFP5}$:GUS (c, f, i) transgenic plants. Results shown are representative of more than 3 independent lines. Bars: 500μm for a, b, c; 300μm for d, e, f; 100μm for g, h, i.

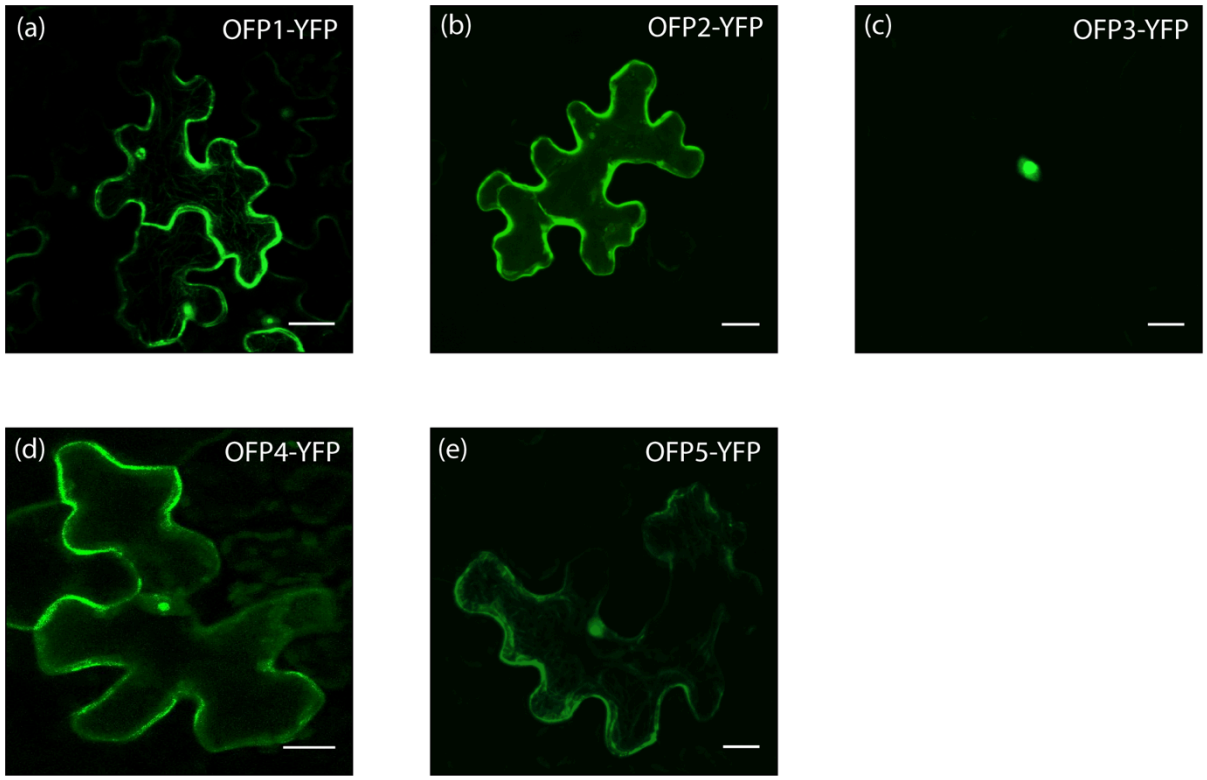

Figure 3.4 Subcellular localization of OFP-YFP fusion proteins in epidermal cells of *N. benthamiana* leaves.

Confocal scanning microscopy observations of OFP1-YFP (a), OFP2-YFP (b), OFP3-YFP (c), OFP4-YFP (d) and OFP5-YFP (e) transiently expressed in tobacco leaf epidermal cells. OFP1-YFP, OFP2-YFP, OFP4-YFP and OFP5-YFP proteins were localized in the nucleus and cytoplasm (a, b, d, e), while OFP3-YFP was exclusively located in the nucleus (c). Scale bars = 20μm.

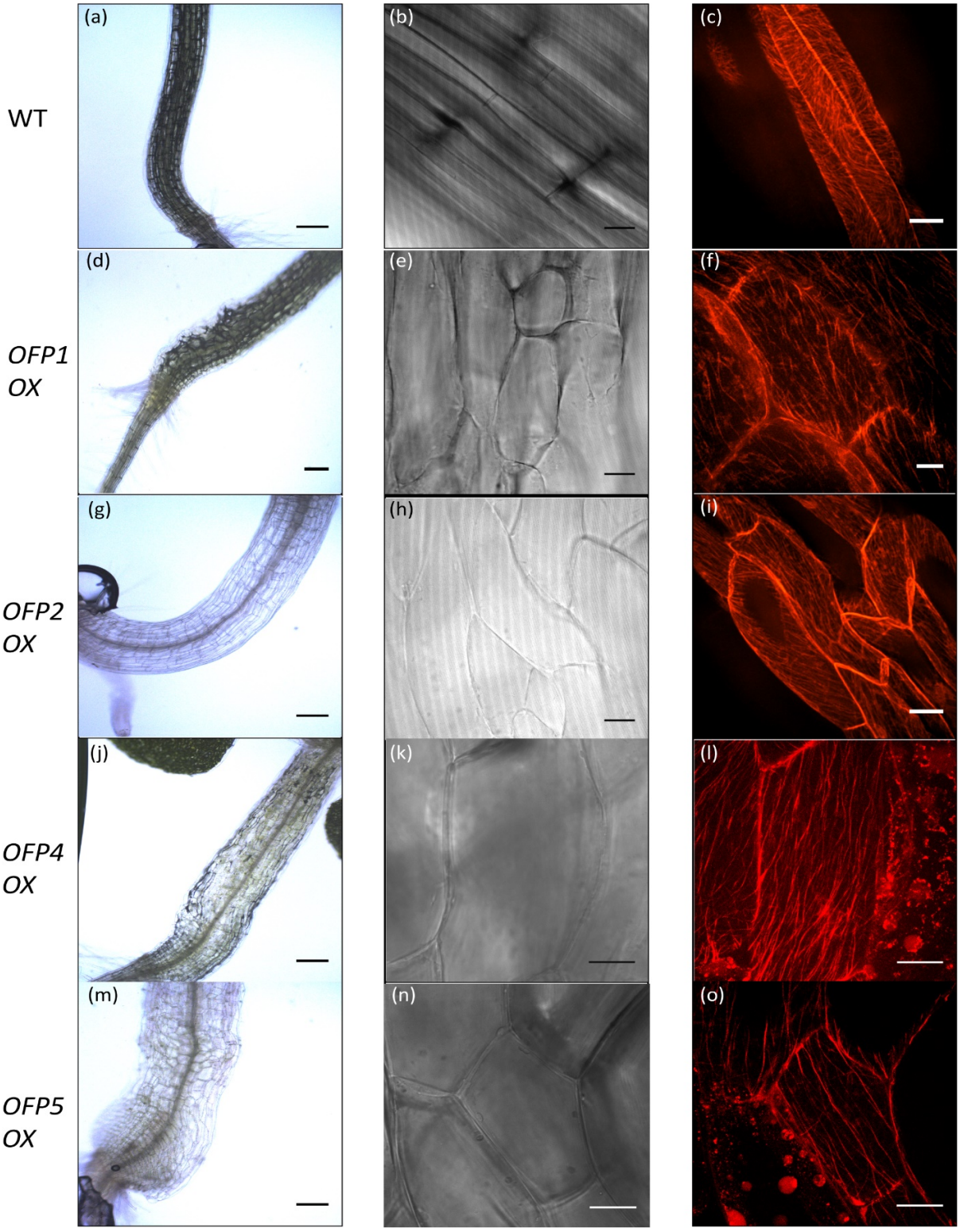
WT
OFP1 OX
OFP2 OX
OFP4 OX
OFP5 OX
(a)
(b)
(c)
(d)
(e)
(f)
(g)
(h)
(i)
(j)
(k)
(l)
(m)
(n)
(o)

Figure 3.5 Hypocotyl phenotypes of wild type (WT) and *OFP* overexpression (*OX*) plants.

Hypocotyls and the hypocotyl epidermal cells of four-day-old wild type (WT) (a, b), *35S:OFP1-YFP* (*OFP1 OX*) (d, e), *35S:OFP2-YFP* (*OFP2 OX*) (g, h), *35S:OFP4-YFP* (*OFP4 OX*) (j, k), and *35S:OFP5-YFP* (*OFP5 OX*) (m, n) seedlings; Overexpression of *OFP1*, *OFP2*, *OFP4* and *OFP5* caused epidermal cells to swell in their hypocotyls. Cortical microtubules were observed in the hypocotyl epidermal cells of WT (c), *OFP1 OX* (f), *OFP2 OX* (i), *OFP4 OX* (l), *OFP5 OX* (o) plants by transforming *OFP* overexpression constructs into the RFP-βTubulin6 (RFP-TUB6) homozygous transgenic plants. After overexpressing *OFP1*, *OFP2*, *OFP4* and *OFP5*, the microtubule orientation was changed to predominantly longitudinal and oblique (f, i, l, o).
Images of c, f, i were taken using different epidermal cells from b, e, h, respectively; Images of l, o were taken using same epidermal cells as k, n, respectively. Bars: 200 μm for a, d, g, j, m; 20 μm for b, c, e, h, i, k, l, n, o; 5 μm for f.

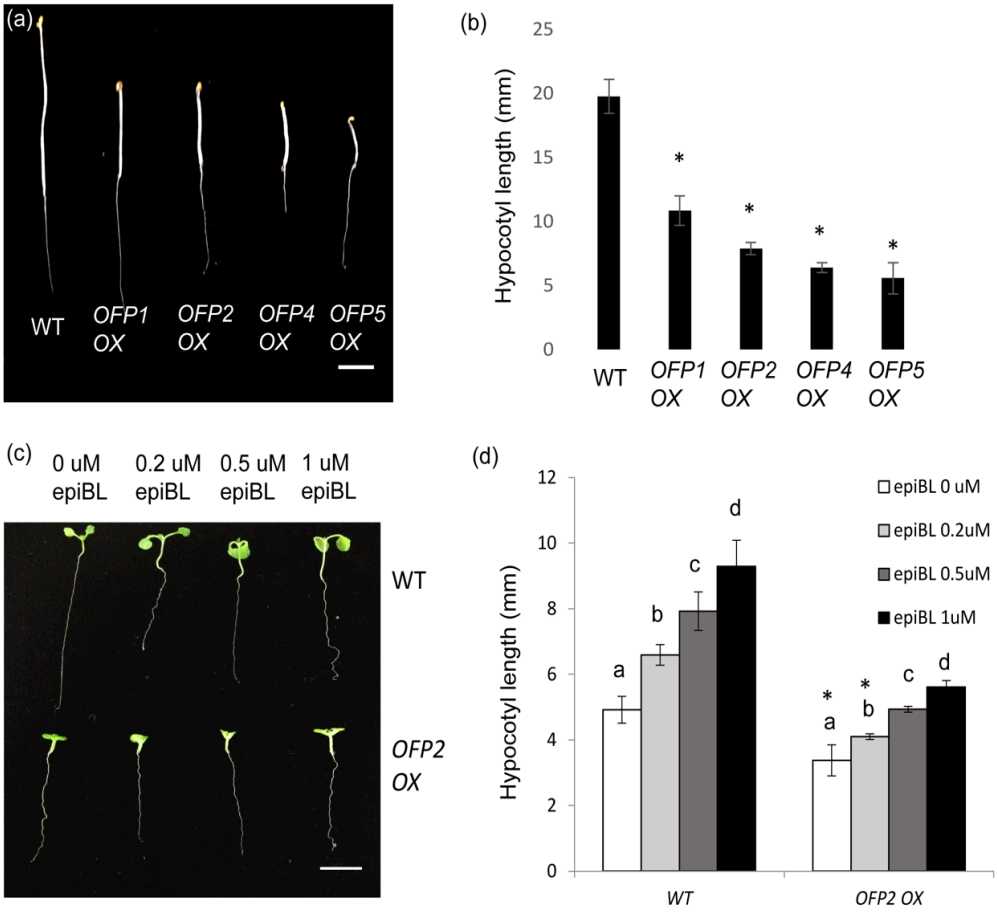

Figure 3.6 BR-deficient related morphological phenotypes of *OFP* overexpression (*OX*) mutants.

(a) Hypocotyl elongation of one-week-old wild type (WT) and *OFP OX* plants grown in the dark. Bars, 5mm.

(b) Statistical analysis of hypocotyl length measurements of dark-grown plants as shown in a. Asterisk (*) indicates the sample is significantly different from WT at P <0.01 determined by Student's T-test. Error bars represent the standard deviations. n= 5-15.

(c) Hypocotyl elongation of one-week-old WT and *OFP2 OX* plants germinated on ½ MS plates containing 0, 0.2, 0.5 or 1 μM epiBL grown in the light. Bars, 10 mm.

Figure 3.6 BR-deficient related morphological phenotypes of *OFP* overexpression (*OX*) mutants.

(d) Hypocotyl length measurements of WT and *OFP2 OX* seedlings germinated on ½ MS plates containing 0, 0.2, 0.5 or 1 μM epiBL in the light as shown in c. Statistical differences among different concentrations of epiBL treatments in the same genotype are labeled with different letters ($P<0.01$, one-way ANOVA followed by Turkey's post hoc test). Asterisk (*) indicates the sample in *OFP2 OX* is significantly different from WT hypocotyl length at 0 μM epiBL treatment at $P <0.01$ determined by Student's T-test. Error bars represent the standard deviations. n= 5-15.

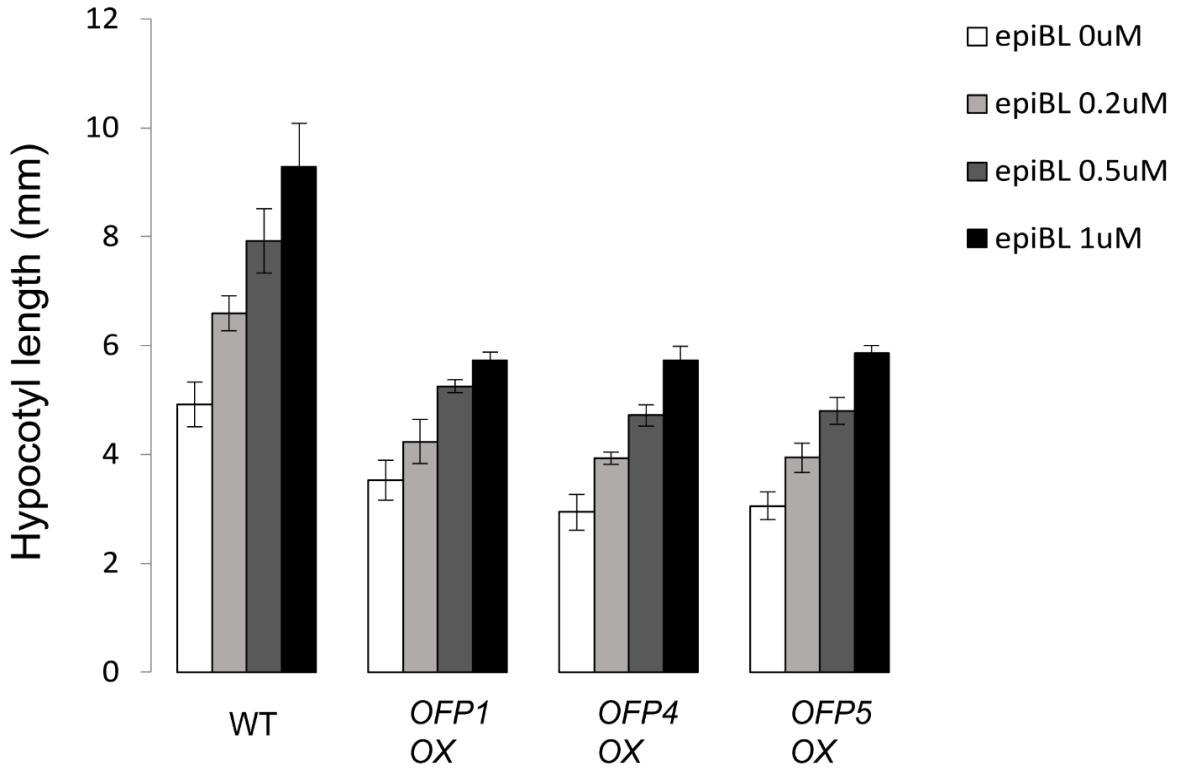

Figure 3.7 Quantification of WT and *OFP OX* hypocotyl length under exogenous BR treatment.

Hypocotyl length measurements of one-week-old WT, *OFP1 OX*, *OFP4 OX*, and *OFP5 OX* seedlings germinated on ½ MS plates containing 0, 0.2, 0.5 or 1 μM epiBL in the light condition. Error bars represent the standard deviations. n= 5-15.

Table 3.2 Identification of the cDNA encoding interactors of OFP4

Gene locus	Protein name	Accession no.	Number of clone	Annotation
AT4G26110	NUCLEOSOME ASSEMBLY PROTEIN 1;1 (NAP1:1)	2120785	1	Nucleotide excision repair (Liu *et al.*, 2009); Cell proliferation and cell expansion (Galichet and Gruissem, 2006)
AT2G19480	NUCLEOSOME ASSEMBLY PROTEIN 1;2 (NAP1;2)	2050424	87	Nucleotide excision repair (Liu *et al.*, 2009)
AT4G28760	TON1 RECRUITING MOTIF 20 (TRM20)	2117823	4	Cytoplasmic-localized protein (Drevensek *et al.*, 2012); unknown function
AT5G14270	BROMODOMAIN AND EXTRATERMINAL DOMAIN PROTEIN 9 (BET9)	2145673	2	Protein phosphorylation; Arabidopsis protein kinase (Nemoto *et al.*, 2011)
AT4G27060	Spiral2 (SPR2)	2136467	1	Microtubule-associated protein (Shoji *et al.*, 2004)

(a)

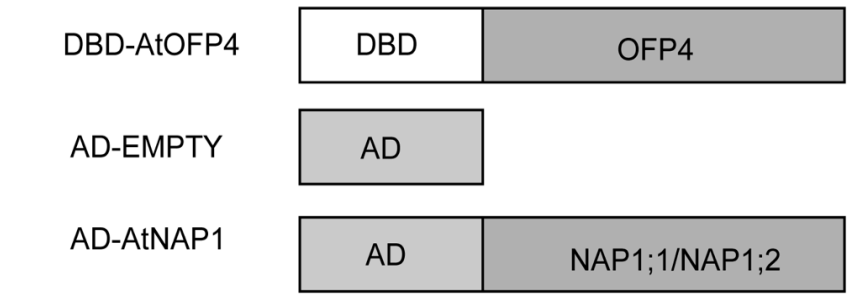

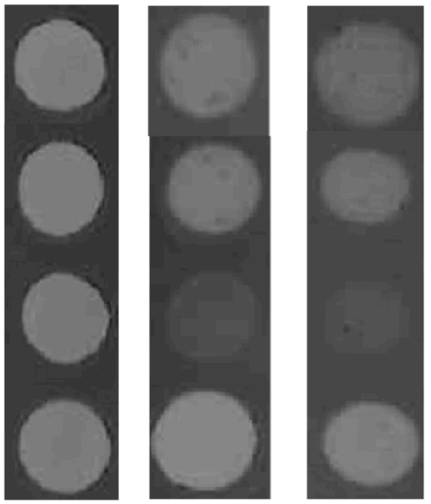

DBD	AD	Interaction
OFP4	NAP1;1	+
OFP4	NAP1;2	+
OFP4 (Negative control)	EMPTY	-
MYB75 (Positive control)	TT8	+

(b)

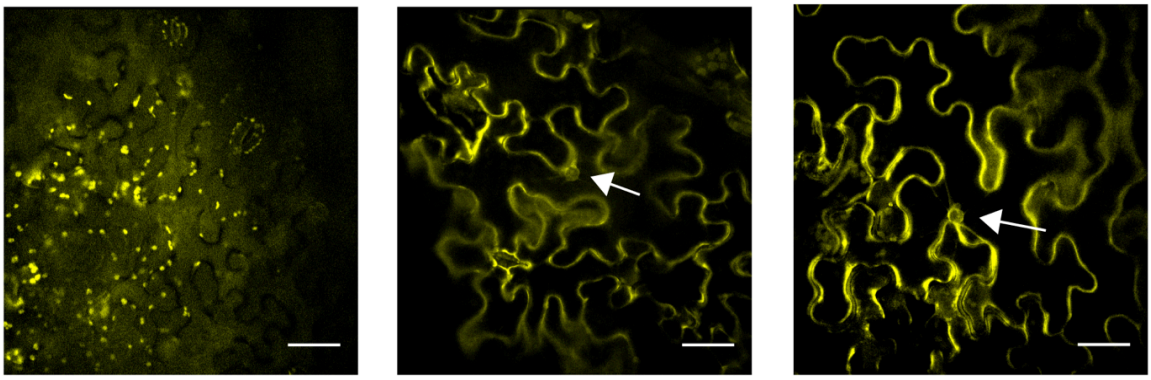

OFP4-nYFP + empty-cYFP (negative control)

OFP4-nYFP + NAP1;1-cYFP

OFP4-nYFP + NAP1;2-cYFP

Figure 3.8 OFP4 interacts with Nucleosome Assembly Protein 1;1 (NAP1;1) and NAP1;2 *in vitro* and *in vivo*.

(a) Yeast two-hybrid assay of OFP4-NAP1 interactions. Top: diagram of used constructs in yeast two-hybrid assays. Bottom: assay of DNA-binding domain (DBD)-OFP4 interaction with activation domain (AD)-NAP1;1 and AD-NAP1;2 using two reporter genes, *HIS3* (assayed on Histidine$^-$ +3AT 40mM medium) and *URA3* (assayed on Uracil$^-$ medium), with growth controls in Trptophan$^-$ Leucine$^-$ medium alone. DBD-OFP4- empty vector interaction was used as a negative control, and MYB75-TT8 interaction was served as a positive control. (b) Bimolecular Fluorescence Assay of OFP4-NAP1 interactions. Left: negative control, image of the representative tobacco leaf epidermal cell co-expressed with OFP4-nYFP and empty-cYFP; Middle and right: images of epidermal cells co-transformed by OFP4-nYFP and NAP1;1/NAP1;2-cYFP together. Scale bars = 50μm.
nYFP: N-terminal enhanced YFP protein; cYFP: C-terminal enhanced YFP protein.

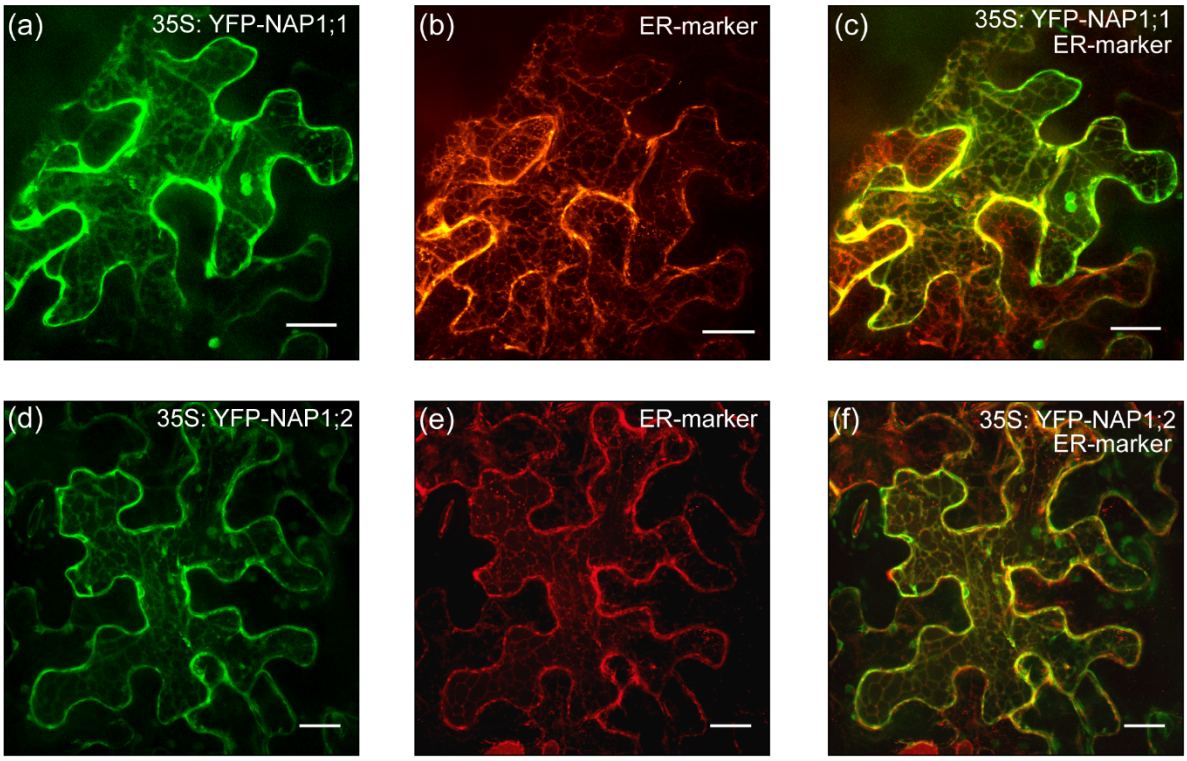

Figure 3.9 NAP1;1 and NAP1;2 are localized to the ER in epidermal cells of *N. benthamiana* leaves.

35S:YFP-NAP1;1 (a) and *35S:YFP-NAP1;2* (d) were co-transformed with ER-marker *HDEL-RFP* (b, e) into epidermal cells of *N. benthamiana* leaves. The colocalization of NAP1;1 and NAP1;2 with ER-marker protein appears as yellow in the merged images (c, f). Scale bars = 20μm.

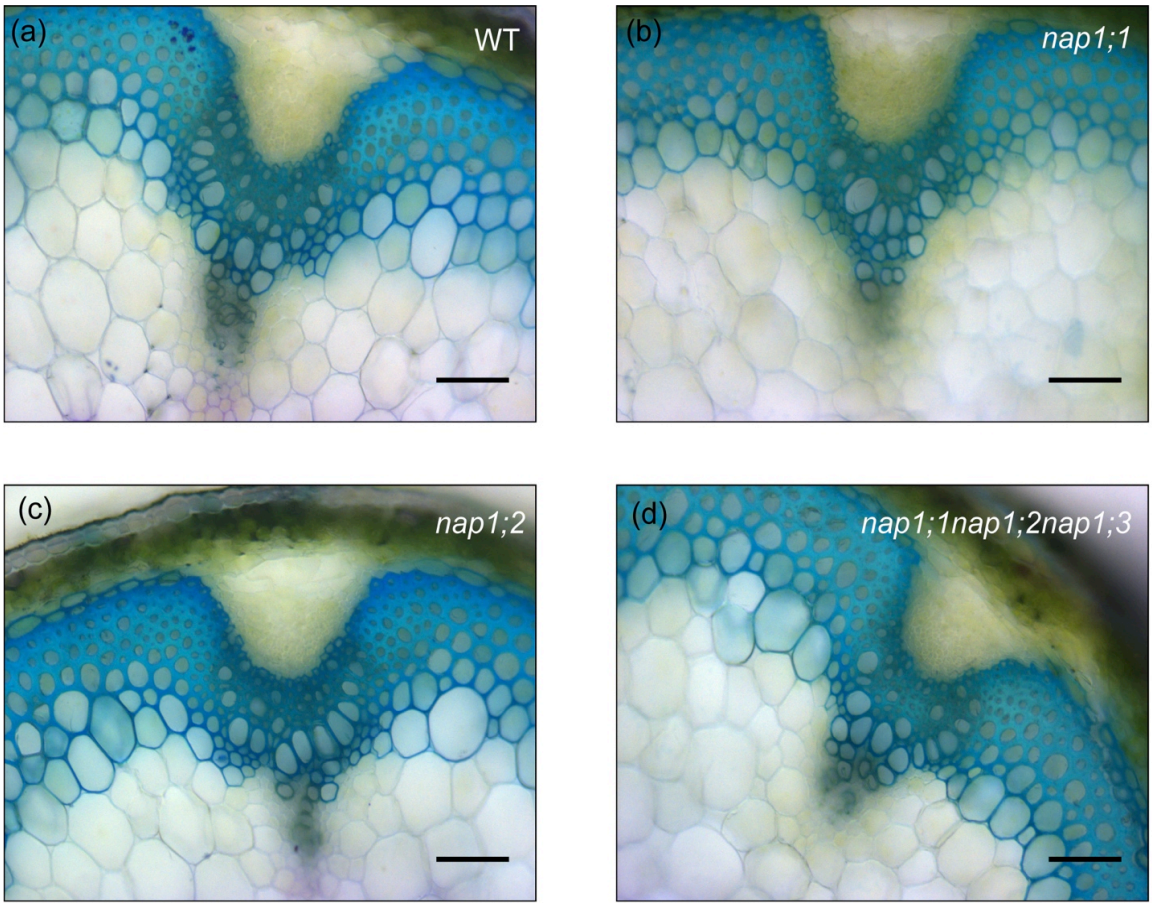

Figure 3.10 Cross-sections of stem vascular bundles in WT, *nap1;1, nap1;2 and nap1;1 nap1;2 nap1;3* triple mutants.

Stem sections stained with toluidine blue. A single representative vascular bundle is shown from each mutant. (a) WT; (b) *nap1;1*; (c) *nap1;2*; (d) *nap1;1 nap1;2 nap1;3*. No obvious differences are shown in xylem or interfascicular fiber morphology between wild type and mutants. Scale bars = 30μm.

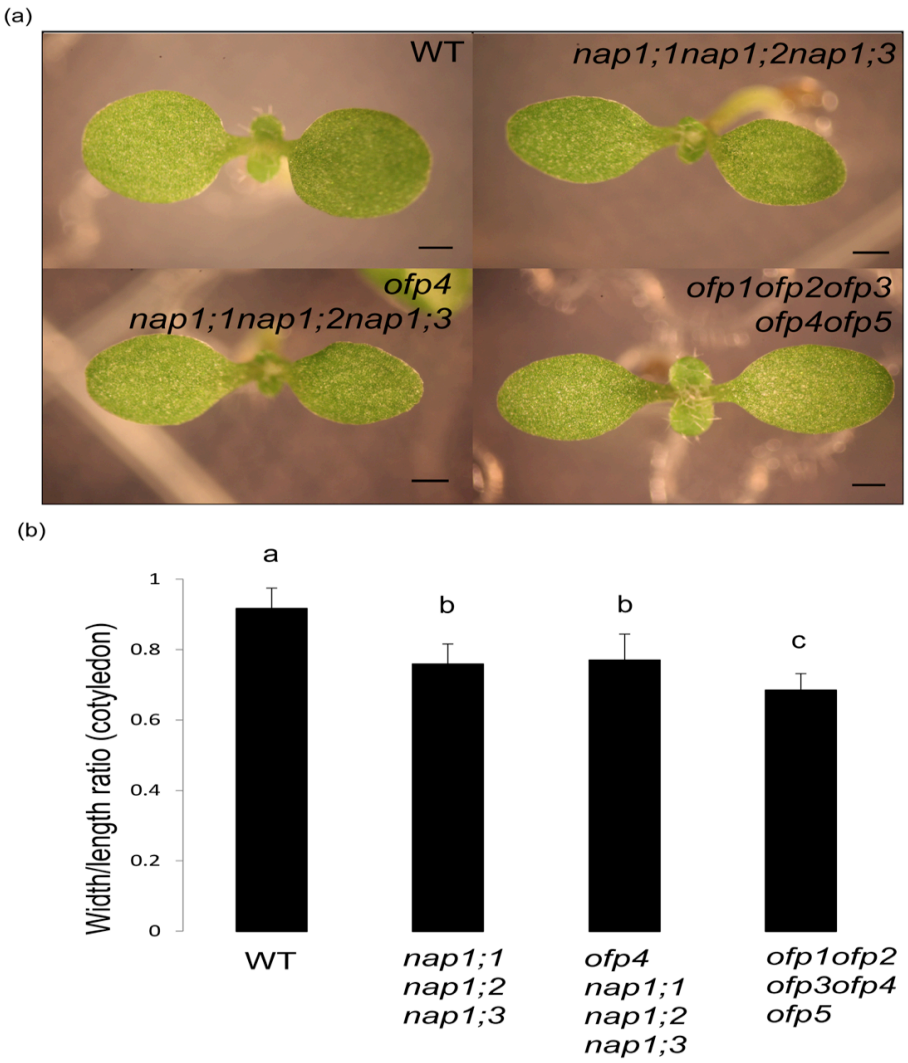

Figure 3.11 Cotyledon phenotypes of *NAP1* and *OFP* loss-of-function mutants

(a) one-week-old wild type (WT), *nap1;1 nap1;2 nap1;3*, *ofp4 nap1;1 nap1;2 nap1;3, ofp1 ofp2 ofp3 ofp4 ofp5* cotyledons; Scale bars = 500 μm.

(b) Statistical analysis of the cotyledon width to length ratio of WT, *nap1;1 nap1;2 nap1;3*, *ofp4 nap1;1 nap1;2 nap1;3, ofp1 ofp2 ofp3 ofp4 ofp5* seedlings as shown in a. Error bars represent the standard deviations; Statistical differences among the samples are labeled with different letters ($P<0.01$, one-way ANOVA followed by Turkey's post hoc test). n = 20-30.

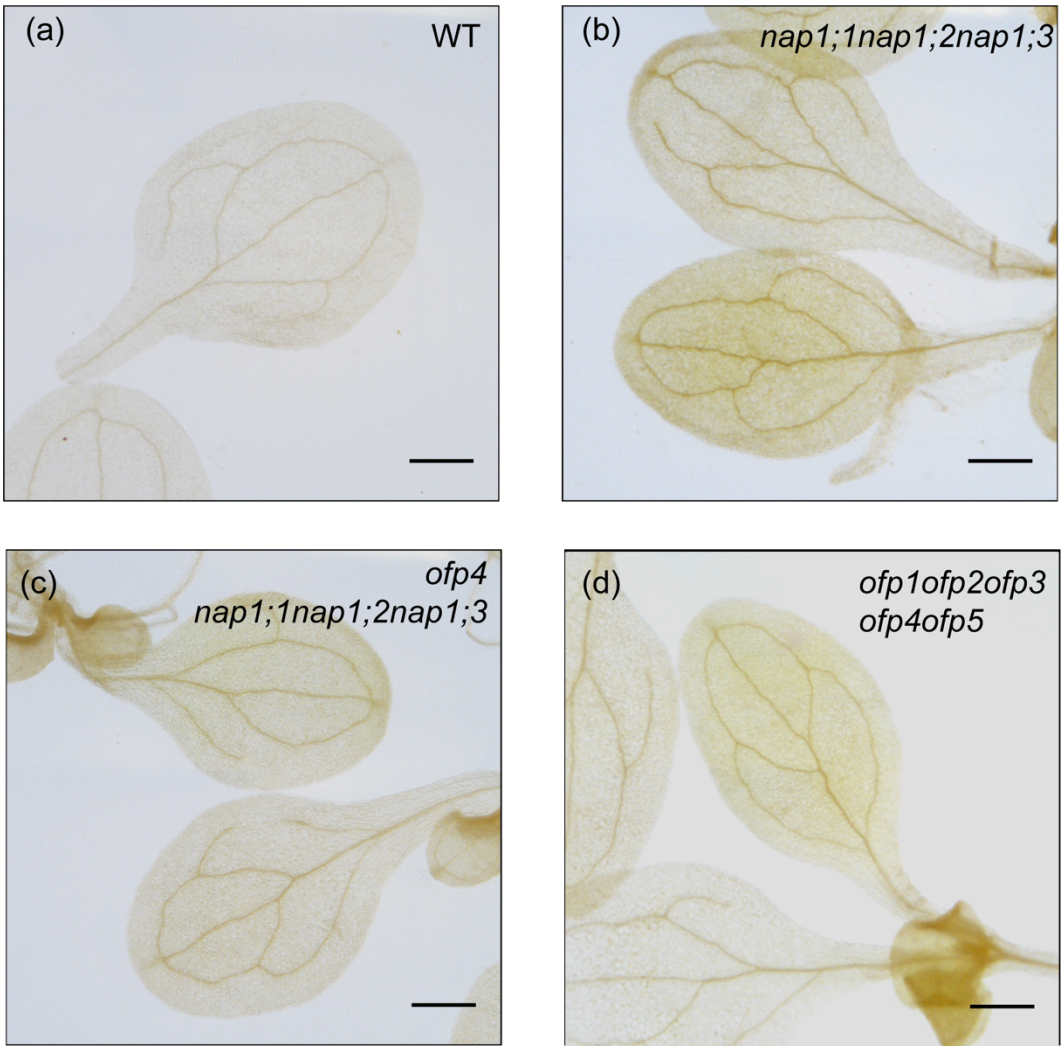

Figure 3.12 Cotyledon vasculature development in *NAP1* and *OFP* loss-of-function mutants.

In one-week-old WT (a), *nap1;1 nap1;2 nap1;3* (b), *ofp4 nap1;1 nap1;2 nap1;3* (c), *ofp1 ofp2 ofp3 ofp4 ofp5* (d) seedlings, no significant differences were found in their cotyledon vasculature forms, and all of them had a similar pattern with two to four closed loops around a single main vein. Scale bars = 2mm.

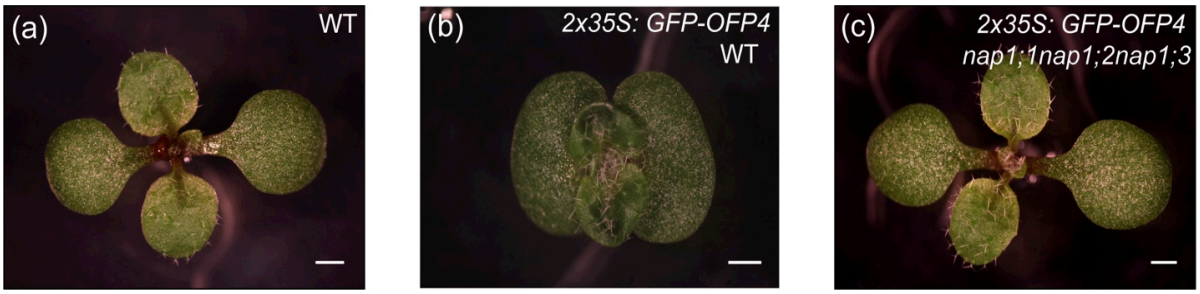

Figure 3.13 Phenotypes of *2 x 35S: GFP-OFP4* transgenic seedlings in WT and *nap1;1 nap1;2 nap1;3* background.

Ten-day-old wild type (WT) (a), *2 x 35S: GFP-OFP4* transgenic seedlings in the WT background (b), and in the *nap1;1 nap1;2 nap1;3* background (c); Scale bars = 500 μm.

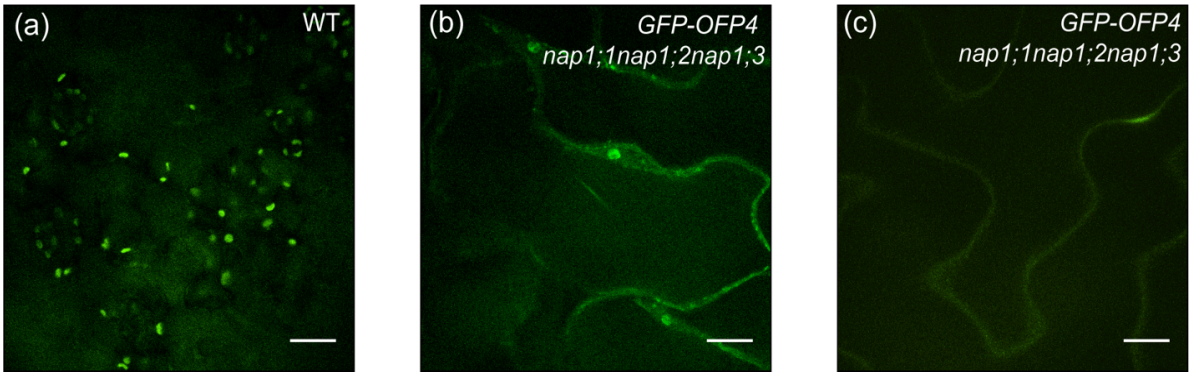

Figure 3.14 GFP-OFP4 expression in *nap1;1 nap1;2 nap1;3* triple mutants.

WT has no fluorescence that serves as a negative control (a). GFP-OFP4 nucleus localization was only detected in a few epidermal cells of *nap1;1 nap1;2 nap1;3* mutants (b), and GFP-OFP4 fluorescence was found in cytoplasm in most of epidermal cells of triple mutants (c). Scale bars = 15 μm.

Chapter 4: Conclusions

4.1 Major findings of the thesis

Owing to the existence of secondary cell walls, large trees and other terrestrial plants are the foundations of ecosystems on earth. Secondary cell wall development requires a complex network of transcriptional regulation, controlling the biosynthetic genes to produce secondary cell walls spatially and temporally. In my thesis, I studied two different family proteins with the potential roles involved in secondary cell wall formation. And I discovered KNAT3, a transcription factor belonging to the KNOX family, is working cooperatively with KNAT7 to regulate secondary cell wall development and provide mechanical support to Arabidopsis stems (Chapter 2). Although expressed in the appropriate temporal and spatial window, I showed OFPs, another family of proteins, instead of participating in secondary cell wall formation as originally hypothesized, actually function to maintain plant hormone homeostasis and regulate the cotyledon development in Arabidopsis (Chapter 3).

4.1.1 *KNAT3* and *KNAT7* function together to activate xylem vessel secondary wall formation

knat7 mutants, one of four *KNOX2* family transcription factors in Arabidopsis, have been reported to have secondary cell wall defects, including irregular xylem (*irx*) and increased fiber wall thickness (Li *et al.*, 2012). However, the functions of other *KNOX2* genes, *KNAT3*, *KNAT4*, and *KNAT5,* involved in plant growth and development and secondary wall formation were unclear. In Chapter 2, the four Arabidopsis *KNOX2* genes were shown to share the same expression patterns, largely being expressed in the cells where secondary cell walls are actively being deposited in inflorescence stems. *knat3*, *knat4*, *knat5* single mutants did not show any obvious phenotypes, while the double mutants of *knat3knat7* manifested an enhanced *irx* phenotype, compared to the other double and single mutants. Pro_{KNAT3}*:KNAT3-GFP* partially rescued the enhanced *irx* phenotype of the double mutants, and resulted in a

phenotype similar to the *knat7* single mutants. This partial complementation suggests that KNAT3 plays a positive role in xylem vessel formation. When *knat3knat7* mutants were transformed with *Pro$_{KNAT7}$:KNAT7-GFP*, the *irx* phenotype was completely recovered, mimicking the lack of phenotype of *knat3* single mutants. Thus, *KNAT3* and *KNAT7* may function redundantly to activate secondary cell wall formation in xylem vessels, where KNAT7 plays a dominant role. My results confirmed previous observation concerning the *knat7 irx* phenotype and extend our understanding of the role of *KNAT3* in xylem vessel secondary wall formation.

4.1.2 *KNAT3* acts antagonistically with *KNAT7* during secondary cell wall formation in interfascicular fibers

In Chapter 2, we confirmed that *knat7* single mutants had thicker interfascicular fiber wall thickness, and increased total lignin contents in inflorescence stems. Also, via RNA-seq analysis, we show an elaborate network of genes involved in the cell wall organizational processes are affected in *knat7* mutants compared with wild-type plants, and conclusively show that KNAT7 is a transcriptional repressor in secondary cell wall formation in interfascicular fibers, as proposed before in Li *et al.* (2012).

Interestingly, Chapter 2 also showed that *knat3knat7* displayed a pendent stem phenotype, culminating a significant reduction in tensile and flexural strength and stiffness in their inflorescence stems. It is very possible that this weak stem phenotype was caused by the extremely thin interfascicular fiber cell walls apparent in *knat3knat7* double mutants. By expressing *Pro$_{KNAT3}$::KNAT3-GFP* in *knat3knat7* double mutants, the thinner fiber secondary wall was restored to a level consistent with the *knat7* single mutants, which suggested that the thicker fiber walls in *knat7* require a functional copy of KNAT3. In addition, by overexpressing *KNAT3*, the secondary cell wall thickness of interfascicular fibers was significantly increased. These findings suggest that *KNAT3* plays a positive role in regulating interfascicular fiber secondary wall formation, acting antagonistically with *KNAT7*. In

support of this conclusion, we observed altered cell wall chemical compositions and significant mis-regulation of associated cell wall related genes in *knat3knat7* double mutants. Previously, it was reported that KNOX2 and KNOX1 had antagonistic roles in plant aerial organ development (Furumizu *et al.*, 2015), and my results provided an additional dimension, implicating *KNAT3* and *KNAT7* as antagonistic interactors regulating secondary wall development in interfascicular fibers.

4.1.3 *OFP* genes are not associated with Brassinosteroid signaling pathway in Arabidopsis

Previous data suggested that OFP1 is able to repress the expression of *GA20ox*, an enzyme involved in Gibberellic acid (GA) biosynthesis that is known to contribute to cell elongation. Contrary, in rice, a number of OsOFP genes have been reported to be involved in the BR signalling pathway (Yang *et al.*, 2016; Xiao *et al.*, 2017; Yang *et al.*, 2018). However, to date, there is no evidence in Arabidopsis linking BR-related functions to OFPs. In Chapter 3, by examining the *OFP* overexpression phenotypes in detail, I observed that *OFP* mis-regulation results in dwarfism, disorganized microtubules, and dark-grown de-etiolated phenotypes mimic the BR-deficient or –signaling mutants. By treating the *OFP* overexpression plants with synthetic BR to distinguish BR-deficient from BR-signalling mutants, I found the short hypocotyl phenotypes in *OFP* overexpression plants were rescued, indicating that the BR signaling pathway is normal in these plants. Further work could be done to test if the *OFP* overexpressor phenotypes are associated with BR biosynthesis, to give new insights about OFP's role in maintaining hormone homeostasis.

4.1.4 OFP proteins regulate cotyledon development by interacting with NAP1

To date, *OFP* overexpression phenotypes have been well studied (Hackbusch *et al.*, 2005; Wang *et al.*, 2007; Li *et al.*, 2011; Wang *et al.*, 2011), but there are only a few reports examining *OFP* loss-of-function mutant phenotypes in Arabidopsis (Li *et al.*, 2011; Wang *et al.*, 2010; Pagnussat *et al.*, 2007). Among them, the secondary cell wall phenotypes of *ofp4*

and the embryo sac development phenotypes of *ofp5* were not replicated in our work. The other phenotypes common to *ofp* mutants were apparent when the plants were subject to different stresses (Wang *et al.*, 2010). Since overexpressing *OFP* would cause pleotropic phenotypes, we hypothesized that the functions of *OFP* are related to plant growth and development even in the normal conditions.

In Chapter 3, by generating the high-ordered loss-of-function mutants, I was able to uncover new phenotypes for *ofp* mutants. The quintuple mutants *ofp1ofp2ofp3ofp4ofp5* displayed abnormal cotyledons with oblong shapes, and the cotyledon width to length ratio was significantly reduced compared with that in wild-type plants. In contrast, *OFP* overexpression plants diplay kidney-shaped cotyledons. Consistent with these phenotypic observations, an analysis of the expression pattern revealed that *OFP1*, *OFP2*, *OFP3*, *OFP4* and *OFP5* were expressed in the cotyledons, providing further support that OFPs function in the cotyledon development in Arabidopsis seedlings.

Previously, it has been shown that the Ovate Family Proteins interact with TALE homeodomain transcription factors regulating different aspects of plant development (Hackbusch *et al.*, 2005; Pagnussat *et al.*, 2007; Li *et al.*, 2011; Zhang *et al.*, 2016). In Chapter 3, in a yeast two-hybrid screen using OFP4 as the bait, I did not observe any TALE protein. Instead, I found that Nucleosome Assembly Protein1, histone chaperones, interacted with OFP4 *in vitro* and *in vivo*. In addition, they were found to interact with one another in the cytoplasm of tobacco leaf epidermal cells. In support of this finding, *NAP1* loss-of-function mutants were shown to display an abnormal cotyledon phenotype, and the kidney-shaped cotyledon phenotype of *OFP* overexpression plants were suppressed when transforming the constitutive overexpressing *OFP* constructs into the *nap1;1nap1;2nap1;3* triple mutants. In addition, by crossing *ofp4* with the *nap1* triple mutants, we did not detect any additive cotyledon phenotypes, and the cotyledon phenotypes of quadruple mutants were similar to the *nap1* triple mutants. All the evidences we found suggest that OFP and NAP proteins can form a complex in Arabidopsis seedlings to regulate cotyledon development.

My findings provide a significant step forward in disclosing the OFP functions in plant growth and development.

4.2 Future directions

Throughout this thesis, I have investigated the functions of Arabidopsis *KNOX2* and *OFP* genes, focusing specifically on their association to plant secondary cell wall development. However, this work has illustrated that *KNOX2* and *OFP* genes also contribute and function as regulators in plant growth and development. As such, several questions have arisen regarding the mechanisms behind these phenotypes, and therefore, I propose future studies should focus specifically on understanding their unique contribution to plant growth and development in Arabidopsis, as outlined below.

4.2.1 Identifying direct target genes of KNAT3 and KNAT7 in different cell tissues

My data (Chapter 2) suggested that KNAT3 may function as a transcriptional activator, regulating secondary cell wall formation in both fibers and xylem vessels, while *KNAT7* may have opposing activities in interfascicular fibers and xylem vessels. RNA-seq analyses identified a number of genes differentially expressed between wild-type, *knat3*, *knat7* and *knat3knat7* stems. However, of the mis-regulated genes, we do not know which ones are directly regulated by KNAT3 and KNAT7, respectively, in different cell types. To address this, I would propose to employ chromatin immunoprecipitation sequencing (ChIP-seq). Since these transcription factors likely display different functions in the distinct cell tissues, we could use cell type-specific promoters to overexpress them to study their functions in different cell types, and couple this to ChIP-seq. More specifically, the fiber-specific promoter *SND1* (Zhong *et al.*, 2006) and xylem vessel-specific promoter *VND7* (Kubo *et al.*, 2005) could be used, and different transgenic plants could be generated by expressing Pro_{SND1}*::KNAT3-GFP*, Pro_{SND1}*::KNAT7-GFP*, Pro_{VND7}*::KNAT3-GFP* and Pro_{VND7}*::KNAT7-GFP* constructs in *knat3knat7* mutants, respectively. The phenotypic analysis of these transgenic plants in secondary cell wall development should confirm our hypothesis about

their functions in different cell types. ChIP-seq using these complemented lines could help identify all the putative binding sites of KNAT3 and KNAT7, which would disclose their direct target genes in each cell type.

4.2.2 Identifying KNAT3 and KNAT7 cell-specific interacting partners

Many studies have shown that protein interactions among TALE homeodomain transcription factors play significant roles in varying aspects of plant development (Hackbusch *et al.*, 2005; Pagnussat *et al.*, 2007; Kim *et al.*, 2013; Liu *et al.*, 2014). KNAT7 has been reported to interact with BLH6, and the interaction appears to enhance KNAT7 repressor activity (Liu *et al.*, 2014). Compared with single mutants, the *knat7blh6* double mutants displayed an enhanced *irx* phenotype, but the fiber wall thickness was not enhanced (Liu *et al.*, 2014). The additive *irx* phenotypes suggests that KNAT7 and BLH6 may function in different pathways to regulate xylem vessel secondary wall formation, while the phenotype in interfascicular fibers implies that KNAT7 forms a complex with BLH6 to impact fiber secondary cell wall development. In addition, KNAT3 was shown to interact with BLH1 in controlling embryo sac development and ABA signalling pathway (Pagnussat *et al.*, 2007; Kim *et al.*, 2013). However, the KNAT3 interacting partners involved in secondary cell wall development remain unclear. Moreover, according to my findings with KNAT7, I hypothesize that the same transcription factor may have different interacting partners in multiple tissues to regulate secondary cell wall formation.

To identify these putative protein complexes in Arabidopsis, the metabolic stable isotope labelling immuno-precipitation mass spectrometry (mSILIP) could be performed. And the transgenic lines mentioned above with *KNAT3* or *KNAT7* expression driven by tissue-specific promoters in the *knat3knat7* background could be used to detect tissue-specific interactors of KNAT3 or KNAT7, respectively. Quantitative immuno-precipitation and mass spectrometry should allow us to distinguish specific from non-specific proteins revealed by co-immunoprecipitation, and employing this strategy, we may be able to identify novel interactors of KNAT3 and KNAT7.

4.2.3 Investigating upstream signals of KNAT3 and KNAT7 involved in secondary cell wall development

Previous research has shown that SND1 and MYB46 are the upstream regulators of KNAT7 (Zhong *et al.*, 2008; Ko *et al.*, 2009). However, KNAT3 is a newly identified transcription factor involved in secondary cell wall formation. It would be interesting to see if KNAT3 and KNAT7 share the same upstream regulators, and if there are other "alternative" regulators controlling KNAT3 and KNAT7 functions in secondary cell wall development. It was reported that the xylem transcriptional network could be manipulated by environmental stresses (Taylor-Teeples *et al.*, 2014a). However, there is little information about the role of KNOX2 in regulating secondary cell wall formation in response to different abiotic stresses. To address these questions, we could use a yeast one-hybrid (Y1H) protein-DNA interaction assays elucidate the direct upstream regulators of KNAT3 and KNAT7. This could be followed by electrophoretic mobility shift assays (EMSA) to confirm the interactions between identified regulators and the promoters of KNAT3 and KNAT7. By treating plants with different abiotic stresses, we could investigate the influence of stresses on the number of *KNAT3* and *KNAT7* upstream regulators in Arabidopsis.

4.2.4 Elucidating the roles of OFP in cotyledon development

In Chapter 3, the *ofp1ofp2ofp3ofp4ofp5* quintuple mutants showed altered cotyledon shapes, but it is unclear how this phenotype manifests. RNA-seq analysis could be conducted on the quintuple mutants to reveal the genes responsible for this unique phenotype. Since overexpressing *OFP1/2/4/5* resulted in kidney-shaped cotyledons, we could generate these same transgenic plants expressing *OFPs* under their native promoters, and again perform mSILIP to identify OFP interactors in *planta*. These approaches may help us improve our understanding of how OFPs contribute to the cotyledon development.

4.2.5 Investigating the relationships between OFP and plant hormones

In addition to the cotyledon phenotype, *OFP* overexpression plants also exhibited shorter hypocotyl and swollen hypocotyl epidermal cells. The data in Chapter 3 highlighted a relationship between OFPs and BR, and we hypothesized that OFP may be involved in BR biosynthesis. Previous research has shown that OFP1 functions as a transcriptional repressor, by inhibiting GA biosynthesis to regulate cell elongation (Wang *et al.*, 2007). Another hormone, Auxin, is also involved in cell elongation. Since crosstalk among Auxin, BR and GA signalling pathways exists (Jung *et al.*, 2010; Bernardo-García *et al.*, 2014; Bai *et al.*, 2012), it would be interesting to see if *OFP* overexpression plants and loss-of-function (quintuple) mutants have any response to different hormones, and if the three hormones can induce or inhibit *OFP* gene expressions.

4.2.6 Characterizing the functions of OFP4-TRM20

van der Knaap *et al.* (2014) carried out a yeast two-hybrid screen using tomato *OVATE* gene as the bait, and they did not detect any TALE transcription factors in their results, which is consistent with my results. However, they identified many candidates from the TONNEAU1 Recruiting Motif (TRM) superfamily, including the otholog of Arabidopsis TRM17/20 (van der Knaap *et al.*, 2014). Interestingly, in my experiment, TRM 20 was also identified as one of the top OFP4 interactors. These findings provide additional confidence and impetus to further study the potential complex of OFP4-TRM20. To verify their interaction in *planta*, BiFC or co-immunoprecipitation could be employed. Moreover, using a reverse genetics approach, we could explore the function(s) of a putative OFP4-TRM20 complex in plant growth and development, using the suite of similar techniques employed in this thesis.

References

Albersheim, P., Darvill, A., Roberts, K., Sederoff, R., and Staehelin, A. (2010). Plant cell walls. Garlandscience. 18-19, 74.

Ambrose, C., Allard, J.F., Cytrynbaum, E.N. and Wasteneys, G.O. (2011) A CLASP-modulated cell edge barrier mechanism drives cell-wide cortical microtubule organization in Arabidopsis. *Nat. Commun.*, **2**, 412–430.

Amoutzias, G.D., Robertson, D.L., Peer, Y. Van de and Oliver, S.G. (2008) Choose your partners: dimerization in eukaryotic transcription factors. *Trends Biochem. Sci.*, **33**, 220–229.

Bai, M.-Y., Shang, J.-X., Oh, E., Fan, M., Bai, Y., Zentella, R., Sun, T. and Wang, Z.-Y. (2012) Brassinosteroid, gibberellin and phytochrome impinge on a common transcription module in Arabidopsis. *Nat. Cell Biol.*, **14**, 810–817.

Bernardo-García, S., Lucas, M. de, Martínez, C., Espinosa-Ruiz, A., Davière, J.M. and Prat, S. (2014) BR-dependent phosphorylation modulates PIF4 transcriptional activity and shapes diurnal hypocotyl growth. *Genes Dev.*, **28**, 1681–1694.

Bhargava, A., Mansfield, S.D., Hall, H.C., Douglas, C.J. and Ellis, B.E. (2010) MYB75 Functions in Regulation of Secondary Cell Wall Formation in the Arabidopsis Inflorescence Stem. *Plant Physiol.*, **154**, 1428–1438.

Bonawitz, N.D. and Chapple, C. (2010) The Genetics of Lignin Biosynthesis: Connecting Genotype to Phenotype. *Annu. Rev. Genet.*, **44**, 337–363.

Brown, D.M., Zeef, L.A.H., Ellis, J., Goodacre, R. and Turner, S.R. (2005) Identification of Novel Genes in Arabidopsis Involved in Secondary Cell Wall Formation Using Expression Profiling and Reverse Genetics. *Plant Cell*, **17**, 2281–2295.

Brown, D.M., Zhang, Z., Stephens, E., Dupree, P. and Turner, S.R. (2009)

Characterization of IRX10 and IRX10-like reveals an essential role in glucuronoxylan biosynthesis in Arabidopsis. *Plant J.*, **57**, 732–746.

Bürglin, T.R. (1997) Analysis of TALE superclass homeobox genes (MEIS, PBC, KNOX, Iroquois, TGIF) reveals a novel domain conserved between plants and animals. *Nucleic Acids Res.*, **25**, 4173–4180.

Carland, F.M., Berg, B.L., Fitzgerald, J.N., Jinamornphongs, S., Nelson, T. and Keith, B. (1999) Genetic Regulation of Vascular Tissue Patterning in Arabidopsis. *Plant Cell*, **11**, 2123–2137.

Chen, F., Tobimatsu, Y., Havkin-Frenkel, D., Dixon, R.A. and Ralph, J. (2012) A polymer of caffeyl alcohol in plant seeds. *Proc. Natl. Acad. Sci.*, **109**, 1772–1777.

Citovsky, V., Lee, L.Y., Vyas, S., Glick, E., Chen, M.H., Vainstein, A., Gafni, Y., Gelvin, S.B. and Tzfira, T. (2006) Subcellular Localization of Interacting Proteins by Bimolecular Fluorescence Complementation in Planta. *J. Mol. Biol.*, **362**, 1120–1131.

Clough, S.J. and Bent, A.F. (1998) Floral dip: A simplified method for Agrobacterium-mediated transformation of *Arabidopsis thaliana*. *Plant J.*, **16**, 735–743.

Coleman, H.D., Park, J.-Y., Nair, R., Chapple, C. and Mansfield, S.D. (2008) RNAi-mediated suppression of p-coumaroyl-CoA 3'-hydroxylase in hybrid poplar impacts lignin deposition and soluble secondary metabolism. *Proc. Natl. Acad. Sci.*, **105**, 4501–4506.

Cosgrove, D. (2005) Growth of the plant cell wall. *Nat. Rev. Mol. Cell Biol.*, **6**, 850–61.

Cosgrove, D.J. and Jarvis, M.C. (2012) Comparative structure and biomechanics of plant primary and secondary cell walls. *Front. Plant Sci.*, **3**, 1–7.

Courtois-Moreau, C.L., Pesquet, E., Sjödin, A., Muñiz, L., Bollhöner, B., Kaneda, M., Samuels, L., Jansson, S. and Tuominen, H. (2009) A unique program for cell death in

xylem fibers of Populus stem. *Plant J.*, **58**, 260–274.

Derelle, R., Lopez, P., Guyader, H. Le and Manuel, M. (2007) Homeodomain proteins belong to the ancestral molecular toolkit of eukaryotes. *Evol. Dev.*, **9**, 212–219.

Dixon, R.A., Srinivasa Reddy, M.S. and Gallego-Giraldo, L. (2014) Monolignol Biosynthesis and its Genetic Manipulation: The Good, the Bad, and the Ugly. *Recent Adv. Polyphen. Res.*, **4**, 1–38.

Donaldson, L.A. (2001) Lignification and lignin topochemistry - An ultrastructural view. *Phytochemistry*, **57**, 859–873.

Donner, T.J., Sherr, I. and Scarpella, E. (2009) Regulation of preprocambial cell state acquisition by auxin signaling in Arabidopsis leaves. *Development*, **136**, 3235–3246.

Douglas, C.J. (1996) Phenylpropanoid metabolism and lignin biosynthesis: From weeds to trees. *Trends Plant Sci.*, **1**, 171–178.

Douglas, S.J., Chuck, G., Dengler, R.E., Pelecanda, L. and Riggs, C.D. (2002) KNAT1 and ERECTA Regulate Inflorescence Architecture in Arabidopsis. *Society*, **14**, 547–558.

Drevensek, S., Goussot, M., Duroc, Y., Christodoulidou, A., Steyaert, S., Schaefer, E., Duvernois, E., Grandjean, O., Vantard, M., Bouchez, D. and Pastuglia, M. (2012) The Arabidopsis TRM1-TON1 Interaction Reveals a Recruitment Network Common to Plant Cortical Microtubule Arrays and Eukaryotic Centrosomes. *Plant Cell*, **24**, 178–191.

Ehlting, J., Mattheus, N., Aeschliman, D.S., Li, E., Hamberger, B., Cullis, I.F., Zhuang, J., Kaneda, M., Mansfield, S.D., Samuels, L., Ritland, K., Ellie, B.E., Bohlmannn, J. and Douglas, C.J. (2005) Global transcript profiling of primary stems from Arabidopsis thaliana identifies candidate genes for missing links in lignin biosynthesis and transcriptional regulators of fiber differentiation. *Plant J.*, **42**, 618–640.

Etchells, J.P., Provost, C.M., Mishra, L. and Turner, S.R. (2013) WOX4 and WOX14 act downstream of the PXY receptor kinase to regulate plant vascular proliferation independently of any role in vascular organisation. *Development*, **140**, 2224–2234.

Etchells, J.P. and Turner, S.R. (2010) The PXY-CLE41 receptor ligand pair defines a multifunctional pathway that controls the rate and orientation of vascular cell division. *Development*, **137**, 767–774.

Fisher, K. and Turner, S. (2007) PXY, a Receptor-like Kinase Essential for Maintaining Polarity during Plant Vascular-Tissue Development. *Curr. Biol.*, **17**, 1061–1066.

Fukuda, H. (1996) XYLOGENESIS : INITIATION , PROGRESSION , AND CELL DEATH. , 299–325.

Funk, V., Kositsup, B., Zhao, C. and Beers, E.P. (2002) The Arabidopsis xylem peptidase XCP1 is a tracheary element vacuolar protein that may be a papain ortholog. *Plant Physiol.*, **128**, 84–94.

Furumizu, C., Alvarez, J.P. aul, Sakakibara, K. and Bowman, J.L. (2015a) Antagonistic roles for KNOX1 and KNOX2 genes in patterning the land plant body plan following an ancient gene duplication. *PLoS Genet.*, **11**, e1004980.

Galichet, A. and Gruissem, W. (2006) Developmentally Controlled Farnesylation Modulates AtNAP1;1 Function in Cell Proliferation and Cell Expansion during Arabidopsis Leaf Development. *Plant Physiol.*, **142**, 1412–1426.

Greco, M., Chiappetta, A., Bruno, L. and Bitonti, M.B. (2012) Xylem tissue specification, patterning, and differentiation mechanisms. *J. Exp. Bot.*, **63**, 695–709.

Groover, A.T., Mansfield, S.D., DiFazio, S.P., Dupper, G., Fontana, J.R., Millar, R. and Wang, Y. (2006) The Populus homeobox gene ARBORKNOX1 reveals overlapping

mechanisms regulating the shoot apical meristem and the vascular cambium. *Plant Mol. Biol.*, **61**, 917–932.

Guo, D., Chen, F., Inoue, K., Blount, J.W. and Dixon, R. (2001) Downregulation of caffeic acid 3-O-methyltransferase and caffeoyl CoA 3-O-methyltransferase in transgenic alfalfa. impacts on lignin structure and implications for the biosynthesis of G and S lignin. *Plant Cell*, **13**, 73–88.

Guo, J., Wang, S., Wang, J., Huang, W.D., Liang, J. and Chen, J.G. (2009) Dissection of the relationship between RACK1 and heterotrimeric G-proteins in Arabidopsis. *Plant Cell Physiol.*, **50**, 1681–1694.

Hackbusch, J., Richter, K., Müller, J., Salamini, F. and Uhrig, J.F. (2005) A central role of Arabidopsis thaliana ovate family proteins in networking and subcellular localization of 3-aa loop extension homeodomain proteins. *P Natl Acad Sci USA*, **102**, 4908–4912.

Hake, S., Smith, H.M.S., Holtan, H., Magnani, E., Mele, G. and Ramirez, J. (2004) the Role of Knox Genes in Plant Development. *Annu. Rev. Cell Dev. Biol*, **20**, 125–51.

Hao, Z. and Mohnen, D. (2014) A review of xylan and lignin biosynthesis: Foundation for studying Arabidopsis irregular xylem mutants with pleiotropic phenotypes. *Crit. Rev. Biochem. Mol. Biol.*, **49**, 212–241.

Hay, A. and Tsiantis, M. (2010) KNOX genes: versatile regulators of plant development and diversity. *Development*, **137**, 3153–3165.

Hirakawa, Y., Kondo, Y. and Fukuda, H. (2010) TDIF Peptide Signaling Regulates Vascular Stem Cell Proliferation via the WOX4 Homeobox Gene in Arabidopsis. *Plant Cell*, **22**, 2618–2629.

Hirakawa, Y., Shinohara, H., Kondo, Y., Inoue, A., Nakanomyo, I., Ogawa, M., Sawa,

S., Ohashi-Ito, K., Mastsubayashi, Y. and Fukuda, H. (2008) Non-cell-autonomous control of vascular stem cell fate by a CLE peptide/receptor system. *Proc. Natl. Acad. Sci.*, **105**, 15208–15213.

Hiratsu, K., Mitsuda, N., Matsui, K. and Ohme-Takagi, M. (2004) Identification of the minimal repression domain of SUPERMAN shows that the DLELRL hexapeptide is both necessary and sufficient for repression of transcription in Arabidopsis. *Biochem. Biophys. Res. Commun.*, **321**, 172–178.

Hongo, S., Sato, K., Yokoyama, R. and Nishitani, K. (2012) Demethylesterification of the Primary Wall by PECTIN METHYLESTERASE35 Provides Mechanical Support to the Arabidopsis Stem. *Plant Cell*, **24**, 2624–2634.

Hu, C.D., Chinenov, Y. and Kerppola, T.K. (2002) Visualization of interactions among bZIP and Rel family proteins in living cells using bimolecular fluorescence complementation. *Mol. Cell*, **9**, 789–798.

Ito, Y., Nakanomyo, I., Hiroyasu, M., Iwamoto, K., Sawa, S., Dohmae, N. and Fukuda, H. (2006) Dodeca-CLE Peptides as Suppressors. *Science* (80), 842–845.

Jin, H. (2000) Transcriptional repression by AtMYB4 controls production of UV-protecting sunscreens in Arabidopsis. *EMBO J.*, **19**, 6150–6161.

Jones, L., Ennos, a R. and Turner, S.R. (2001) Cloning and characterization of *irregular xylem4* (*irx4*): a severely lignin-deficient mutant of *Arabidopsis*. *Plant J.*, **26**, 205–216.

Jouanin, L., Goujon, T., Nadaï, V. de, Martin, M.T., Mila, I., Vallet, C., Poller, B., Yoshinaga, A., Chabbert, B., Petit-Conil, M. and Lapierre, C. (2000) Lignification in transgenic poplars with extremely reduced caffeic acid O-methyltransferase activity. *Plant Physiol.*, **123**, 1363–74.

Jung, J.H., Lee, M. and Park, C.M. (2010) A transcriptional feedback loop modulating signaling crosstalks between auxin and brassinosteroid in Arabidopsis. *Mol. Cells*, **29**, 449–456.

Kerstetter, R., Vollbrecht, E., Lowe, B., Veit, B., Yamaguchi, J. and Hake, S. (1994) Sequence-Analysis and Expression Patterns Divide the Maize Knotted1-Like Homeobox Genes into 2 Classes. *Plant Cell*, **6**, 1877–1887.

Kim, D., Cho, Y.H., Ryu, H., Kim, Y., Kim, T.H. and Hwang, I. (2013) BLH1 and KNAT3 modulate ABA responses during germination and early seedling development in Arabidopsis. *Plant J.*, **75**, 755–766.

Kim, W.C., Ko, J.H., Kim, J.Y., Kim, J., Bae, H.J. and Han, K.H. (2013) MYB46 directly regulates the gene expression of secondary wall-associated cellulose synthases in Arabidopsis. *Plant J.*, **73**, 26–36.

Kimura, S., Koenig, D., Kang, J., Yoong, F.Y. and Sinha, N. (2008) Natural Variation in Leaf Morphology Results from Mutation of a Novel KNOX Gene. *Curr. Biol.*, **18**, 672–677.

Knaap, E. van der, Chakrabarti, M., Chu, Y.H., Clevenger, J.P., Illa-Berenguer, E., Huang, Z., Keyhaninejad, N., Mu, Q., Sun, L., Wang, Y. and Wu, S. (2014) What lies beyond the eye: the molecular mechanisms regulating tomato fruit weight and shape. *Front. Plant Sci.*, **5**, 1–13.

Ko, J.-H., Kim, W.C. and Han, K.H. (2009) Ectopic expression of MYB46 identifies transcriptional regulatory genes involved in secondary wall biosynthesis in Arabidopsis. *Plant J.*, **60**, 649–665.

Ko, J.H., Yang, S.H., Park, A.H., Lerouxel, O. and Han, K.H. (2007) ANAC012, a member of the plant-specific NAC transcription factor family, negatively regulates xylary fiber development in Arabidopsis thaliana. *Plant J.*, **50**, 1035–1048.

Kondo, Y., Fujita, T., Sugiyama, M. and Fukuda, H. (2015) A novel system for xylem cell differentiation in arabidopsis thaliana. *Mol. Plant*, **8**, 612–621.

Kondo, Y., Ito, T., Nakagami, H., Hirakawa, Y., Saito, M., Tamaki, T., Shirasu, K. and Fukuda, H. (2014) Plant GSK3 proteins regulate xylem cell differentiation downstream of TDIF-TDR signalling. *Nat. Commun.*, **5**, 1–11.

Kubo, M., Udagawa, M., Nishikubo, N., Horiguchi, G., Yamaguchi, M., Ito, J., Mimura, T., Fukuda, H. and Demura, T. (2005) Transcription switches for protoxylem and metaxylem vessel formation. *Genes Dev.*, **19**, 1855–1860.

Lee, C., Teng, Q., Huang, W., Zhong, R. and Ye, Z.-H. (2010) The Arabidopsis Family GT43 Glycosyltransferases Form Two Functionally Nonredundant Groups Essential for the Elongation of Glucuronoxylan Backbone. *Plant Physiol.*, **153**, 526–541.

Lee, D., Meyer, K., Chapple, C. and Douglasa, C.J. (1998) Antisense suppression of 4-Coumarate: Coenzyme A Ligase activity in Arabidopsis leads to altered lignin subunit composition. , **9**, 1985–1998.

Li, E., Bhargava, A., Qiang, W., Friedmann, M.C., Forneris, N., Savidge, R.A., Johnson, L.A., Mansfield, S.D., Ellis, B.E. and Douglas, C.J. (2012) The Class II KNOX gene KNAT7 negatively regulates secondary wall formation in Arabidopsis and is functionally conserved in Populus. *New Phytol.*, **194**, 102–115.

Li, E., Wang, S., Liu, Y., Chen, J. and Douglas, C.J. (2011) OVATE FAMILY PROTEIN4 (OFP4) interaction with KNAT7 regulates secondary cell wall formation in Arabidopsis thaliana. , **4**, 328–341.

Li, J. and Nam, K.H. (2002) Regulation of Brassinosteroid Signaling by a GSK3 / SHAGGY-Like Kinase. *Science (80-.).*, **295**, 1299–1301.

Li, Y., Qian, Q., Zhou, Y., Yan, M., Sun, L., Zhang, M., Fu, Z., Wang, Y., Han, B., Pang, X., Chen, M. and Li, J. (2003) *BRITTLE CULM1* , which encodes a COBRA-like protein , affects the mechanical properties of rice plants. *Plant Cell*, **15**, 2020–2031.

Lie, C., Kelsom, C. and Wu, X. (2012) WOX2 and STIMPY-LIKE/WOX8 promote cotyledon boundary formation in Arabidopsis. *Plant J.*, **72**, 674–682.

Liu, D., Sun, W., Yuan, Y., Zhang, N., Hayward, A., Liu, Y. and Wang, Y. (2014) Phylogenetic analyses provide the first insights into the evolution of OVATE family proteins in land plants. *Ann. Bot.*, **113**, 1219–1233.

Liu, J., Eck, J. Van, Cong, B. and Tanksley, S.D. (2002) A new class of regulatory genes underlying the cause of pear-shaped tomato fruit. *Proc. Natl. Acad. Sci. U. S. A.*, **99**, 13302–6.

Liu, Y. and Douglas, C.J. (2015) A role for OVATE FAMILY PROTEIN1 (OFP1) and OFP4 in a BLH6-KNAT7 multi-protein complex regulating secondary cell wall formation in Arabidopsis thaliana. *Plant Signal. Behav.*, **10**, e1033126.

Liu, Y., You, S., Taylor-Teeples, M., Li, W.L., Schuetz, M., Brady, S.M. and Douglas, C.J. (2014a) BEL1-LIKE HOMEODOMAIN6 and KNOTTED ARABIDOPSIS THALIANA7 Interact and Regulate Secondary Cell Wall Formation via Repression of REVOLUTA. *Plant Cell Online*, **26**, 4843–4861.

Liu, Z., Schneider, R., Kesten, C., Zhang, Y., Somssich, M., Zhang, Y., Fernie, A.R. and Persson, S. (2016) Cellulose-Microtubule Uncoupling Proteins Prevent Lateral Displacement of Microtubules during Cellulose Synthesis in Arabidopsis. *Dev. Cell*, **38**, 305–315.

Liu, Z., Zhu, Y., Gao, J., Yu, F., Dong, A. and Shen, W.H. (2009) Molecular and reverse genetic characterization of NUCLEOSOME ASSEMBLY PROTEIN1 (NAP1) genes

unravels their function in transcription and nucleotide excision repair in Arabidopsis thaliana. *Plant J.*, **59**, 27–38.

Long, J. a, Moan, E.I., Medford, J.I. and Barton, M.K. (1996) A member of the KNOTTED class of homeodomain proteins encoded by the STM gene of Arabidopsis. *Nature*, **379**, 66–69.

Lüscher, B. (2001) Function and regulation of the transcription factors of the Myc/Max/Mad network. *Gene*, **277**, 1–14.

MacMillan, C.P., Mansfield, S.D., Stachurski, Z.H., Evans, R. and Southerton, S.G. (2010) Fasciclin-like arabinogalactan proteins: Specialization for stem biomechanics and cell wall architecture in Arabidopsis and Eucalyptus. *Plant J.*, **62**, 689–703.

Magnani, E. and Hake, S. (2008) KNOX lost the OX: the Arabidopsis KNATM gene defines a novel class of KNOX transcriptional regulators missing the homeodomain. *Plant Cell*, **20**, 875–87.

Marita, J.M., Ralph, J., Hatfield, R.D. and Chapple, C. (1999) NMR characterization of lignins in Arabidopsis altered in the activity of ferulate 5-hydroxylase. *Proc. Natl. Acad. Sci.*, **96**, 12328–12332.

Mazur, E., Kurczyńska, E.U. and Friml, J. (2014) Cellular events during interfascicular cambium ontogenesis in inflorescence stems of Arabidopsis. *Protoplasma*, **251**, 1125–1139.

McCarthy, R.L., Zhong, R. and Ye, Z.H. (2009) MYB83 is a direct target of SND1 and acts redundantly with MYB46 in the regulation of secondary cell wall biosynthesis in arabidopsis. *Plant Cell Physiol.*, **50**, 1950–1964.

McFarlane, H.E., Döring, A. and Persson, S. (2014) The Cell Biology of Cellulose Synthesis. *Annu. Rev. Plant Biol.*, **65**, 69–94.

Meents, M.J., Watanabe, Y. and Samuels, A.L. (2018) The cell biology of secondary cell wall biosynthesis. , 1–19.

Mellerowicz, E.J., Baucher, M., Sundberg, B. and Boerjan, W. (2001) Unravelling cell wall formation in the woody dicot stem. *Plant Mol. Biol.*, **47**, 239–274.

Mi, H., Muruganujan, A. and Thomas, P.D. (2013) PANTHER in 2013: Modeling the evolution of gene function, and other gene attributes, in the context of phylogenetic trees. *Nucleic Acids Res.*, **41**, 377–386.

Mitsuda, N., Iwase, A., Yamamoto, H., Yoshida, M., Seki, M., Shinozaki, K. and Ohme-Takagi, M. (2007) NAC Transcription Factors, NST1 and NST3, Are Key Regulators of the Formation of Secondary Walls in Woody Tissues of Arabidopsis. *Plant Cell Online*, **19**, 270–280.

Mottiar, Y., Vanholme, R., Boerjan, W., Ralph, J. and Mansfield, S.D. (2016) Designer lignins: Harnessing the plasticity of lignification. *Curr. Opin. Biotechnol.*, **37**, 190–200.

Mueller, S.C. and Malcolm Brown, R. (1980) Evidence for an intramembrane component associated with a cellulose microfibril-synthesizing complex in higher plants. *J. Cell Biol.*, **84**, 315–326.

Mukherjee, K., Brocchieri, L. and Bürglin, T.R. (2009) A comprehensive classification and evolutionary analysis of plant homeobox genes. *Mol. Biol. Evol.*, **26**, 2775–2794.

Nakano, Y., Yamaguchi, M., Endo, H., Rejab, N.A. and Ohtani, M. (2015) NAC-MYB-based transcriptional regulation of secondary cell wall biosynthesis in land plants. *Front. Plant Sci.*, **6**, 1–18.

Napier, R.M., Fowke, L.C., Hawes, C., Lewis, M. and Pelham, H.R. (1992) Immunological evidence that plants use both HDEL and KDEL for targeting proteins to the

endoplasmic reticulum. *J. Cell Sci.*, **102**, 261–71.

Nemoto, K., Seto, T., Takahashi, H., Nozawa, A., Seki, M., Shinozaki, K., Endo, Y. and Sawasaki, T. (2011) Autophosphorylation profiling of Arabidopsis protein kinases using the cell-free system. *Phytochemistry*, **72**, 1136–1144.

Nixon, B.T., Mansouri, K., Singh, A., Du, J., Davis, J.K., Lee, J.G., Slabaugh, E., Vandavasi, V.G., O'Neil, H., Roberts, E.M., Roberts, A.W., Yingling, Y.G. and Haigler, C.H. (2016) Comparative Structural and Computational Analysis Supports Eighteen Cellulose Synthases in the Plant Cellulose Synthesis Complex. *Sci. Rep.*, **6**, 1–14.

Oda, Y. and Fukuda, H. (2012) Secondary cell wall patterning during xylem differentiation. *Curr. Opin. Plant Biol.*, **15**, 38–44.

Oehme, D.P., Downton, M.T., Doblin, M.S., Wagner, J., Gidley, M.J. and Bacic, A. (2015) Unique Aspects of the Structure and Dynamics of Elementary I β Cellulose Microfibrils Revealed by Computational Simulations. *Plant Physiol.*, **168**, 3–17.

Ohashi-Ito, K., Oda, Y. and Fukuda, H. (2010) *Arabidopsis* VASCULAR-RELATED NAC-DOMAIN6 Directly Regulates the Genes That Govern Programmed Cell Death and Secondary Wall Formation during Xylem Differentiation. *Plant Cell*, **22**, 3461–3473.

Ohman, D., Demedts, B., Kumar, M., Gerber, L., Gorzsas, A., Goeminne, G., Hedenstrom, M., Ellis, B., Boerjan, W. and Sundberg, B. (2013) MYB103 is required for FERULATE-5-HYDROXYLASE expression and syringyl lignin biosynthesis in Arabidopsis stems. *Plant J.*, **73**, 63–76.

Pagnussat, G.C., Yu, H.J. and Sundaresan, V. (2007) Cell-Fate Switch of Synergid to Egg Cell in Arabidopsis eostre Mutant Embryo Sacs Arises from Misexpression of the BEL1-Like Homeodomain Gene BLH1. *Plant Cell Online*, **19**, 3578–3592.

Pawar, P.M.-A., Koutaniemi, S., Tenkanen, M. and Mellerowicz, E.J. (2013) Acetylation of woody lignocellulose: significance and regulation. *Front. Plant Sci.*, **4**, 1–8.

Peña, M.J., Kulkarni, A.R., Backe, J., Boyd, M., O'Neill, M.A. and York, W.S. (2016) Structural diversity of xylans in the cell walls of monocots. *Planta*, **244**, 589–606.

Pesquet, E., Korolev, A. V., Calder, G. and Lloyd, C.W. (2010) The Microtubule-Associated Protein AtMAP70-5 Regulates Secondary Wall Patterning in Arabidopsis Wood Cells. *Curr. Biol.*, **20**, 744–749.

Porth, I., Klápště, J., Skyba, O., . (2013) Populus trichocarpa cell wall chemistry and ultrastructure trait variation, genetic control and genetic correlations. *New Phytol.*, **197**, 777–90.

Rennie, E.A. and Scheller, H.V. (2014) Xylan biosynthesis. *Curr. Opin. Biotechnol.*, **26**, 100–107.

Robinson, A.R. and Mansfield, S.D. (2009) Rapid analysis of poplar lignin monomer composition by a streamlined thioacidolysis procedure and near-infrared reflectance-based prediction modeling. *Plant J.*, **58**, 706–714.

Rodriguez-Gacio, M. del C., Iglesias-Fernandez, R., Carbonero, P. and Matilla, A.J. (2012) Softening-up mannan-rich cell walls. *J. Exp. Bot.*, **63**, 3975–3988.

Sakakibara, K., Nishiyama, T., Deguchi, H. and Hasebe, M. (2008) Class 1 KNOX genes are not involved in shoot development in the moss Physcomitrella patens but do function in sporophyte development. *Evol. Dev.*, **10**, 555–566.

Samuels, A.L., Kaneda, M. and Rensing, K.H. (2006) The cell biology of wood formation: from cambial divisions to mature secondary xylemThis review is one of a selection of papers published in the Special Issue on Plant Cell Biology. *Can. J. Bot.*, **84**, 631–639.

Scheller, H.V. and Ulvskov, P. (2010) Hemicelluloses. *Annu. Rev. Plant Biol.*, **61**, 263–289.

Schneider, R., Tang, L., Lampugnani, E.R., Barkwill, S., Lathe, R., Zhang., Y., McFarlane, H.E., Pesquet, E., Niittyla, T., Mansfield, S.D., Zhou, Y. and Persson, S. (2017) Two Complementary Mechanisms Underpin Cell Wall Patterning during Xylem Vessel Development. *Plant Cell*, **29**, 2433-2449.

Serikawa, K., Martinez-Laborda, A., Kim, H. and Zambryski, P. C. (1997) Localization of expression of KNAT3, a class 2 knotted1-like gene. *Plant J.*, **11(4)**, 853–861.

Shi, C.-L., Stenvik, G.-E., Vie, A.K., Bones, A.M., Pautot, V., Proveniers, M., Aalen, R.B. and Butenko, M.A. (2011) Arabidopsis Class I KNOTTED-Like Homeobox Proteins Act Downstream in the IDA-HAE/HSL2 Floral Abscission Signaling Pathway. *Plant Cell*, **23**, 2553–2567.

Shigeta, T., Yasuda, D., Mori, T., Yoshimitsu, Y., Nakamura, Y., Yoshida, S., Asami, T., Okamoto, S. and Matsuo, T. (2011) Characterization of brassinosteroid-regulated proteins in a nuclear-enriched fraction of Arabidopsis suspension-cultured cells. *Plant Physiol. Biochem.*, **49**, 985–995.

Shoji, T., Narita, N.N., Hayashi, K., Asada, J., Hamada, T., Sonobe, S., Nakajima, K. and Hashimoto, T. (2004) Plant-specific microtubule-associated protein SPIRAL2 is required for anisotropic growth in Arabidopsis. *Plant Physiol.*, **136**, 3933–3944.

Signal.salk.edu. (2018). Salk_010386, accessed 22 Feb. 2018, <http://signal.salk.edu/cgi-bin/tdnaexpress?JOB=TEXT&TYPE=DATA&QUERY=SALK_010386.38.25.x>.

Taylor-Teeples, M., Lin, L., Lucas, M. de, Turco, G., Toal, T.W., Gaudinier, A., Young, N.F., Trabucco, G.M., Veling, M.T., Lamothe, R., Handakumbura, P.P., Xiong, G., Wang, C., Corwin, J., Tsoukalas, A., Zhang, L., Ware, D., Pauly, M., Kliebenstein, D.J., Dehesh, K., Tagkopoulos, I., Breton, G., Pruneda-Paz, J.L., Ahnert, S.E., Kay, S.A.,

Hazen, S. P. and Brady, S.M. (2014a) An Arabidopsis gene regulatory network for secondary cell wall synthesis. *Nature*, **517**, 571–575.

Taylor, N.G. (2000) Multiple Cellulose Synthase Catalytic Subunits Are Required for Cellulose Synthesis in Arabidopsis. *Plant Cell Online*, **12**, 2529–2540.

Taylor, N.G., Howells, R.M., Huttly, A.K., Vickers, K. and Turner, S.R. (2003) Interactions among three distinct CesA proteins essential for cellulose synthesis. *Proc. Natl. Acad. Sci.*, **100**, 1450–1455.

Taylor, N.G., Laurie, S. and Turner, S.R. (2000) Multiple Cellulose Synthase Catalytic Subunits Are Required for Cellulose Synthesis in Arabidopsis. *Plant Cell*, **12**, 2529–2539.

Taylor, N.G., Scheible, W.R., Cutler, S., Somerville, C.R. and Turner, S.R. (1999) The irregular xylem3 locus of Arabidopsis encodes a cellulose synthase required for secondary cell wall synthesis. *Plant Cell*, **11**, 769–780.

Tobimatsu, Y., Chen, F., Nakashima, J., Escamilla-Trevino, L.L., Jackson, L., Dixon, R.A. and Ralph, J. (2013) Coexistence but Independent Biosynthesis of Catechyl and Guaiacyl/Syringyl Lignin Polymers in Seed Coats. *Plant Cell*, **25**, 2587–2600.

Trapnell, C., Roberts, A., Goff, L., Pertea, G., Kim, D., Kelley, D.R., Pimentel, H., Salzberg, S.L., Rinn, J.L. and Pachter, L. (2012) Differential gene and transcript expression analysis of RNA-seq experiments with TopHat and Cufflinks. *Nat. Protoc.*, **7**, 562–578.

Truernit, E., Siemering, K.R., Hodge, S., Grbic, V. and Haseloff, J. (2006) A map of KNAT gene expression in the Arabidopsis root. *Plant Mol. Biol.*, **60**, 1–20.

Tsuda, K., Ito, Y., Sato, Y. and Kurata, N. (2011) Positive autoregulation of a KNOX gene is essential for shoot apical meristem maintenance in rice. *Plant Cell*, **23**, 4368–4381.

Turner, S.R. (1997) Collapsed Xylem Phenotype of Arabidopsis Identifies Mutants Deficient in Cellulose Deposition in the Secondary Cell Wall. *Plant Cell Online*, **9**, 689–701.

Turnera, S.R. and Somerville, C.R. (1997) Collapsed Xylem Phenotype of Arabidopsis ldentifies Mutants Deficient in Cellulose Deposition in the Secondary Cell Wall. , **9**, 689–701.

Ursache, R., Miyashima, S., Chen, Q., Vaten, A., Nakajima, K., Carlsbecker, A., Zhao, Y., Helariutta, Y. and Dettmer, J. (2014) Tryptophan-dependent auxin biosynthesis is required for HD-ZIP III-mediated xylem patterning. *Development*, **141**, 1250–1259.

Ursache, R., Nieminen, K. and Helariutta, Y. (2013) Genetic and hormonal regulation of cambial development. *Physiol. Plant.*, **147**, 36–45.

Vanholme, R., Cesarino, I., Rataj, K., Xiao, Y., Sundin, L., Goeminne, G., Kim, H., Cross, J., Morreel K., Araujo, P., Welsh, L., Haustraete, J., McClellam, C., Vanholme, B., Ralph, J., Simpson, G.G., Halpin, C., Boerjan, W. (2013) Caffeoyl Shikimate Esterase (CSE) Is an Enzyme in the Lignin Biosynthetic Pathway in Arabidopsis. *Science*, **342**, 1327–1329.

Velasquez, S.M., Ricardi, M.M., Dorosz, J.G., Fernandez, P.V., Nadra, A.D., Pol-Fachin, L., Egelund, J., Gille, S., Harholt, J., Cianacia, M., Verli, H., Pauly, M., Bacic, A., Olsen, C.E., Ulvskov, P., Petersen, B.L., Somerville, C., Lusem, N.D. and Esteves, J.M. (2011) O-Glycosylated Cell Wall Proteins Are Essential in Root Hair Growth. *Science*, **332**, 1401–1403.

Venglat, S.P., Dumonceaux, T., Rozwadowski, K., Parnell, L., Babic, V., Keller, W., Martienssen, R., Selvaraj, G. and Datla, R. (2002) The homeobox gene BREVIPEDICELLUS is a key regulator of inflorescence architecture in Arabidopsis. *Proc. Natl. Acad. Sci.*, **99**, 4730–4735.

Vollbrecht, E., Reiser, L. and Hake, S. (2000) Shoot meristem size is dependent on inbred background and presence of the maize homeobox gene, knotted1. *Development*, **127**, 3161–3172.

Vollbrecht, E., Veit, B., Sinha, N. and Hake, S. (1991) The developmental gene Knotted-1 is a member of a maize homeobox gene family. *Nature*, **350**, 241–243.

Wang, H., Avci, U., Nakashima, J., Hahn, M.G., Chen, F. and Dixon, R.A. (2010) Mutation of WRKY transcription factors initiates pith secondary wall formation and increases stem biomass in dicotyledonous plants. *Proc. Natl. Acad. Sci.*, **107**, 22338–22343.

Wang, H., Zhao, Q., Chen, F., Wang, M. and Dixon, R.A. (2011) NAC domain function and transcriptional control of a secondary cell wall master switch. *Plant J.*, **68**, 1104–1114.

Wang, S., Chang, Y. and Ellis, B. (2016) Overview of OVATE FAMILY PROTEINS, A Novel Class of Plant-Specific Growth Regulators. *Front. Plant Sci.*, **7**, 1–8.

Wang, S., Chang, Y., Guo, J. and Chen, J.-G. (2007) Arabidopsis Ovate Family Protein 1 is a transcriptional repressor that suppresses cell elongation. *Plant J.*, **50**, 858–872.

Wang, S., Chang, Y., Guo, J., Zeng, Q., Ellis, B.E. and Chen, J.G. (2011) Arabidopsis Ovate family proteins, a novel transcriptional repressor family, control multiple aspects of plant growth and development. *PLoS One*, **6**.

Wang, Y.K., Chang, W.C., Liu, P.F., Hsiao, M.K., Lin, C.T., Lin, S.M. and Pan, R.L. (2010) Ovate family protein 1 as a plant Ku70 interacting protein involving in DNA double-strand break repair. *Plant Mol. Biol.*, **74**, 453–466.

Weng, J.K., Mo, H. and Chapple, C. (2010) Over-expression of F5H in COMT-deficient Arabidopsis leads to enrichment of an unusual lignin and disruption of pollen wall formation. *Plant J.*, **64**, 898–911.

Wu, A.-M., Hornblad, E., Voxeur, A., Gerber, L., Rihouey, C., Lerouge, P. and Marchant, A. (2010) Analysis of the Arabidopsis IRX9/IRX9-L and IRX14/IRX14-L Pairs of Glycosyltransferase Genes Reveals Critical Contributions to Biosynthesis of the Hemicellulose Glucuronoxylan. *Plant Physiol.*, **153**, 542–554.

Xiao, Y., Liu, D., Zhang, G., Tong, H. and Chu, C. (2017) Brassinosteroids Regulate OFP1, a DLT Interacting Protein, to Modulate Plant Architecture and Grain Morphology in Rice. *Front. Plant Sci.*, **8**, 1–13.

Yamaguchi, M., Goue, N., Igarashi, H., Ohtani, M., Nakano, Y., Mortimer, J.C., Nishikubo, N., Kubo, M., Katayama, Y., Kakegawa, K., Dupree, P. and Demura, T. (2010) VASCULAR-RELATED NAC-DOMAIN6 and VASCULAR-RELATED NAC-DOMAIN7 Effectively Induce Transdifferentiation into Xylem Vessel Elements under Control of an Induction System. *Plant Physiol.*, **153**, 906–914.

Yamaguchi, M., Mitsuda, N., Ohtani, M., Ohme-takagi, M., Kato, K. and Demura, T. (2011) VASCULAR-RELATED NAC-DOMAIN 7 directly regulates the expression of a broad range of genes for xylem vessel formation. , 579–590.

Yamaguchi, M., Ohtani, M., Mitsuda, N., Kubo, M., Ohme-Takagi, M., Fukuda, H. and Demura, T. (2010) VND-INTERACTING2, a NAC Domain Transcription Factor, Negatively Regulates Xylem Vessel Formation in *Arabidopsis*. *Plant Cell*, **22**, 1249–1263.

Yang, C., Ma, Y., He, Y., Tian, Z. and Li, J. (2018) OsOFP19 modulates plant architecture by integrating the cell division pattern and brassinosteroid signaling. *Plant J.*, 489–501.

Yang, C., Shen, W., He, Y., Tian, Z. and Li, J. (2016) OVATE Family Protein 8 Positively Mediates Brassinosteroid Signaling through Interacting with the GSK3-like Kinase in Rice. *PLoS Genet.*, **12**, 1–15.

Yang, J.H. and Wang, H. (2016) Molecular Mechanisms for Vascular Development and

Secondary Cell Wall Formation. *Front. Plant Sci.*, **7**, 1–8.

Yin, Y., Wang, Z.Y., Mora-Garcia, S., Li, J., Yoshida, S., Asami, T. and Chory, J. (2002) BES1 accumulates in the nucleus in response to brassinosteroids to regulate gene expression and promote stem elongation. *Cell*, **109**, 181–191.

Zeng, W., Lampugnani, E.R., Picard, K.L., Song, L., Wu, A.M., Farion, I.M., Zhao, J., Ford, K., Doblin, M.S. and Bacic, A. (2016) Asparagus IRX9, IRX10, and IRX14A Are Components of an Active Xylan Backbone Synthase Complex that Forms in the Golgi Apparatus. *Plant Physiol.*, **171**, 93–109.

Zhang, J., Elo, A. and Helariutta, Y. (2011) Arabidopsis as a model for wood formation. *Curr. Opin. Biotechnol.*, **22**, 293–299.

Zhang, L., Zhang, X., Ju, H., Chen, J., Wang, S., Wang, H., Zhao, Y. and Chang, Y. (2016) Ovate family protein1 interaction with BLH3 regulates transition timing from vegetative to reproductive phase in Arabidopsis. *Biochem. Biophys. Res. Commun.*, **470**, 492–497.

Zhao, C., Avci, U., Grant, E.H., Haigler, C.H. and Beers, E.P. (2008) XND1, a member of the NAC domain family in Arabidopsis thaliana, negatively regulates lignocellulose synthesis and programmed cell death in xylem. *Plant J.*, **53**, 425–436.

Zhao, Q. (2016) Lignification: Flexibility, Biosynthesis and Regulation. *Trends Plant Sci.*, **21**, 713–721.

Zhao, Q. and Dixon, R.A. (2011) Transcriptional networks for lignin biosynthesis: More complex than we thought? *Trends Plant Sci.*, **16**, 227–233.

Zhao, Q., Wang, H., Yin, Y., Xu, Y., Chen, F. and Dixon, R.A. (2010) Syringyl lignin biosynthesis is directly regulated by a secondary cell wall master switch. *Proc. Natl. Acad.*

Sci., **107**, 14496–14501.

Zhong, R. (2005) Arabidopsis Fragile Fiber8, Which Encodes a Putative Glucuronyltransferase, Is Essential for Normal Secondary Wall Synthesis. *Plant Cell Online*, **17**, 3390–3408.

Zhong, R. (1997) Disruption of Interfascicular Fiber Differentiation in an Arabidopsis Mutant. *Plant Cell Online*, **9**, 2159–2170.

Zhong, R., Demura, T. and Ye, Z.H. (2006) SND1, a NAC Domain Transcription Factor, Is a Key Regulator of Secondary Wall Synthesis in Fibers of Arabidopsis. *Plant Cell Online*, **18**, 3158–3170.

Zhong, R., Lee, C., Zhou, J., McCarthy, R.L. and Ye, Z.H. (2008a) A Battery of Transcription Factors Involved in the Regulation of Secondary Cell Wall Biosynthesis in Arabidopsis. *Plant Cell Online*, **20**, 2763–2782.

Zhong, R., Lee, C., Zhou, J., McCarthy, R.L. and Ye, Z.-H. (2008b) A Battery of Transcription Factors Involved in the Regulation of Secondary Cell Wall Biosynthesis in Arabidopsis. *Plant Cell Online*, **20**, 2763–2782.

Zhong, R., Richardson, E.A. and Ye, Z.-H. (2007) The MYB46 Transcription Factor Is a Direct Target of SND1 and Regulates Secondary Wall Biosynthesis in Arabidopsis. *Plant Cell Online*, **19**, 2776–2792.

Zhong, R., Richardson, E.A. and Ye, Z.H. (2007) Two NAC domain transcription factors, SND1 and NST1, function redundantly in regulation of secondary wall synthesis in fibers of Arabidopsis. *Planta*, **225**, 1603–1611.

Zhong, R. and Ye, Z.H. (2015) The Arabidopsis NAC transcription factor NST2 functions together with SND1 and NST1 to regulate secondary wall biosynthesis in fibers of

inflorescence stems. *Plant Signal. Behav.*, **10**, 1–7.

Zhong, R. and Ye, Z.H. (2012) MYB46 and MYB83 bind to the SMRE sites and directly activate a suite of transcription factors and secondary wall biosynthetic genes. *Plant Cell Physiol.*, **53**, 368–380.

Zhong, R. and Ye, Z.H. (2007) Regulation of cell wall biosynthesis. *Curr. Opin. Plant Biol.*, **10**, 564–572.

Zhou, J., Lee, C., Zhong, R. and Ye, Z.H. (2009) MYB58 and MYB63 Are Transcriptional Activators of the Lignin Biosynthetic Pathway during Secondary Cell Wall Formation in Arabidopsis. *Plant Cell*, **21**, 248–266.

Zhou, J., Zhong, R. and Ye, Z.H. (2014) Arabidopsis NAC domain proteins, VND1 to VND5, are transcriptional regulators of secondary wall biosynthesis in vessels. *PLoS One*, **9,** e105726.

Zhu, Y., Dong, A., Meyer, D., Pichon, O., Renou, J.P., Cao, K. and Shen, W.H. (2006) Arabidopsis NRP1 and NRP2 encode histone chaperones and are required for maintaining postembryonic root growth. *Plant Cell*, **18**, 2879–2892.

Zimmermann, I.M., Heim, M.A., Weisshaar, B. and Uhrig, J.F. (2004) Comprehensive identification of Arabidopsis thaliana MYB transcription factors interacting with R/B-like BHLH proteins. *Plant J.*, **40**, 22–34.